Backman, J., Duncan, R. A., et al., 1988
Proceedings of the Ocean Drilling Program, Initial Reports, Vol. 115

8. SITE 710[1]

Shipboard Scientific Party[2]

HOLE 710A

Date occupied: 0515 L, 9 June 1987

Date departed: 2300 L, 9 June 1987

Time on hole: 17 hr, 45 min

Position: 04°18.7'S, 60°58.8'E

Water depth (sea level; corrected m, echo-sounding): 3824.3

Water depth (rig floor; corrected m, echo-sounding): 3834.8

Bottom felt (m, drill pipe): 3822.5

Penetration (m): 209.7

Number of cores: 22

Total length of cored section (m): 209.7

Total core recovered (m): 185.2

Core recovery (%): 88

Oldest sediment cored:
Depth (mbsf): 209.7
Nature: nannofossil ooze/chalk
Age: early Oligocene
Measured velocity (km/s): 1.502

HOLE 710B

Date occupied: 0145 L, 10 June 1987

Date departed: 0800 L, 10 June 1987

Time on hole: 6 hr, 15 min

Position: 04°18.7'S, 60°58.8'E

Water depth (sea level; corrected m, echo-sounding): 3824.3

Water depth (rig floor; corrected m, echo-sounding): 3834.8

Bottom felt (m, drill pipe): 3821.0

Penetration (m): 83.4

Number of cores: 9

Total length of cored section (m): 83.4

Total core recovered (m): 72.1

Core recovery (%): 86

Oldest sediment cored:
Depth (mbsf): 83.4
Nature: nannofossil clay
Age: late Miocene
Measured velocity (km/s): 1.402

Principal results: Site 710 is located in the western equatorial Indian Ocean at 4°18.7'S and 60°58.8'E, at a water depth of 3812 m. The site lies on the central Madingley Rise, a regional topographic high between the Carlsberg Ridge and the northern Mascarene Plateau (Fig. 1). More specifically, Site 710 was drilled on a fairly broad northeast-trending terrace showing a sediment thickness of about 400 m and internally coherent seismic reflectors (see "Seismic Stratigraphy" section, this chapter). At a depth of 3812 m, near the present-day sedimentary lysocline, Site 710 is well suited for the purpose of studying the Neogene history of carbonate flux and dissolution. Its topographical location on a flat terrace adjacent to elevated grounds should also provide information on downslope transport processes.

We cored two holes continuously at Site 710. Hole 710A terminated in nannofossil ooze/chalk of early Oligocene age at 209.7 mbsf. We used the advanced hydraulic piston corer (APC) for the upper 13 cores and the extended core barrel (XCB) for the remaining nine deeper cores. The total recovery was 88%, and again the XCB gave good recovery (87%). Nine APC cores were taken at Hole 710B, to a total depth of 83.4 m (86% recovery). Major lithologies are as follows:

Unit I (0–69 mbsf) is divided into two subunits. Subunit IA consists of light yellowish grey nannofossil ooze containing about 5%–10% biogenic silica and about 80% carbonate. Thin (2–5 cm) turbidites occur occasionally, composed of white foraminifer nannofossil oozes. This subunit is interpreted to reflect oxidizing conditions. A greenish color, which presumably reflects more reducing conditions, separates Subunit IB from IA. Quasi-rhythmical changes in color occur throughout Unit I, which probably represent differential dissolution of the biogenic carbonate. The deepest core in Unit I (115-710A-8H) shows signs of disturbance, with sharp nonhorizontal contacts, possibly reflecting slumping. Also the bio- and magnetostratigraphic records indicate that the lowermost part of Unit I is disturbed. Unit I encompasses the interval from the Pleistocene to the late Miocene (0–8 Ma).

Unit II (69–132 mbsf) consists of clay-bearing nannofossil ooze and nannofossil clay. Its upper limit coincides with a marked change in carbonate content, from average values around 80% to values around 60%. This boundary marks an episode of severe carbonate dissolution, which explains the high noncarbonate (clay) fraction. The carbonate content increases to values around 70% toward the deeper part of Unit II, although the entire unit is characterized by strongly variable carbonate percentages. The noncarbonate fraction is mainly clays. This unit is confined to the Miocene (8–24 Ma).

Unit III (132–209.7 mbsf) consists of alternating nannofossil oozes and chalks of early Miocene to early Oligocene age (24–33 Ma). The carbonate content is consistently high, around 90%, although the planktonic foraminifers are largely dissolved. Figure 2 summarizes the cored stratigraphic sequence.

Summary of Interpretation

Site 710 contains the first good magnetostratigraphic record to be obtained during Leg 115. After considerable effort, the magnetostratigraphers succeeded in locating the source of magnetic overprint from the core barrels. Demagnetization of these APC core barrels immediately resulted in clearer reversal boundaries. However, the orienting device did not function properly, nor did the sediments cored with the XCB yield reliable results. Hence, the magnetostratigraphic control ends at about 22 Ma. Magnetic susceptibility records, analyzed at 5-cm intervals, again proved superior for the purpose of interhole correlations, revealing even minor offsets across core boundaries (see "Paleomagnetics" section, this chapter).

The carbonate content record, based on one sample per 0.75 m from Hole 710A, contains a "high-frequency" component (see "Geochemistry" section, this chapter) which, when smoothed, displays a quasi-cyclical character. Dry-bulk densities vary from values of 0.7 to 1.25 g/cm^3 (see "Physical Properties" section, this chapter), where the highest values are observed in the middle-early Miocene nanno-

[1] Backman, J., Duncan, R. A., et al., 1988. *Proc. ODP, Init. Repts.*, 115: College Station, TX (Ocean Drilling Program).

[2] Shipboard Scientific Party is as given in the list of Participants preceding the contents, with the addition of Isabella Premoli Silva, Dipartimento di Scienze della Terra, Universitá di Milano, Via Mangiagalli 34, I-20129 Milano, Italy.

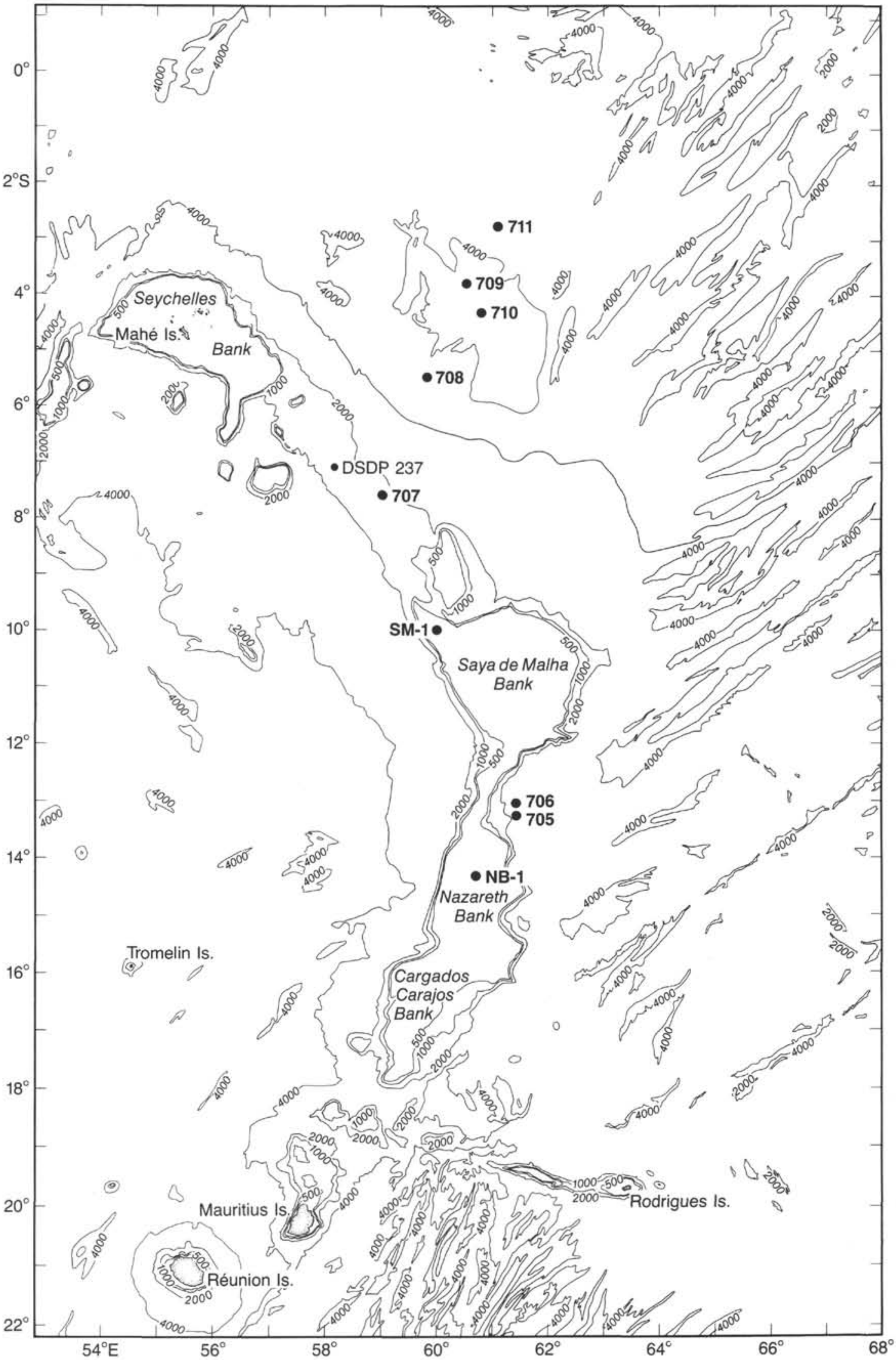

Figure 1. Bathymetric map showing location of Site 710 and other Leg 115 sites (after Fisher et al., 1971). Depth in meters.

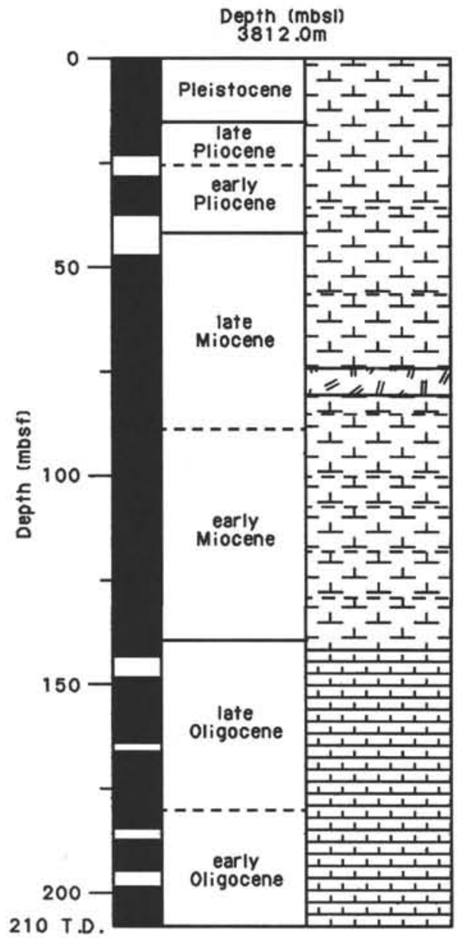

Figure 2. Stratigraphic summary of Site 710. Black column represents recovered section.

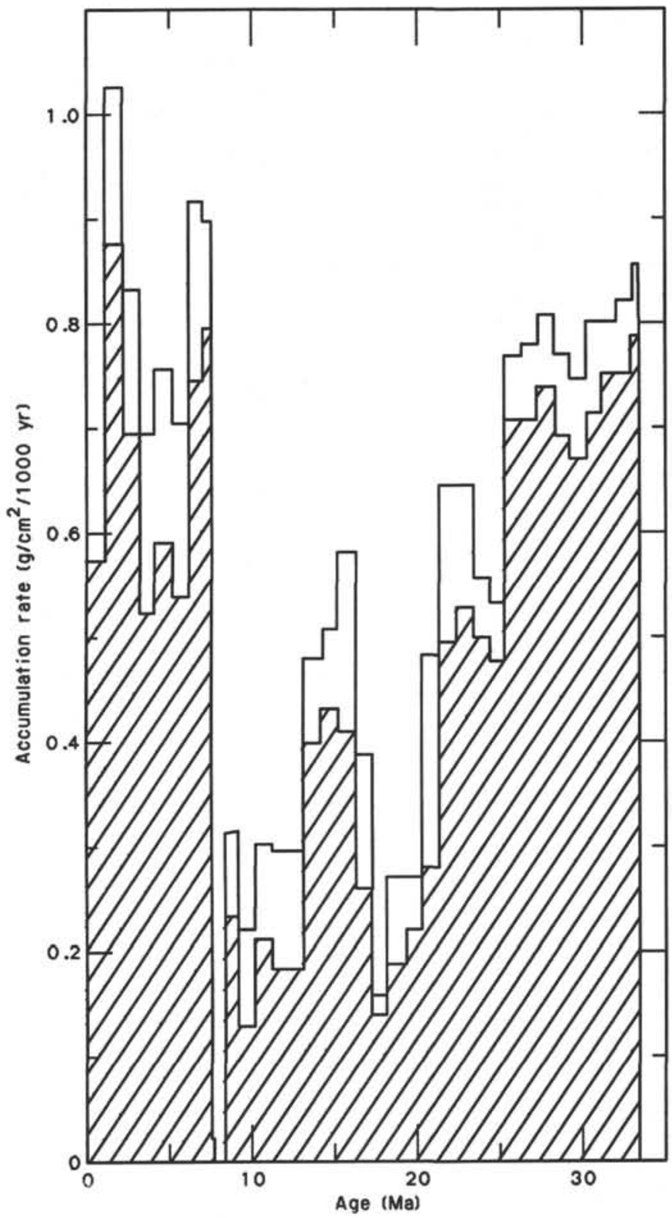

Figure 3. Mass accumulation rates of bulk sediment (unfilled area) and biogenic calcium carbonate (diagonal lines) plotted vs. age at Hole 710A. We excluded data from Core 115-710A-8H due to core disturbances that we interpreted as being caused by sedimentological processes. This appears as a gap in the record between 7.4 and 8.2 Ma. The data represent preliminary estimates of mean values within 1-m.y. time increments.

fossil clays. Preliminary estimates of bulk and carbonate mass accumulation rates are shown in Figure 3.

In comparison with the nearby (800 m shallower) Site 709, Site 710 exhibits generally lower late Miocene through Pleistocene bulk accumulation rates, but a proportionately higher accumulation of the noncarbonate fraction (Fig. 3). It appears reasonable to ascribe this difference to carbonate dissolution at the deeper Site 710. The early Miocene bulk accumulation is virtually identical at the two sites, yielding values of about 0.5–0.6 g/cm^2/1000 yr. A 25% difference in bulk accumulation rates, however, existed between the two sites during late Oligocene times (25–33 Ma), where the higher rates occurred at the deeper Site 710. Because we used the same set of biostratigraphic criteria at both sites for deriving age models, we consider the difference to reflect true differences in depositional modes. Moreover, because the two sites are separated by only 30 nmi, it appears likely that the pelagic input should have been similar in any given time interval.

The average bulk and carbonate accumulation rates are 0.80 and 0.70 g/cm^2/1000 yr, respectively, at Site 710, and 0.56 and 0.52 g/cm^2/1000 yr, respectively, at Site 709 between 25 and 33 Ma. Thus, more carbonate was deposited at Site 710 despite the fact that dissolution of carbonate was more intense at this deeper site (88% of the bulk at Site 710 as compared with 93% at Site 709). This depositional pattern suggests that winnowing affected the shallower Site 709, transporting fine-grained material downslope to be redeposited on the terrace at Site 710. Why this pattern should be confined to the late Oligocene remains to be answered.

BACKGROUND AND OBJECTIVES

Site 710 is one of five sites drilled at different water depths from the Mascarene Plateau (Site 707), the Madingley Rise (Sites 709, 710, and 711), and the surrounding abyssal plains (Site 708; Fig. 4). The broader strategy for drilling this bathymetric transect is presented in the Site 707 chapter (see "Background and Objectives" section, "Site 707" chapter, this volume). Site 710 is located at a water depth of 3812 m, some 30 nmi southeast of Site 709, and is thus at an intermediate depth relative to Site 709 (3038 m) and Site 711 (4429 m). We drilled Site 710 for the purpose of retrieving a complete Neogene sediment sequence that we could use to study the flux of pelagic carbonate and its dissolution at depth.

Biogenic carbonate dissolves at all water depths below the depth of the saturation horizon of calcite, but enhanced dissolution usually begins at some depth well below that horizon

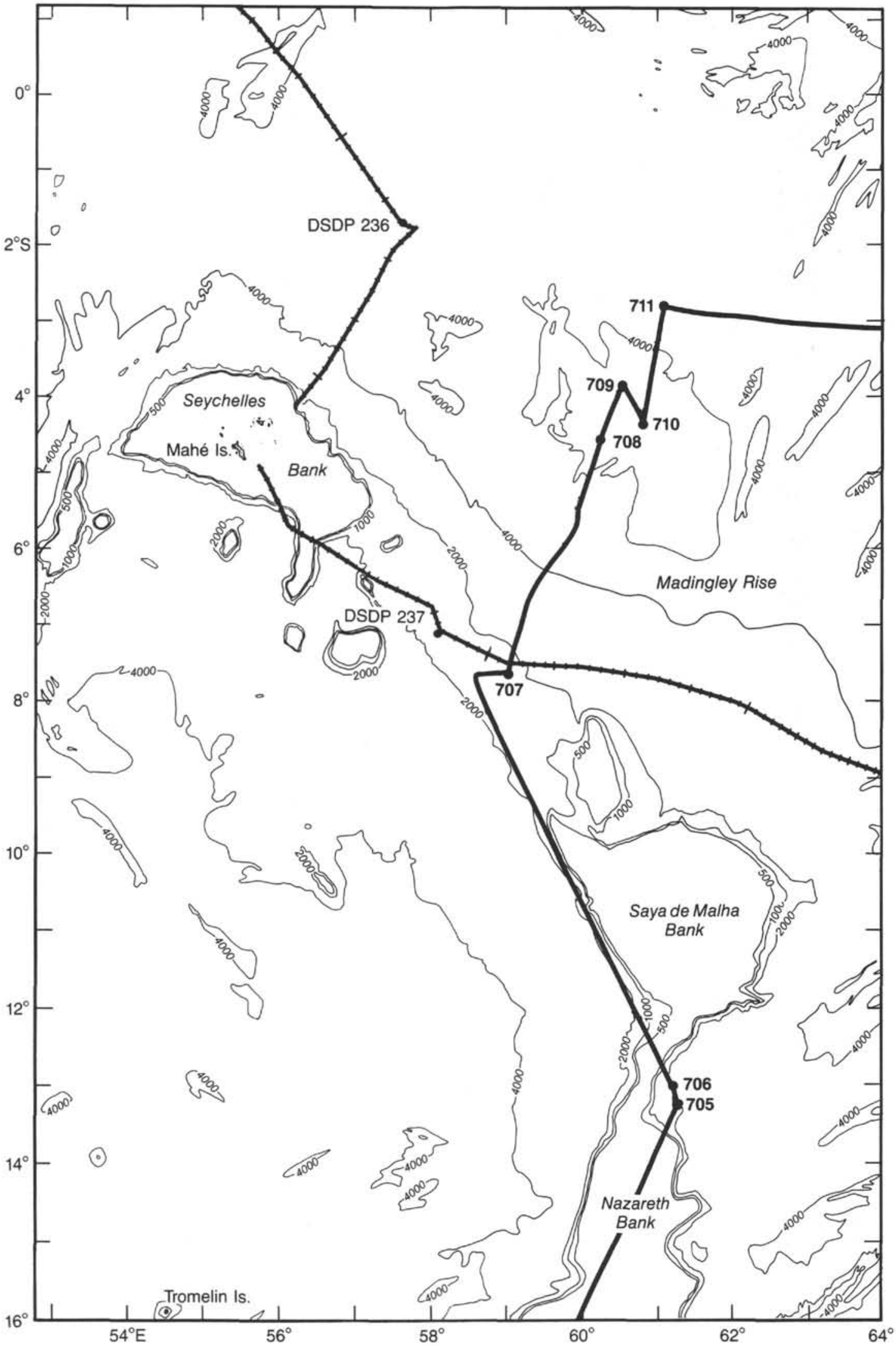

Figure 4. Expanded view of the bathymetric features around the northern Mascarene Plateau and the location of Site 710 (after Fisher, Bunce, et al., 1974). Shown for reference is the track line of the *Glomar Challenger* on DSDP Leg 24 as well as the track line for ODP Leg 115 made by *JOIDES Resolution*. Depth in meters.

(Peterson, 1966; Takahashi, 1975). Moreover, the two main components of the carbonate input to the ocean floor, planktonic foraminifers and coccolithophorids, show major differences in preservational states when the depth of the sedimentary lysocline is approached (Berger, 1973; Roth and Berger, 1975). At a depth of about 3812 m, Site 710 is ideally located for the study of time-dependent variability in the relative position of the foraminiferal and nannofossil lysoclines. Extreme excursions in the depth position of the carbonate-compensation depth (CCD) are also likely to be preserved in the Neogene sequence at Site 710. Furthermore, Sites 709, 710, and 711 are all located on ocean crust of similar age (basal Eocene; Schlich, 1982) in a narrowly confined geographic area, which indicates that their relative bathymetric separations are unlikely to have changed through time, although they are all subject to subsidence.

In order to pursue the proposed studies, it is of paramount importance to establish a highly resolved time control. We expect that carbonate dissolution at Site 710 has concentrated the noncarbonate fraction sufficiently to yield adequate geomagnetic field intensities. Thus, the sediments at Site 710 should provide an excellent opportunity for direct calibration between equatorial Indian Ocean microfossil marker species and the magnetostratigraphic record.

OPERATIONS

Hole 710A

We prepared the same APC/XCB bottom-hole assembly (BHA) we used on the previous sites and lowered it to the seafloor. The mud line was established at 3812 m, where APC coring advanced the hole to 3936.9 m (124.9 mbsf) in 13 coring runs. We deployed orientation instruments beginning with Core 115-710A-4H until we made the change to XCB. Coring with the APC recovered 111.5 m of core for an 89.2% recovery rate. When the pull-out force reached 30,000 lb, we replaced the APC system with the XCB system.

We ran the XCB system nine times, advancing the hole to 4021.7 m (209.7 mbsf) and recovering 73.7 m of core for a recovery rate of 86.9%. Again, we recovered high-quality cores in both soupy chalk ooze and clays with the experimental XCB cutting shoe with seal.

Total penetration was 209.7 mbsf to 4021.7 m, with 185.2 m of core recovered for a total recovery rate of 88% (Table 1).

Hole 710B

With the BHA back on bottom, we established the mud line at 3810.5 m. The APC was deployed nine times to 3893.9 m (83.4 mbsf). With the coring objective met, we tripped out the drill string and made preparations to get under way for Site CARB-4B. Total penetration was 83.4 mbsf to 3893.9 m, with 72 m of core recovered for a total recovery rate of 86% (Table 1).

Site 710 to Site 711 (CARB-4B)

The beacon was recalled and back on board at 1145 hr, 10 June 1987. The ship was under way at 1500 hr and was over Site CARB-4B by 2200 hr, after traveling approximately 94 nmi.

LITHOSTRATIGRAPHY

Introduction

Site 710 was the third of five sites in the carbonate dissolution profile. The site is located on the southeastern flank of the Madingley Rise, at a water depth of 3812 m, which is the approximate depth of the present-day carbonate lysocline.

The sediments at Site 710 contain varying calcium carbonate contents; thus, we have subdivided them into three separate units on the basis of clay (or carbonate) content and degree of lithification. Two subunits further divide Unit I. Each of these lithologies is described below.

Table 1. Coring summary, Site 710.

Core no.	Date (June 1987)	Time (local)	Depth (mbsf)	Cored (m)	Recovered (m)	Recovery (%)
115-710A-						
1H	9	0530	0–9.5	9.5	9.49	99.9
2H	9	0615	9.5–19.2	9.7	9.62	99.2
3H	9	0700	19.2–28.8	9.6	4.67	48.6
4H	9	0800	28.8–38.3	9.5	9.76	103.0
5H	9	0830	38.3–47.9	9.6	0	0
6H	9	0930	47.9–57.5	9.6	9.56	99.6
7H	9	1030	57.5–67.1	9.6	9.55	99.5
8H	9	1115	67.1–76.6	9.5	9.20	96.8
9H	9	1200	76.6–86.2	9.6	9.90	103.0
10H	9	1300	86.2–95.8	9.6	9.87	103.0
11H	9	1345	95.8–105.5	9.7	9.84	101.0
12H	9	1430	105.5–115.2	9.7	10.12	104.3
13H	9	1530	115.2–124.9	9.7	9.91	102.0
14X	9	1630	124.9–132.4	7.5	9.26	123.0
15X	9	1715	132.4–142.1	9.7	7.19	74.1
16X	9	1815	142.1–151.8	9.7	7.36	75.9
17X	9	1900	151.8–161.4	9.6	9.06	94.4
18X	9	2000	161.4–171.1	9.7	7.25	74.7
19X	9	2045	171.1–180.8	9.7	9.35	96.4
20X	9	2130	180.8–190.4	9.6	8.75	91.1
21X	9	2215	190.4–200.1	9.7	8.74	90.1
22X	9	2300	200.1–209.7	9.6	6.75	70.3
115-710B-						
1H	10	0215	0–6.5	6.5	6.53	100.0
2H	10	0300	6.5–16.2	9.7	9.59	98.8
3H	10	0345	16.2–25.8	9.6	9.73	101.0
4H	10	0430	25.8–35.3	9.5	9.48	99.8
5H	10	0515	35.3–44.9	9.6	9.51	99.0
6H	10	0600	44.9–54.5	9.6	8.79	91.5
7H	10	0645	54.5–64.2	9.7	9.23	95.1
8H	10	0730	64.2–73.8	9.6	0	0
9H	10	0815	73.8–83.4	9.6	9.20	95.8

Unit I: Cores 115-710A-1H to -8H (0.0–69.1 mbsf) and Cores 115-710B-1H to -7H (0.0-64.2 mbsf); Age: Pleistocene to late Miocene.

Unit I consists predominantly of clay-bearing nannofossil ooze containing about 80% calcium carbonate. We divided Unit I into two subunits on the basis of color and inferred oxidation state of the sediments.

Subunit IA: Sections 115-710A-1H-1 to 115-710A-4H, CC (0.0–38.3 mbsf), and Sections 115-710B-1H-1 to 115-710B-6H-2, 75 cm (0.0–47.2 mbsf); Age: Pleistocene to early Pliocene.
Subunit IB: Sections 115-710A-5H-1 to 115-710A-8H-2, 47 cm (47.9–69.1 mbsf), and Sections 115-710B-6H-2, 75 cm, to Section 115-710B-7H, CC (47.2–64.2 mbsf); Age: early Pliocene to late Miocene.

Unit IA consists mostly of clay-bearing nannofossil ooze. It is considered to be oxidized because it is colored various shades of yellow and brown: white (10YR 8/2), light gray (10YR 7/2), and very pale brown (10YR 7/3). Mottling due to bioturbation is common throughout this interval. These sediments contain several percentages of biogenic silica; estimates based on smear slides show a maximum of 6% diatoms, 8% radiolarians, 4% sponge spicules, and 1% silicoflagellates. Foraminiferal content is less than 5% in all smear slides of the dominant lithology.

Color changes resulting from variable clay/carbonate ratios average about 30 per core throughout this interval. Variations in the carbonate contents by about 5%–10% are responsible for these color changes. The color changes are mirrored by changes in magnetic susceptibility (see "Paleomagnetics" section, this chapter). As a result, magnetic susceptibility has proved to be an excellent tool for identifying more precisely the location of lithologic boundaries and for correlating between Holes 710A and 710B (Fig. 5). We can correlate low values of magnetic susceptibility with carbonate-rich sediments, with the lowest values in the nearly pure carbonate turbidites. An interesting feature observed in this particular example (Fig. 5) is the erosion of strata A′ and B in Hole 710A by turbidite A.

Carbonate turbidites are a common feature found throughout Unit IA. We can easily recognize these turbidites because they are white (10YR 8/2, 9/2) and are nearly pure calcium carbonate. They have sharp, erosional basal contacts and gradational upper contacts, and they are often size graded. We recognized 10 turbidites throughout this interval at Hole 710A and observed nine at Hole 710B. The turbidites are classified as foraminifer-nannofossil oozes. One of these turbidites is pictured in Figure 6.

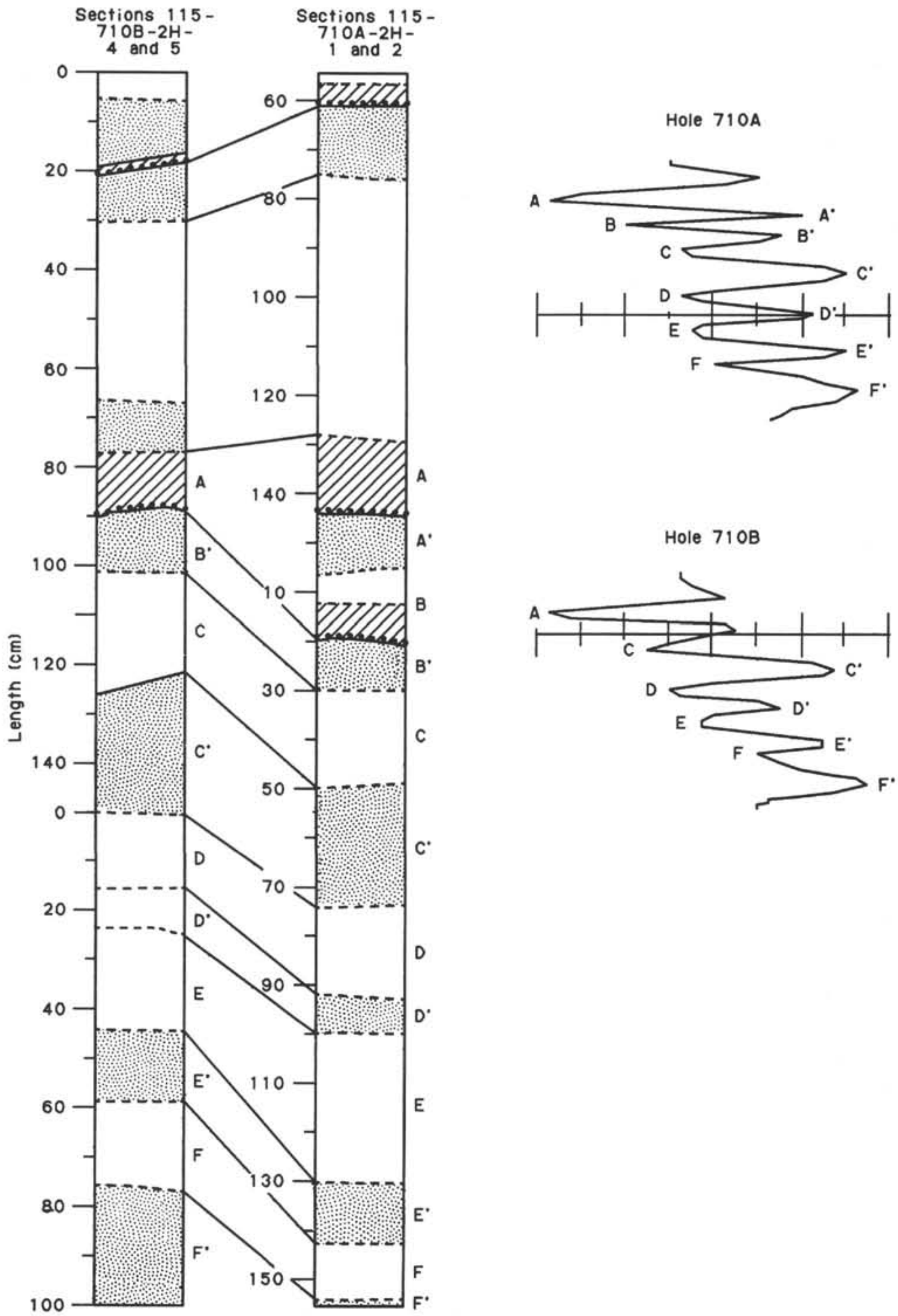

Figure 5. Example of correlation (left) between the same lithologic intervals in Holes 710A and 710B (Sections 115-710B-2H-4 and -5; Sections 115-710A-2H-1 and -2). Also shown (right) are the magnetic susceptibility data (see "Paleomagnetics" section, this chapter) from part of the same interval. Correlative units are labeled. Stippled patterns represent slightly darker, clay-rich beds; diagonal lines represent turbidites.

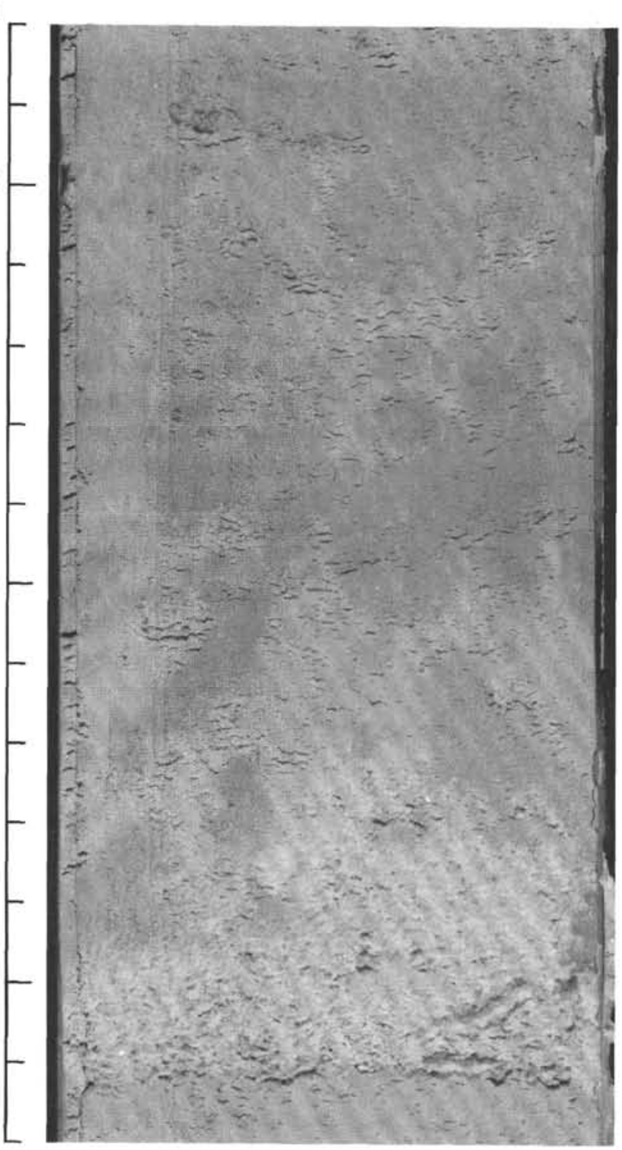

Figure 6. A typical foraminifer nannofossil ooze turbidite (115-710A-4H-2, 33–47 cm).

Unit IA changes gradationally downward over the course of Section 115-710B-6H-2 into a white (5Y 8/1, 5G 8/1) to light-gray colored (10YR 7/2), pyrite-stained, clay-bearing nannofossil ooze. The distinction between Units IA and IB is presumed to be dependent upon the oxidation state of the sediments: sediments in Unit IB have undergone microbial sulfate reduction, dissolution of iron-oxyhydroxide phases, and the precipitation of pyrite. Otherwise, the sediment in Unit IB is similar in composition to the overlying sediment.

Unit II: Sections 115-710A-8H-2, 47 cm, to 115-710A-14X, CC (69.1–132.4 mbsf), and Core 115-710B-9H (73.8–83.4 mbsf); Age: late Miocene to early Miocene.

Unit II consists predominantly of clay-bearing nannofossil ooze with subordinate amounts of clay-nannofossil ooze and radiolarian-bearing, nannofossil clay. With the exception of two short intervals, we can infer that Unit II is entirely oxidized because of its yellowish-brown colors: white (10YR 8/2), very pale brown (10YR 7/3, 7/4), pale yellow (2.5Y 7/4), light yellowish brown (2.5Y 6/4, 10YR 6/4), and yellowish brown (10YR 5/4). Color changes due to variable amounts of clay (or carbonate), are common again and average about 30 per core throughout this interval. Overall, the carbonate content varies from lows of about 30% to high values (exclusive of turbidites) of about 75%. Foraminifers are rare in these sediments, with smear slides containing from 0% to 3%. Biogenic silica in the form of radiolarians and sponge spicules varies from 0% to 15%. Mottling due to bioturbation is also common in this unit.

Carbonate turbidites are more abundant in Unit II than in either the overlying or underlying sediments. We observed about 20 turbidites in this interval in Hole 710A. The turbidites, as observed in Unit IA, are carbonate-rich, foraminifer-nannofossil oozes and have sharp erosional basal contacts, with gradational, bioturbated upper contacts. An example is shown in Figure 7.

Two short intervals of Unit II are apparently microbially reduced: 115-710A-8H-4, 75 cm, to 115-710A-8H-5, 110 cm, and 115-710A-9H-6, 86 cm, to 115-710A-10H-1, 49 cm. The occurrence of sulfate reduction in these sediments, but not elsewhere in Unit II, is in accord with high sedimentation rates and, hence, rapid burial. This interpretation, at least in the first interval, is consistent with paleontological evidence (see "Biostratigraphy" section, this chapter), which suggests that the sediments above Section 115-710A-8H-4, 75 cm, are older than the sediments shortly below this sample. We have interpreted the overlying 3.3 m of sediment as a slump. Sedimentological evidence in favor of this view includes the distinctive color, sharp nonhorizontal top and bottom contacts, the lack of internal color changes otherwise numerous in surrounding sediments, and the overall homogeneity of the sedimentary texture.

We also observed slumping in Sections 115-710A-10H-5, 60–130 cm, and 115-710A-10H-6, 25–102 cm, and in Sections 115-710A-11H-3, 130 cm, to 115-710A-11H-4, 70 cm. In the first of these three intervals, the slumped material was originally a turbidite composed of foraminifer-nannofossil ooze, interbedded with a 3-cm-thick nannofossil clay. This interval was rolled over on itself and then apparently overturned. Directly underlying

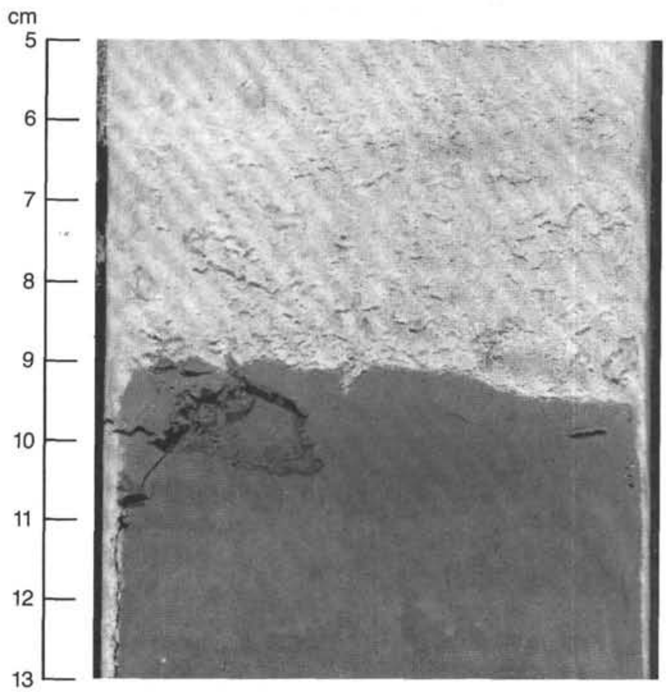

Figure 7. The erosional basal contact of a turbidite (115-710A-10H-5, 5–13 cm).

the slump is a normal microfault with 6 cm of apparent offset (Fig. 8). It is likely that seismic activity produced both the slumping and the microfault. Paleontological evidence also supports slumping in this interval, indicating a 3.0-m.y. hiatus at 90 cm in Section 115-710A-10H-5.

In the last of the three slumped intervals (Sections 115-710A-11H-3 and 115-710A-11H-4), a folded, gray, altered-ash layer reveals contorted bedding (Fig. 9). In this case, the slumped sediment is clayey nannofossil ooze. Paleontological evidence (see "Biostratigraphy" section, this chapter) suggests that downslope transport of well-preserved nannofossils may have taken place within this interval.

Unit III: Sections 115-710A-15X-1 to 115-710A-22X, CC (132.4-209.7 mbsf); Age: early Miocene to early Oligocene.

Near the break between Cores 115-710A-14X and 115-710A-15X, the sediments become more carbonate rich and somewhat

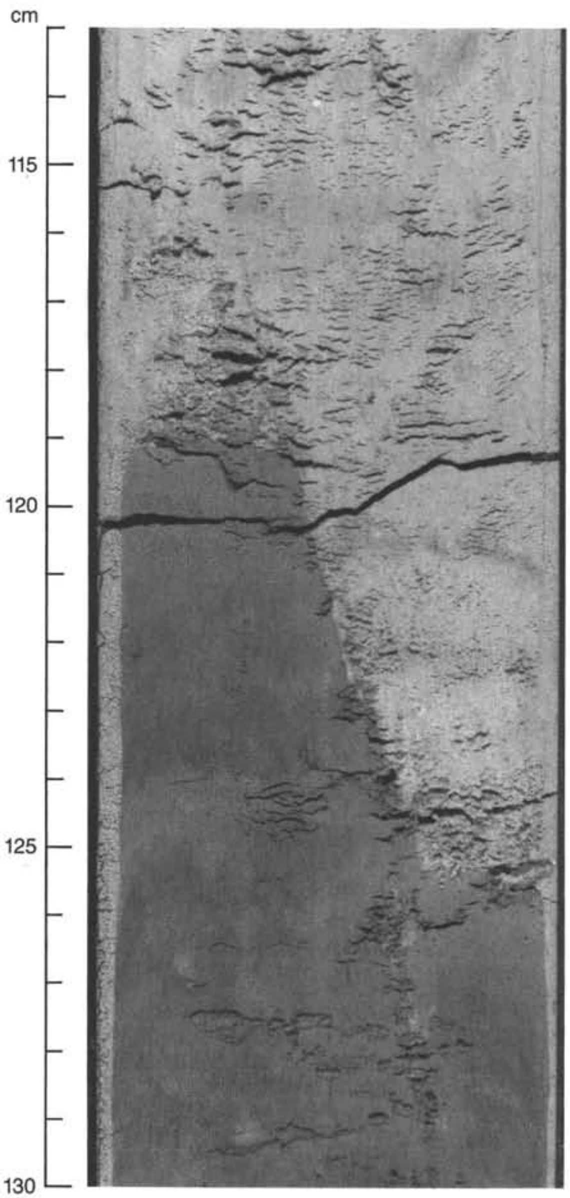

Figure 8. Normal microfault at the base of a slumped interval (115-710A-10H-5, 113–130 cm).

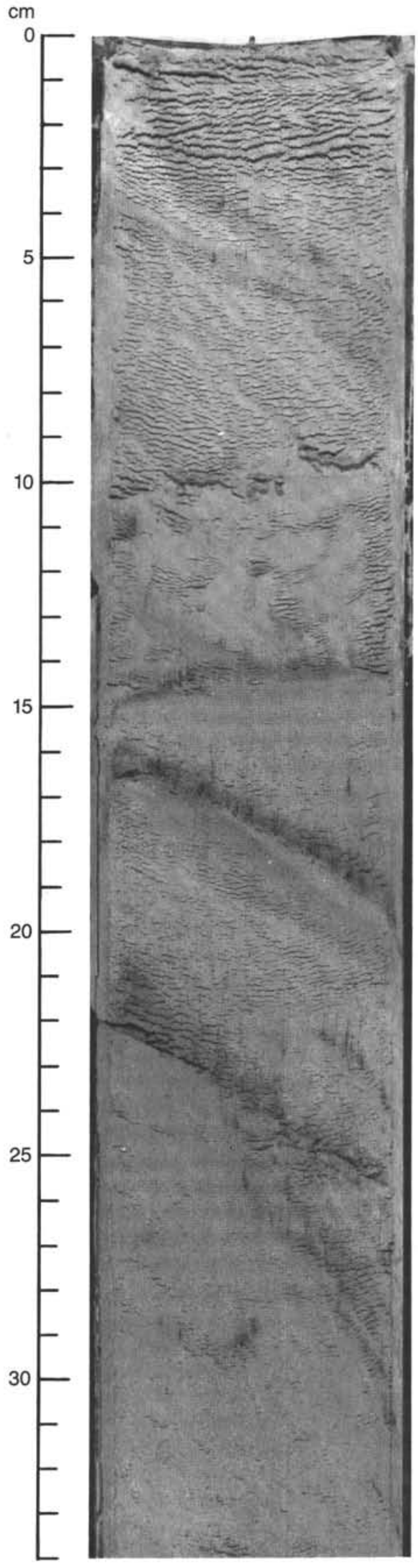

Figure 9. Contorted bedding within a slumped interval, revealed by pyritic staining of a possible altered-ash layer (115-710A-11H-4, 0–34 cm).

lithified. Sediments of Unit III are described as nannofossil oozes and nannofossil chalks. They average about 90% calcium carbonate and are either white (10YR 8/2, N9), light gray (109YR 7/2), or very pale brown (10YR 8/3). These colors imply oxidizing conditions of diagenesis. There are no recognizable turbidites throughout this entire unit and an average of only about three color changes per core. Foraminifers are a minor component of these sediments, forming about 2% of the total sediment. There is essentially no biogenic silica in Cores 115-710A-15X through 115-710A-19X, but in deeper cores radiolarians and sponge spicules make up to 3% of the total lithologies.

Figure 10 illustrates the distribution of lithologic units in Holes 710A and 710B.

BIOSTRATIGRAPHY

Introduction

The 209.7-m-thick sedimentary sequence penetrated by two holes at Site 710 consists of (1) approximately 20 m of Pleistocene to upper Pliocene nannofossil ooze; (2) a minor unconformity in the upper Pliocene equivalent to a time interval of about 0.7 m.y.; and (3) a 190-m-thick, continuous sequence of upper Pliocene through lower Oligocene nannofossil ooze and chalk.

Calcareous nannofossils are generally abundant throughout the section, with significant variation in their state of preservation. The upper Neogene assemblages are strongly affected by dissolution, whereas those from the lower Miocene and Oligocene have better preservation.

Planktonic foraminifers are abundant and moderately well preserved in the Pleistocene, abundant and poorly preserved in the upper Pliocene, and severely dissolved in older sediments. Faunal assemblages consist mainly of a few solution-resistant forms and abundant fragments, preventing a planktonic foraminiferal zonation below the upper Pliocene. Benthic foraminifers occur throughout the dissolved carbonate sequence as dissolution residues.

Radiolarians are common in the Quaternary through upper Miocene interval, being moderately well to well preserved. They are absent in the middle and lower Miocene and are sparse and generally poorly preserved in the Oligocene.

Diatoms are restricted to the interval from the Pleistocene through the uppermost Miocene. They are common to abundant and fairly well preserved in the Pleistocene section. As preservation worsens downcore, the abundance decreases, and no diatoms are preserved in the lower Neogene and Oligocene.

The good paleomagnetic record obtained in both Holes 710A and 710B down to the lower Miocene allows a direct calibration of calcareous nannofossil datums with magnetostratigraphy through most of the Neogene, and of siliceous microfossil datums with magnetostratigraphy for the upper Miocene through Pleistocene interval.

A biostratigraphic summary for Site 710 is presented in Figure 11.

Calcareous Nannofossils

Hole 710A penetrated a 209.7-m-thick sedimentary sequence of early Oligocene to Pleistocene age. Calcareous nannofossils are generally abundant, but their preservational state is variable. In many samples of the Neogene sequence, placoliths are etched and often almost totally dissolved, while the discoasters are generally remarkably well preserved and show little sign of overgrowth. In the Miocene, however, dissolved assemblages often alternate with assemblages in which discoasters are overgrown and the placoliths are well preserved. These latter assemblages are found within probable redeposited sediments. In the lowermost Miocene and in the Oligocene, the preservation is

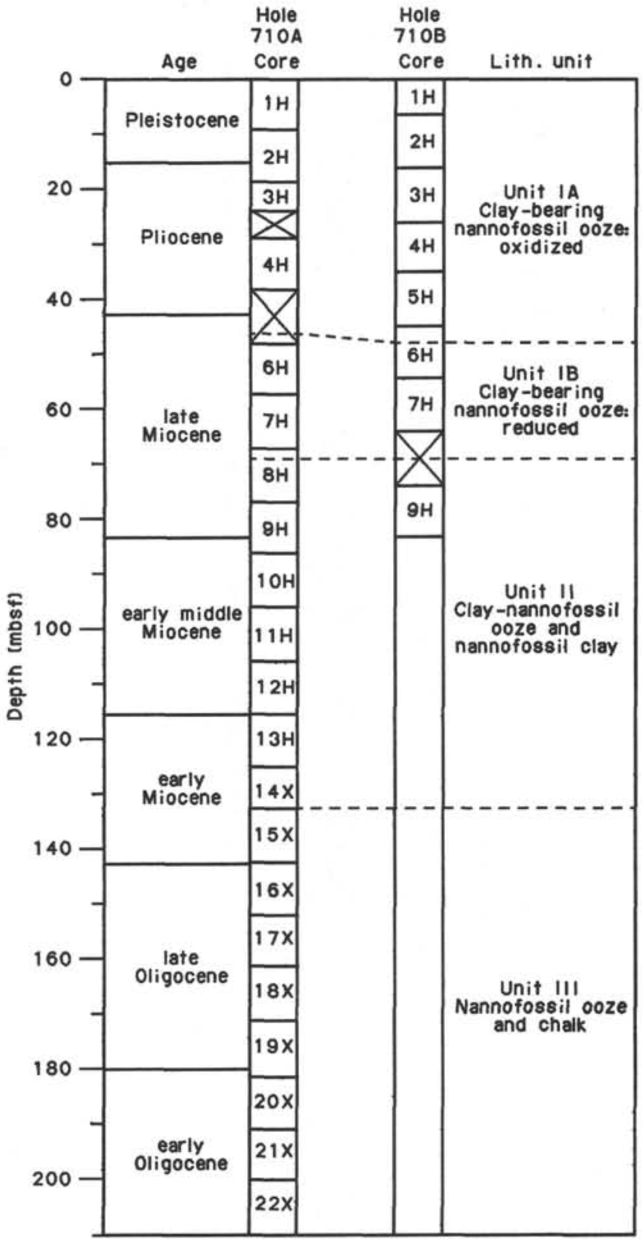

Figure 10. Summary lithologic diagram for Holes 710A and 710B.

generally good, even though the discoasters show evidence of overgrowth.

Preliminary analysis of the calcareous nannofossils of Hole 710A indicates that the Miocene sequence is affected by episodes of sediment redeposition. Redeposition is indicated not only by the above-mentioned contrasts in preservation, but also by the presence of at least one anomalous superposition of biozones in the upper Miocene.

The nine cores of Hole 710B were supposed to recover an identical sequence to that retrieved in the upper nine cores of Hole 710A. An examination of section samples, however, revealed a duplicated coring of the Pleistocene sequence at Hole 710B. We will discuss this finding in the following section.

Pleistocene

We observed a Pleistocene assemblage in the top 15 m of sediments at Hole 710A and in the top 25.5 m of sediments at Hole

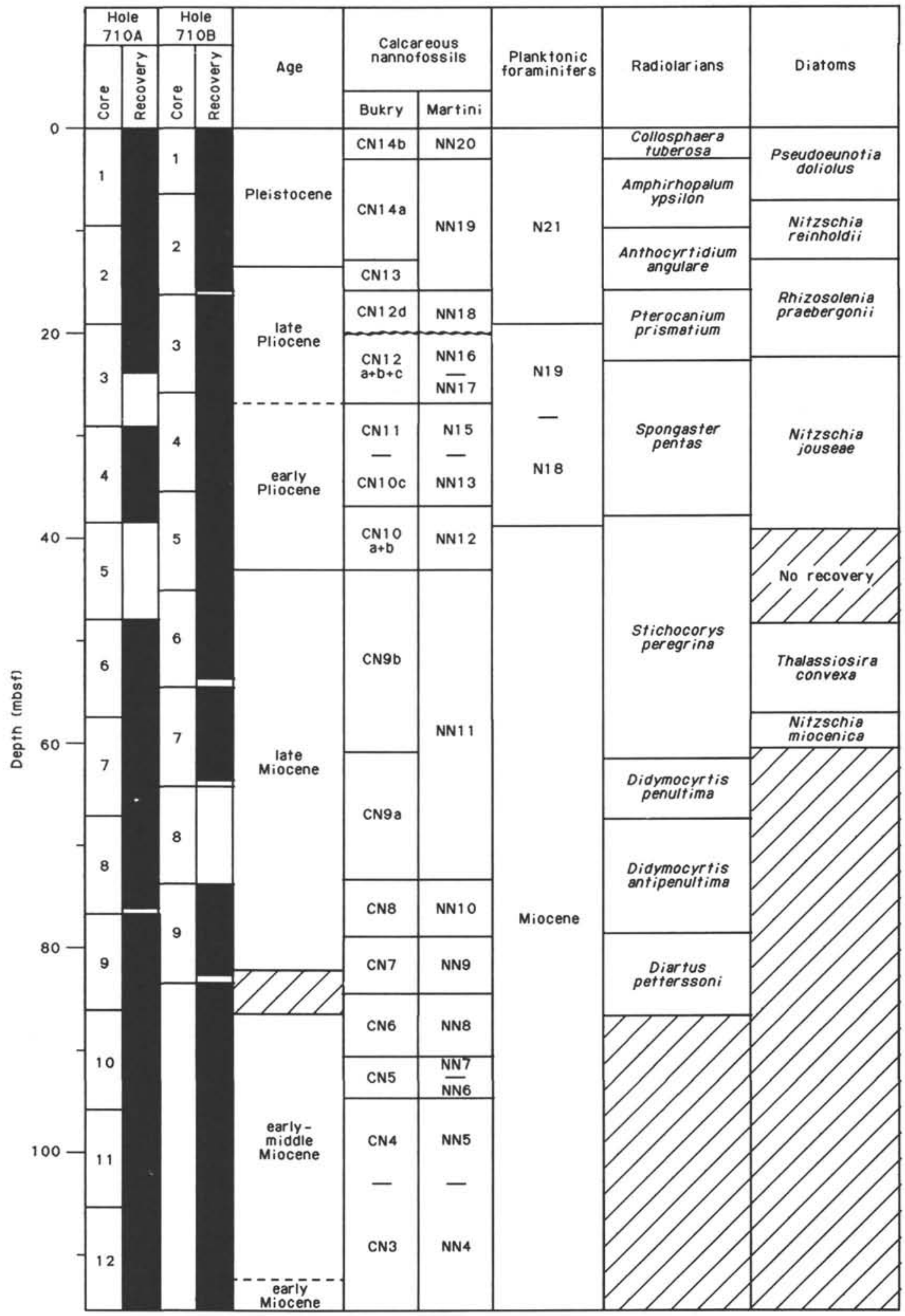

Figure 11. Biostratigraphic summary for Site 710. Black bars represent recovery in Holes 710A and 710B.

710B. Closely spaced samples were examined for the entire Quaternary sequence in both holes, and the results obtained are summarized below.

Nannoflora assignable to the uppermost Quaternary Zone CN15 were observed throughout Section 115-710B-1H-1. *Emiliania huxleyi*, the marker species of Zone CN15, is completely missing from Sample 115-710A-1H-1, 43–44 cm. Thus, the presence of Zone CN15 is not clear for the recovered sediment of Hole 710A.

We recognized the last occurrence (LO) of *Pseudoemiliania lacunosa* (base of Subzone CN14b) in Sample 115-710A-1H-3, 10 cm, and the top of the small *Gephyrocapsa* Zone can be

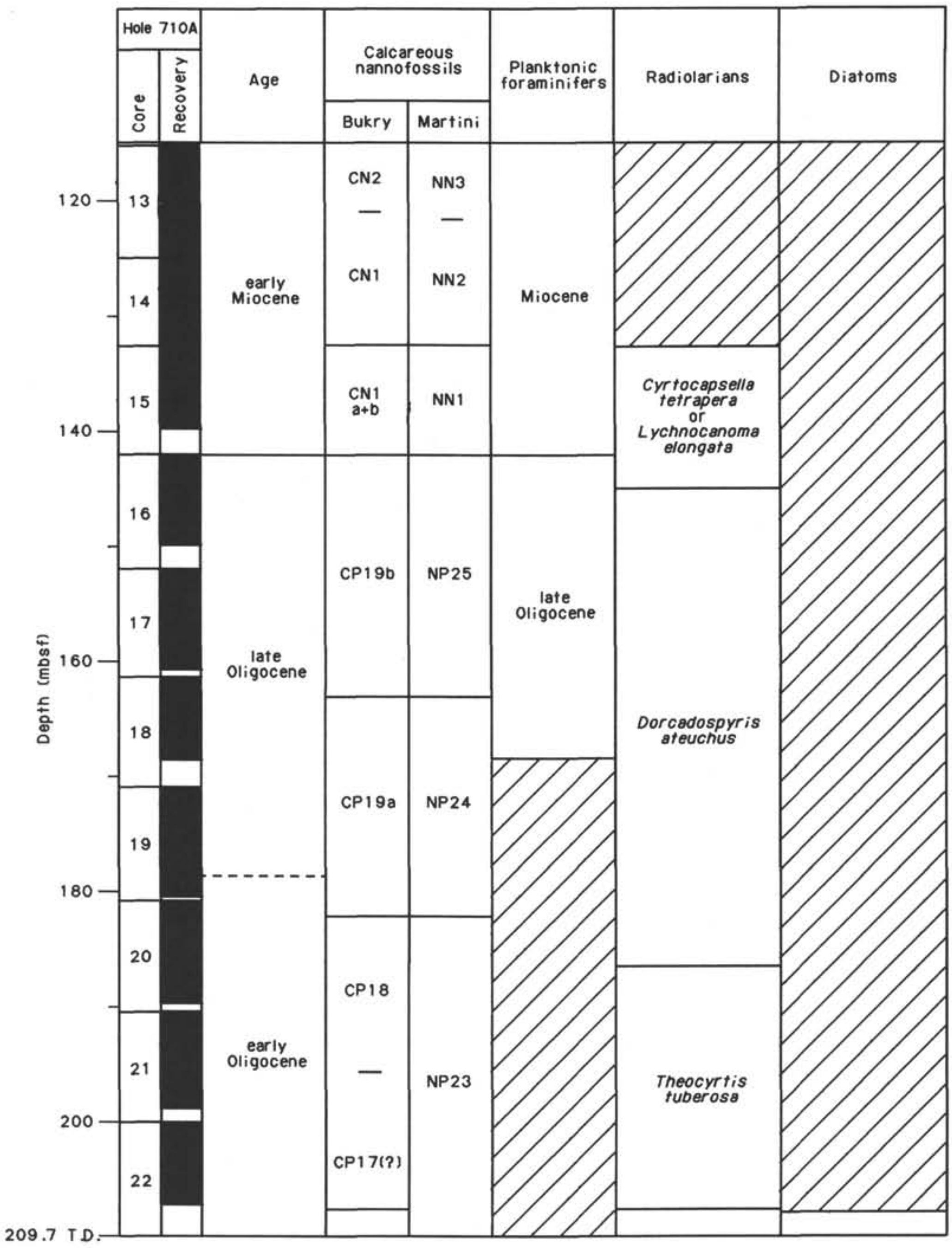

Figure 11 (continued).

placed at Sample 115-710A-1H-6, 120 cm. *Helicosphaera sellii* and *Calcidiscus macintyrei* are absent in Sample 115-710A-2H-3, 43–44 cm, but they coexist in Sample 115-710A-2H-4, 43–44 cm. We also observed the first occurrence (FO) of *Gephyrocapsa oceanica* (base of CN14a) in this sample. The Pliocene-Pleistocene boundary is likely located between Samples 115-710A-2H-4, 43–44 cm, and 115-710A-2H-5, 43–44 cm, in which *Discoaster brouweri* was not observed.

For Hole 115-710B, the LO of *P. lacunosa* was recognized in Sample 115-710B-1H-4, 90 cm. We identified the small *Gephyrocapsa* Zone between Samples 115-710B-2H-2, 150 cm, and 115-710B-2H-3, 150 cm, and detected the LOs of *H. sellii* and *C. macintyrei* in Samples 115-710B-2H-5, 70 cm, and 115-710B-2H-6, 40 cm, respectively. We placed the FO of *G. oceanica* between Sample 115-710B-2H-6, 120 cm, and Sample 115-710B-2H-6, 140 cm.

We assigned the short interval between Sample 115-710B-2H-6, 140 cm, and Section 115-710B-2H, CC, to Zone CN13. Thus, the upper two cores of Hole 710B recovered a complete sequence of Pleistocene sediment. The underlying Core 115-710B-3H, however, again recovered the succession of upper Pleistocene nannoflora observed in the lower half of Core 115-710B-1H through the upper half of Core 115-710B-2H.

Pliocene

Ceratolithus acutus is present in Section 115-710A-4H, CC, and *Discoaster quinqueramus* was observed in the core catcher of underlying Core 115-710A-5H. The Miocene/Pliocene boundary, therefore, is likely to be located within the empty Core 115-710A-5H. We located the boundary between the lower and the upper Pliocene between Section 115-710A-3H, CC, and Sample 115-710A-4H-1, 31 cm, where we detected the last *Reticulofenestra pseudoumbilica* and *Sphenolithus abies* specimens. The Pliocene sequence is estimated to be approximately 25 m thick.

We recognized the LOs of *Discoaster brouweri*, *D. pentaradiatus*, and *D. surculus* in Samples 115-710A-2H-7, 30 cm, 115-710A-3H-1, 90 cm, and 115-710A-3H-1, 30 cm, respectively. *Discoaster tamalis* is rare, and its last occurrence has not been monitored. The short spacing between the LO of *D. brouweri* and *D. pentaradiatus* (separated from each other in time by about 0.5 m.y.) indicates that some sediments may have been lost between Cores 115-710A-2H and 115-710A-3H. We recovered specimens from the lower Pliocene only in Core 115-710A-4H, which we therefore assigned to the CN10c–CN11 zonal interval because *Ceratolithus rugosus* (together with *C. acutus)* is present from the very base of the core.

Miocene

We located the Oligocene-Miocene boundary in Sample 115-710A-16X-1, 30 cm, on the basis of the LO of *Sphenolithus ciperoensis.* The Miocene epoch is therefore represented by about 100 m of sediments in Hole 710A. As noted in Sites 707, 708, and 709, the sediment accumulation rates are different in each series and are particularly high in the late Miocene.

The base of upper Miocene Zone CN9 was recorded in Sample 115-710A-8H-4, 90 cm. Zone CN9, whose duration is estimated to be about 3.2 m.y., is therefore more than 25 m thick. However, in this time interval there is strong evidence of slumping of older material. At the top of Section 115-710A-8H-4, an oblique contact is present between brown clays and white nannofossil ooze. A sample collected in the brown clays (115-710A-8H-4, 75 cm) yielded a nannofossil assemblage indicative of Zone CN7b, while a sample collected in the underlying white ooze (115-710A-8H-4, 79 cm) yielded a nannofossil assemblage indicative of Zone CN9a. We need to perform detailed micropaleontologic and sedimentologic analyses in order to ascertain the full extent of the slumped material in this as well as in underlying intervals.

Upper Miocene Zone CN8 (NN10) is located between Samples 115-710A-8H-4, 130 cm, and 115-710A-9H-2, 90 cm. We detected Zone CN7, which straddles the middle upper Miocene boundary, between Samples 115-710A-9H-2, 90 cm, and 115-710A-9H-5, 90 cm. We recognized middle Miocene Zone CN6 (NN8) between Samples 115-710A-9H-6, 30 cm, and 115-710A-10H-3, 90 cm. The LO of *Sphenolithus heteromorphus* occurs in Sample 115-710A-10H-6, 90 cm. The CN5 interval, therefore, is represented by approximately 4 m of sediments in the lower part of Core 115-710A-10H.

We did not differentiate Zones CN4 (middle Miocene) and CN3 (straddling the lower middle Miocene boundary). The base of Zone CN3 was recognized in Sample 115-710A-12H-6, 90 cm, where the FO of *S. heteromorphus* was detected. In the middle and upper lower Miocene sequence of Cores 115-710A-11H and 115-710A-12H, samples which show strong evidence of dissolution alternate with others in which the preservation is better and discoasters are overgrown. Those samples with dissolved assemblages probably represent the *in-situ* pelagic sediments, while the samples with better preservation are derived from sediments redeposited from shallower water sites.

Sphenolithus belemnos, whose FO defines the base of Zone CN2, was recorded only in Section 115-710A-12, CC. In the underlying sample (115-710A-13H-1, 30 cm), *S. belemnos* is missing, while *Triquetrorhabdulus carinatus* (indicative of Zone CN1) is present. The interval between the latter sample and Section 115-710A-14X, CC, has been assigned to Zone CN1c (NN2) on the basis of the co-occurrence of *T. carinatus* and *Discoaster druggii*. Because *T. carinatus* and *Sphenolithus delphix* are both present and *D. druggii* is absent, we assigned Core 115-710A-15H to Subzones CN1a–CN1b (NN1).

Oligocene

The interval from Section 115-710A-16X-1 (142 mbsf) to the bottom of the hole (209.7 mbsf) yielded abundant Oligocene nannofossil assemblages whose preservational state was generally good. The LO of *Sphenolithus distentus* (base of Subzone CP19b) was placed between Samples 115-710A-18X-1, 43–44 cm, and 115-710A-18X-2, 43–44 cm. The FO of *Sphenolithus ciperoensis* (base of Subzone CP19a) occurs between Samples 115-710A-20X-1, 43–44 cm, and 115-710A-20X-1, 130 cm.

As in Sites 707 and 709, the FO of *Sphenolithus distentus* was again difficult to locate. We found *S. distentus* occurring continuously above Section 115-710A-21X-2, but it was absent in the lower five sections of Core 115-710A-21X. In the upper three sections of Core 115-710A-22X, however, we again observed a few specimens of forms which resemble *S. distentus.* This sphenolith is absent, and we recognized neither *Reticulofenestra umbilica* nor *Ericsonia formosa* in the lower half of Core 115-710A-22X. Therefore, we assigned the lower half of the deepest core to Zone CP17. Considering the controversial occurrence of *S. distentus* in Sites 707 and 709, however, the entire interval ranging from Section 115-710A-20X-1 to the bottom of the hole is tentatively assigned to Zones CP18–CP17.

Planktonic Foraminifers

Neogene

Planktonic foraminifers are abundant and moderately well preserved in Section 115-710A-1H, CC. They are also abundant in Section 115-710A-2H, CC, but poorly preserved with a high degree of fragmentation. From Section 115-710A-3H, CC, down to the base of the Neogene sequence, preservation deteriorates. As dissolution progresses, fewer whole planktonic foraminifers are found, whereas foraminiferal fragments are abundant and dominate the residues.

Sections 115-710A-1H, CC, and 115-710A-2H, CC, are assigned to upper Pliocene Zone N21 based on the presence of *Globorotalia tosaensis* and *G. limbata*. The LO of the latter species occurs in the upper Pliocene at the previous sites, indicating a late Pliocene age for Section 115-710A-1H, CC, even though nannofossil data indicate a younger age (Pleistocene at this level). Section 115-710A-2H, CC, contains rare *Globigerinoides fistulosus*, indicating an age younger than 2.9 Ma. The faunal assemblage in Sections 115-710A-1H, CC, and 115-710A-2H, CC, is dominated by abundant *Globorotalia tumida* (whole and fragmented specimens), *G. limbata*, *Neogloboquadrina dutertrei*, and *Globigerinoides sacculifer*.

From Section 115-710A-3H, CC, down, whole planktonic foraminifers are less common whereas fragments are abundant. Only a few solution-resistant forms are found. We attributed Sections 115-710A-3H, CC, and 115-710A-4H, CC, to the lower Pliocene (zonal interval N20–N19 to N18) on the basis of the co-occurrence of *G. tumida* and *Sphaeroidinellopsis subdehiscens*. *Globoquadrina altispira* are rare in Section 115-710A-4H, CC. There was no recovery from Core 115-710A-5H.

In Sections 115-710A-6H, CC, through 115-710A-9H, CC, residues are almost entirely made up of foraminiferal fragments, common radiolarians, and rare sponge spicules. The fauna consists of only a few resistant forms, including rare *Sphaeroidinellopsis* and *Globoquadrina venezuelana*; no zonal assignment is possible. Nannofossil data indicate a late Miocene age for that interval, in agreement with the absence of *G. tumida* (a Pliocene-Pleistocene species). A few specimens of encrusted *Globo-*

rotalia plesiotumida were found in Section 115-710A-7H, CC. Rare *Globigerina nepenthes* occur in Sections 115-710A-8H, CC, and 115-710A-9H, CC.

Sections 115-710A-10H, CC, through 115-710A-15X, CC, are assigned to the middle to lower Miocene on the basis of nannofossil data. No planktonic foraminiferal zonation is possible in this interval due to the rarity of planktonic foraminifers. The residue greater than 63 μm is very small and consists essentially of foraminiferal fragments, rare benthic foraminifers, fish teeth, echinoid spines, glass debris, sponge spicules, and radiolarians. The last three components are abundant in the lowest section (115-710A-15X, CC).

Paleogene

A dissolution residue assemblage of Oligocene-age planktonic foraminifers occurs in Sections 115-710A-16X, CC, through 115-710A-18X, CC; only a few fragments of planktonic foraminifers are found at the bottom of the hole (Sections 115-710A-19X, CC, to 115-710A-22X, CC). The faunas, consisting of only a few resistant species, are diagnostic of the later Oligocene in general, but we could determine few zones. Species present include the *Globoquadrina tripartita* group, *G. sellii*, *Catapsydrax unicavus*, *C. dissimilis*, and *Paragloborotalia nana*. Sample 115-710A-21X-3, 38 cm, can be attributed to Zone P20, probably the later portion. Sample 115-710A-22X-3, 38 cm, also belongs to Zone P20.

Benthic Foraminifers

Benthic foraminifers at Site 710 exist as dissolution residues in the moderately to heavily dissolved carbonates which occur throughout the sequence. In general, these residue faunas contain only a few species of few genera; that is, diversity and dominance are both low. In most residues, the benthic foraminifers are small in size, as the larger specimens have been removed by dissolution. In only a few samples (for example, Section 115-710A-8H, CC) are the benthic foraminifers actually concentrated by dissolution of the planktonic foraminifers.

As dissolution progresses, fewer genera are found in the residues. The order of appearance as a function of improving preservation from almost no benthic foraminifers at the foraminiferal CCD is as follows:

1. *Oridorsalis umbonatus*; gyroidinids; pullenids; *Globocassidulina subglobosa*; miliolids, especially *Pyrgo* and *Triloculina*; *Nuttalides umbonifera*; and *Epistominella exigua*.
2. Stilostomellids, usually smooth forms of *Stilostomella lepidula* or *S. abyssorum*, and the very large species *S. insecta* and *S. nuttalli*; favocassidulinids; nonalate fissurinids; unornamented planulinids, such as *P. wuellerstorfi*; and agglutinated benthic foraminifers with very fine particles, such as *Eggerella bradyi*.
3. Large, striate *Chrysalogonium* spp.; melonids, especially the smooth, poreless species such as *Melonis pacificum* or the poreless morph of *M. barleeanum*; the smooth buliminid, *Buliminella grata*, and its Neogene derivative, *Laticarinina* (with a megalospheric proloculus); deep-water, unornamented cibicidids, including *Cibicides kullenbergi* and *C. havanensis*; the smooth anomalinids; and the finely particulate vulvulinids, especially the spiroplectaminid morph.

Pleistocene dissolution residues (Sections 115-710A-1H, CC, to 115-710A-2H, CC) differ from those below because of the predominance of very small forms, including *G. subglobosa*, *E. exigua*, and *N. umbonifera*, as well as the greater abundance of the last two species. They are about equally abundant at this site.

Despite dissolution, the uppermost Miocene faunas are slightly different and can be compared with the better preserved, deep-water faunas at Site 709. That is, we could recognize a dissolution residue containing elements of the tropical, intermediate-water, Car Nicobar fauna found at Site 709 in Section 115-710A-6H, CC, by the large size of the individuals, the greater diversity of the fauna, the presence of numerous striate nodosarid and chrysalogonium fragments, and the characteristic species or morphs of that fauna. Because nannofossils indicate redeposition through this interval, it is not clear whether this better preserved fauna is in place.

Oligocene dissolution residues contain the same genera and phenotypes, but species are different in the Oligocene. Even large striate fragments of *Chrysalogonium* occur in the Oligocene residues. One exception involves the thick-walled heterolepid, *Heterolepa grimsdalei*, which occurs in all but the most strongly dissolved samples. Its Neogene counterpart, *H. dohmi*, does not appear at this site.

All but one fauna appear to be in place and to represent abyssal depths.

Radiolarians

Radiolarians are common and moderately to well preserved in the Quaternary through upper Miocene interval at Site 710. In the middle and lower Miocene interval, radiolarians are absent entirely. In the Oligocene, the radiolarian assemblages are sparse and generally poorly preserved, allowing only an approximate zonal age determination. The lowermost material recovered at Site 710 is of early Oligocene age, corresponding to the *Theocyrtis tuberosa* Zone.

Quaternary

Sample 115-710A-1H-4, 70 cm, through Section 115-710A-1H, CC, are of early Pleistocene age corresponding to the *Amphirhopalum ypsilon* Zone. Diagnostic taxa include *Stylatractus universus*, *Pterocorys campanula*, *Theocorythium trachelium*, *Anthocyrtidium nigriniae*, and *A. ophirense*. Samples 115-710A-2H-2, 70 cm, through 115-710A-2H-4, 70 cm, are of early Pleistocene age, corresponding to the *Anthocyrtidium angulare* Zone.

Pliocene

Samples 115-710A-2H-6, 70 cm, through 115-710A-3H-2, 70 cm, are of late Pliocene age, corresponding to the *Pterocanium prismatium* Zone. Diagnostic taxa include *P. prismatium*, *Lamprocyrtis neoheteroporus*, *A. michelinae*, *A. zanguebaricum*, *Spongaster tetras*, and *Pterocorys campanula*.

Samples 115-710A-3H-3, 95 cm, through 115-710A-4H-6, 70 cm, are of early Pliocene age, corresponding to the *Spongaster pentas* Zone. Diagnostic taxa include *Stichocorys peregrina*, *Pterocanium prismatium*, *Amphirhopalum ypsilon*, *Spongaster tetras*, *Anthocyrtidium michelinae*, and *A. jenghisi*.

Section 115-710A-4H, CC, through Sample 115-710A-7H-2, 70 cm, belong to the *Stichocorys peregrina* Zone, which spans the Pliocene/Miocene boundary. Diagnostic taxa in this interval include *Phormostichoartus doliolum*, *P. fistula*, *Solenosphaera omnitubus*, *Spongaster berminghami*, *S. peregrina*, and *Lychnodyctium audax*. Taxa are common and well preserved in both these cores.

Miocene

We assigned Sample 115-710A-7H-4, 70 cm, through Section 115-710A-7H, CC, to the *Didymocyrtis penultima* Zone of late Miocene age. Radiolarians are few and moderately well preserved. Diagnostic taxa include *Siphostichartus corona*, *D. penultima*, *Stichocorys delmontensis*, *Anthocyrtidium pliocenica*, and rare specimens of *D. antepenultima*.

Sample 115-710A-8H-2, 70 cm, through Section 115-710A-8H, CC, may be assigned to the *D. antepenultima* Zone of late Miocene age. Radiolarians in this interval are common and well preserved. Diagnostic taxa include *Diartus hughesi*, *D. antepe-*

nultima, *A. pliocenica*, *Dendrospyris bursa*, and *Stichocorys delmontensis*.

We placed Sample 115-710A-9H-2, 70 cm, through Section 115 710A-9H, CC, in the *Diartus petterssoni* Zone, based on common specimens of *D. petterssoni*.

Sections 115-710A-10H, CC, through 115-710A-14X, CC (95.8–132.4 mbsf) are barren of radiolarians. This stratigraphic interval corresponds to the middle and early Miocene.

Section 115-710A-15X, CC, contains rare and poorly preserved radiolarian fragments of earliest Miocene age, probably equivalent to the *Cyrtocapsella tetrapera* Zone or the *Lychnocanoma elongata* Zone. Taxa present include *Calocycletta robusta*, *Dorcadospyris ateuchus*, *D. papilio*, and *Dendrospyris bursa*.

Oligocene

We assigned Sections 115-710A-16X, CC, through 115-710A-19X, CC (151.8–180.8 mbsf) to the *Dorcadospyris ateuchus* Zone of late Oligocene age. Radiolarians are generally rare and poorly to moderately preserved. Diagnostic taxa in this interval include *D. ateuchus*, *D. papilio*, *Theocyrtis annosa*, *Lithocyclia angusta*, and *Theocorys spongoconus*.

Sections 115-710A-20X, CC, through 115-710A-22X, CC (190.4–209.7 mbsf) may be assigned to the *Theocyrtis tuberosa* Zone of early Oligocene age. Radiolarians in this interval are few and moderately well preserved. Diagnostic taxa include *Tristylospyris triceros*, *Artophormis gracilis*, *Lithocyclia angusta*, *L. crux*, *Theocorys spongoconus*, *T. tuberosa*, *Dictyoprora pirum*, and *Dorcadospyris spinosa*.

Diatoms

In the two holes at Site 710, diatoms are restricted to the interval from the Pleistocene through the uppermost part of the upper Miocene. The diatoms are common to abundant and fairly well preserved in the Pleistocene sections. As preservation worsens, diatom abundance decreases in the upper Miocene: no diatom valves are present in the early Neogene and Paleogene sequences of Site 710.

Neogene

A fairly poorly preserved assemblage in Sample 115-710A-1H-5, 101–102 cm, is referred to the late Pleistocene *Pseudoeunotia doliolus* Zone based on the presence of *P. doliolus* and the absence of *Nitzschia reinholdii*.

The diatom assemblages in Section 115-710A-1H, CC, and Sections 115-710B-1H, CC, through 115-710B-3H, CC, are moderate to well preserved, and the diversified assemblages include the age-diagnostic species *P. doliolus*, *Nitzschia fossilis*, and *N. reinholdii*. Also present is the silicoflagellate, *Mesocena quadrangula*, whose stratigraphic range is confined to the upper part of the *N. reinholdii* Zone.

Section 115-710A-2H, CC, is referred to the middle part of the *Rhizosolenia praebergonii* Zone based on the presence of *R. praebergonii* and the rare occurrence of *Thalassiosira convexa* var. *aspinosa*.

Sections 115-710A-3H, CC, 115-710A-4H, CC, and 115-710B-4H, CC, have diversified diatom assemblages, including the age-diagnostic species *Nitzschia jouseae*, *N. reinholdii*, and *Thalassiosira oestrupii*. The lack of *R. praebergonii* places these samples in the *N. jouseae* Zone.

No core-catcher material was available from Core 115-710A-5H. The diatom flora of Section 115-710B-5H, CC, is diversified and includes *T. convexa* var. *aspinosa* and *Nitzschia cylindrica*, thus locating the sample in the middle part of the *T. convexa* Zone. In Sample 115-710A-6H-5, 47–48 cm, and Section 115-710B-6H, CC, the presence of *Nitzschia miocenica* places the sample in the lower part of the *T. convexa* Zone.

The assemblage of Section 115-710A-6H, CC, which is affected by silica dissolution, contains *N. reinholdii* and *N. cylindrica*, but lacks *T. convexa* var. *aspinosa*. The sample is tentatively placed in the lower part of the *N. miocenica* Zone.

No diatoms are found in the lower Neogene sections of Site 710.

PALEOMAGNETICS

Introduction

Paleomagnetic measurements of the sediments from Site 710 provide magnetostratigraphic data from most of the APC cores recovered. Problems with the orienting device (see "Paleomagnetics" section, "Explanatory Notes" chapter, this volume) and with the core-barrel remagnetization effect (see "Paleomagnetics" section, "Site 709" chapter, this volume) complicate the interpretation. However, the results appear to give a reliable magnetostratigraphy through much of this Neogene section.

Results

We measured 18 APC cores recovered from Holes 710A and 710B with the pass-through cryogenic magnetometer system before and after 5-mT demagnetization treatment. In addition, we subjected at least one discrete sample from each section to progressive alternating-field (AF) demagnetization. Our analysis of the APC cores collected at Site 710 gave the location of 79 reversal boundaries in Holes 710A and 710B (Table 2). Records of magnetic declination along with a preliminary interpretation of polarity stratigraphy are shown in Figure 12. For the most part, 180° shifts in declination have been indicated as magnetozone boundaries; however, many shifts appear to be spurious and have not been interpreted as polarity reversals. In general, the inclination shifts at reversal boundaries are not well defined in the pass-through records because the small changes at this low-latitude site are usually obscured by remagnetization effects. An analysis of discrete samples, however, often gives the polarity sense more clearly.

Discussion

In general, the paleomagnetic data generated at this site appear reliable, and we can make a reasonable correlation with the magnetic polarity time scale on the basis of the available biostratigraphic data (see "Biostratigraphy" section, this chapter). Good biostratigraphic control insures that the interpretation of the magnetostratigraphy is largely correct, although there may be errors in some of the more detailed correlations shown in Table 2.

The importance of having confirmatory biostratigraphic data is exemplified by the interpretation made for the upper sections of Hole 710B. The normal polarity zone just above 20 mbsf might appear to correspond to the Olduvai subchronozone as found in Hole 710A. However, it is much more likely that this zone represents the lower Brunhes, given the evidence for recoring of the same sequence (see "Biostratigraphy" section, this chapter, as well as the discussion in "Magnetic Susceptibility" below).

The declination record shown in Figure 12 shows many shifts which probably do not correspond to polarity reversals. These include the obvious shifts in declination at the breaks between cores as well as less obvious effects. For example, side lobes in the pass-through magnetometer's horizontal response functions will cause the measured declination to reverse in a thin zone of relatively low intensity. Also, slumped zones like the one identified in Core 115-710A-10H (see "Lithostratigraphy" section, this chapter) or areas of pervasive core-barrel remagnetization will show erratic declination changes. Consideration of all the

Table 2. Magnetic polarity reversal boundaries identified in APC cores from Site 710.

Section interval (cm)	Depth (mbsf)	Sense	Chron	Age (Ma)
115-710A-				
1H-5, 50	6.5	R-N	Brunhes/Matuyama	0.73
2H-4, 140	15.4	N-R	Olduvai (T)	1.66
3H-1, 90	20.1	N-R	Matuyama/Gauss	2.47
4H-1, 110	29.9	R-N	Cochiti (O)	3.97
4H-2, 100	31.3	N-R	? (spurious?)	
4H-4, 1	33.3	N-R	Nunivak (T)	4.10
4H-4, 90	34.2	R-N	Nunivak (O)	4.24
4H-5, 110	35.9	N-R	Sidufjall (T)	4.40
4H-6, 70	37.0	R-N	Sidufjall (O)	4.47
4H-7, 1	37.8	N-R	Thvera (T)	4.57
6H-2, 30	49.7	N-R	C3AN2 (T)	5.68
6H-4, 20	52.6	R-N	C3AN2 (0)	5.89
7H-2, 130	60.3	N-R	C4N1 (T)	6.70
7H-3, 110	61.6	R-N	C4N1 (0)	6.78
7H-4, 10	62.1	N-R	C4N2 (T)	6.85
7H-6, 120	66.2	R-N	C4N3 (0)	7.41
8H-5, 110	74.2	N-R	C4AN1 (T)	7.90
8H-6, 1	74.6	R-N	?	
8H-6, 20	74.8	N-R	?	
9H-1, 70	77.3	N-R	C4AN2 (T)	8.41
9H-2, 1	78.1	R-N	C4AN2 (O)	8.50
9H-2, 120	79.3	N-R	C4AN3 (T)	8.71
9H-3, 10	79.7	R-N	C4AN3 (O)	8.80
9H-3, 40	80.0	N-R	C5N1 (T)	8.92
9H-6, 60	84.7	R-N	C5N1 or N2 (O)	
11H-2, 120	98.5	R-N	C5ACN (O)	14.08
11H-3, 30	99.1	N-R	C5ADN (T)	14.20
11H-5, 50	102.3	R-N	C5ADN (O)	14.66
11H-7, 1	104.8	N-R	C5BN1 (T) ?	14.87
11H-7, 40	105.2	R-N	C5BN1 (O) ?	14.96
12H-3, 120	109.7	N-R	C5CN1 (T)	16.22
12H-5, 20	111.7	R-N	C5CN3 (O)	16.98
12H-5, 130	112.8	N-R	C5DN1 (T)	17.57
12H-6, 30	113.3	R-N	C5DN1 or N2 (O)	
12H-7, 20	114.7	N-R	C5EN (T) ?	18.56
13H-1, 50	115.7	N-R	C6N (T)	19.35
13H-3, 30	118.5	R-N	C6N (O)	20.45
13H-3, 140	119.6	N-R	C6AN1 (T)	20.88
13H-4, 30	120.0	R-N	C6AN1 (O)	21.16
13H-4, 90	120.6	N-R	C6AN2 (T)	21.38
13H-5, 50	121.7	R-N	C6AN2 (O)	21.71
13H-6, 10	122.8	N-R	C6AAN1 (T) ?	21.90
13H-6, 40	123.1	R-N	C6AAN1 (O) ?	22.06
13H-7, 20	124.4	N-R	C6AAN2 (T) ?	22.25
13H-7, 50	124.7	R-N	C6AAN2 (O) ?	22.35
115-710B-				
2H-1, 120	7.7	R-N	Brunhes/Matuyama	0.73
3H-3, 80	20.0	R-N	Brunhes/Matuyama	0.73
4H-1, 20	26.0	N-R	Kaena (O)	2.99
4H-1, 40	26.2	R-N	Mammoth (T)	3.08
4H-1, 90	26.7	N-R	Mammoth (O)	3.18
4H-2, 100	28.3	R-N	Gauss/Gilbert	3.40
4H-5, 20	32.0	N-R	Cochiti (T)	3.88
4H-5, 130	33.1	R-N	Cochiti (O)	3.97
4H-6, 130	34.6	N-R	(spurious?)	
5H-1, 90	36.2	N-R	Sidufjall (T)	4.40
5H-2, 50	37.3	R-N	Sidufjall (O)	4.47
5H-2, 130	38.1	N-R	Thvera (T)	4.57
5H-4, 90	40.7	R-N	Thvera (O)	4.77
6H-2, 50	46.9	N-R	C3AN1 (T)	5.35
6H-3, 130	49.2	R-N	C3AN1 (O)	5.53
6H-2, 70	50.1	N-R	?	
6H-2, 90	50.3	R-N	?	
6H-2, 110	50.5	N-R	C3AN2 (T)	5.68
6H-4, 50	52.9	R-N	C3AN2 (O)	5.89
7H-2, 110	57.1	N-R	C3AN3 (T)	6.37
7H-3, 70	58.2	R-N	?	
7H-3, 110	58.6	N-R	?	
7H-4, 1	59.0	R-N	C3AN3 (O)	6.50
7H-5, 1	60.5	N-R	?	
7H-5, 20	60.7	R-N	?	
7H-5, 70	61.2	N-R	C4N1 (T)	6.70
7H-6, 30	62.3	R-N	C4N1 (O)	6.78
7H-6, 100	63.0	N-R	C4N2 (T)	6.85
9H-3, 1	76.8	R-N	C4AN1 (O)	8.21
9H-3, 70	77.5	N-R	C4AN2 (T)	8.41
9H-4, 20	78.5	R-N	C4AN2 (O)	8.50
9H-5, 1	79.8	N-R	C4AN3 (T)	8.71
9H-5, 50	80.3	R-N	C4AN3 (O)	8.80
9H-5, 80	80.6	N-R	C5N1 (T)	8.92

Note: Depth values in columns 1 and 2 are determined from pass-through results and have an associated error of 10–20 cm. Sense = active sense of reversal; Chron = associated magnetic polarity chron boundary. (O) indicates onset of polarity chron, (T) indicates termination, and more tentative correlations are shown by "?".

available data (including pass-through records of inclination and intensity as well as discrete sample results) has helped us to identify most of these problematic sections.

Magnetic Susceptibility

We made whole-core magnetic susceptibility measurements at intervals of 6 cm on all sections of cores recovered from Holes 710A and 710B. Measurements were made with a Bartington Susceptibility Meter (Model MS1) and a whole-core, pass-through sensor coil of 80-mm inner diameter (Model MS2C). Figures 13, 14, and 15 show the results of these measurements.

The strong lithologic control of susceptibility variations at this site is clearly emphasized by the striking similarity (negative correlation) between the susceptibility profile of Hole 710A (Fig. 13) and the plot of the carbonate content (wt%) for the same hole (see Fig. 21). We can divide the lithostratigraphic record of Hole 710A into four main subsections according to its magnetic susceptibility profile, as follows.

1. Between 0 and approximately 40+ mbsf (the exact depth is not known due to lack of recovery; the equivalent depth in Hole 710B is 47 mbsf), magnetic susceptibility values are generally between 5 and 15 $\times 10^{-6}$ cgs. Variations in susceptibility within this particular interval reflect changes in sediment color and clay content (see "Lithostratigraphy" section, this chapter). The sediments are of Pliocene-Pleistocene age and consist of white to light yellowish brown or buff-colored, clay-bearing nannofossil oozes with occasional calc-turbidites (Unit IA-see "Lithostratigraphy" section, this chapter). The colors of these sediments suggest that they have remained in an oxidized state since they were deposited (e.g., Lyle, 1983); thus, any magnetic iron oxides and/or oxyhydroxides which they originally contained will have been preserved unaltered (or further oxidized, but not magnetically disordered).

2. Below approximately 40+ mbsf, to a depth of 67 mbsf, susceptibility values fall to between 2 and 7 $\times 10^{-6}$ cgs. This interval corresponds to a sequence of upper Miocene to lower Pliocene clay-bearing nannofossil oozes (see "Lithostratigraphy" section for Unit IB), which are similar in composition to those described above, but in which pore waters became anoxic post-depositionally, possibly due to a high initial C_{org} content, thus imparting gray or greenish gray hues to the sediment. Under reducing conditions, any magnetic iron oxides or oxyhydroxides originally in the sediment are likely to have been dissolved (i.e., bacterially dissociated) during suboxic diagenesis of organic matter in the sediment (e.g., Froelich et al., 1979; Canfield and Berner, 1987). This effect may have been responsible for the general decrease in susceptibility values in this interval. As NRM-carrying magnetic minerals originally in the sediment were destroyed, only paramagnetic iron-bearing minerals like clays, ferromagnesian silicates, pyrite, etc., were left to contribute to susceptibility values (e.g., Karlin and Levi, 1983, 1985; Karlin et al., 1987).

3. Between 67 mbsf and approximately 135 mbsf, susceptibility values are generally higher than elsewhere in the profile (i.e., between 10 and 50 $\times 10^{-6}$ cgs). This interval corresponds to an oxidized sequence of lower to middle Miocene clayey-nannofossil oozes and nannofossil clays (see "Lithostratigraphy" section for Unit II). The generally lower carbonate content (see Fig. 21) and higher susceptibility values in this interval may tentatively be related to increased dissolution of carbonate and biogenic silica constituents in the sediment during the early and middle Miocene. We observed similar variations in carbonate and susceptibility trends at Sites 708 and 709 for the same stratigraphic intervals (see "Paleomagnetics" sections, "Site 708" and "Site 709" chapters, this volume). Biogenic silica components virtually disappear from this interval of Hole 710A, while planktonic foraminifers are severely fragmented, and benthic fora-

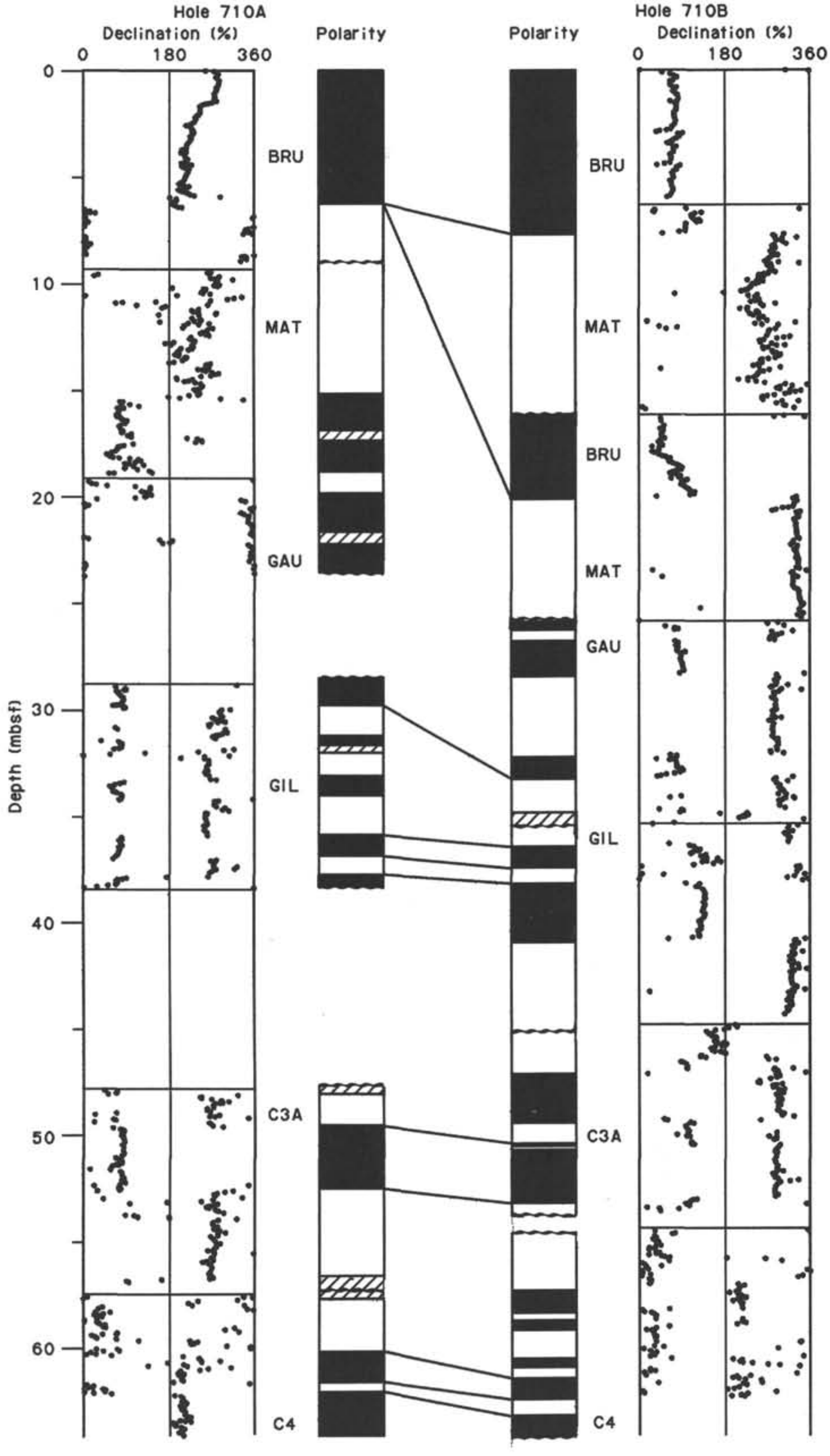

Figure 12. Declination records and magnetic polarity interpretation from APC cores for Holes 710A (left) and 710B (right). Black indicates zones of presumed normal polarity; white, zones of reversed polarity. Diagonal lines indicate disturbed zones of inconsistent magnetics. Horizontal lines on declination panel indicate core breaks; wavy lines on polarity panel indicate corresponding breaks in recovery.

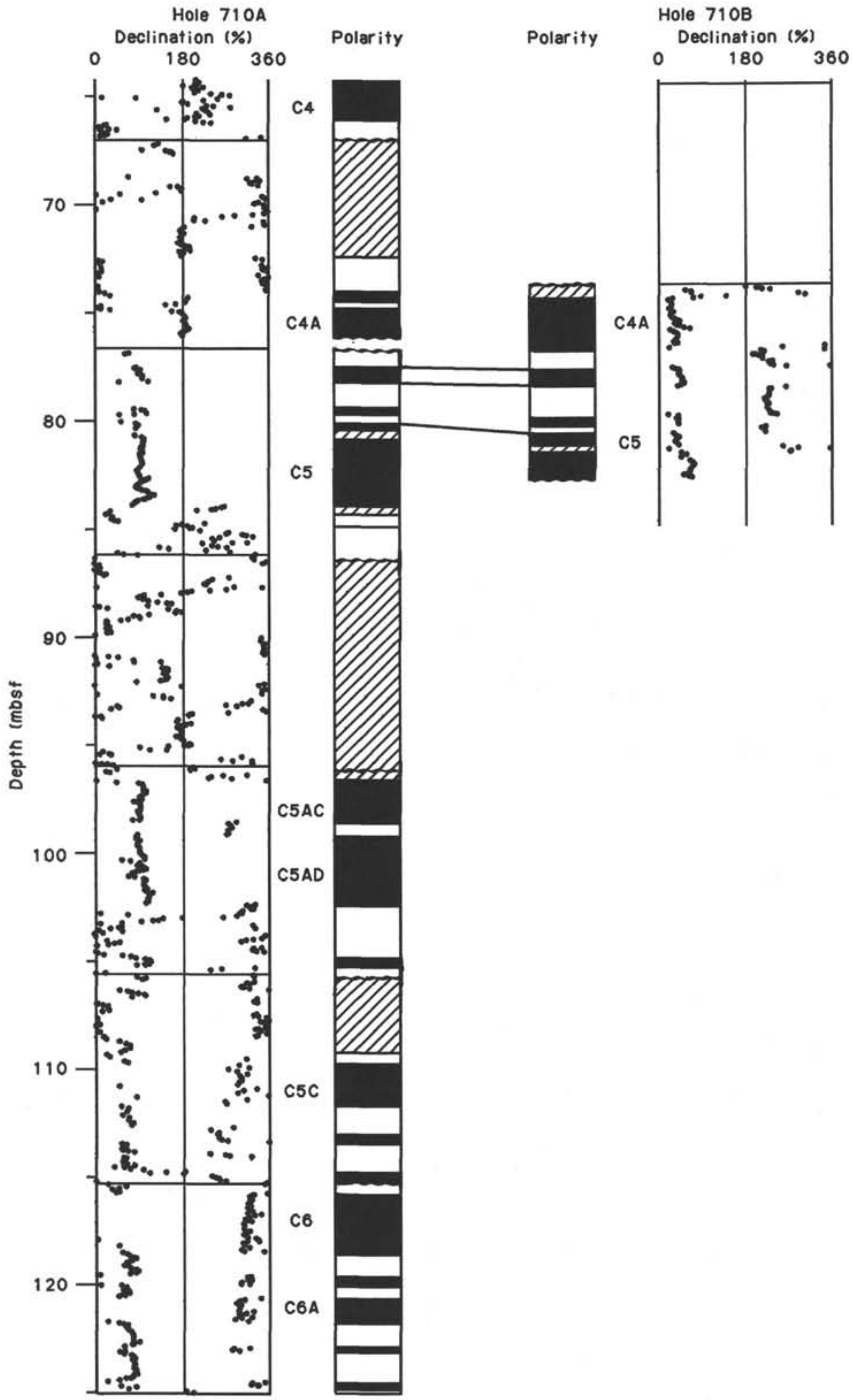

Figure 12 (continued).

minifers and coccoliths also show some signs of dissolution (see "Lithostratigraphy" and "Biostratigraphy" sections, this chapter). There are two horizons of lower susceptibility values within this interval: (1) at approximately 84–86 mbsf, corresponding to a short section of gray or greenish-gray colored, reduced sediment (see "Lithostratigraphy" section, this chapter); and (2) at 93–107 mbsf, corresponding to an interval of higher carbonate content in the sediment (see Fig. 21), possibly the result of a

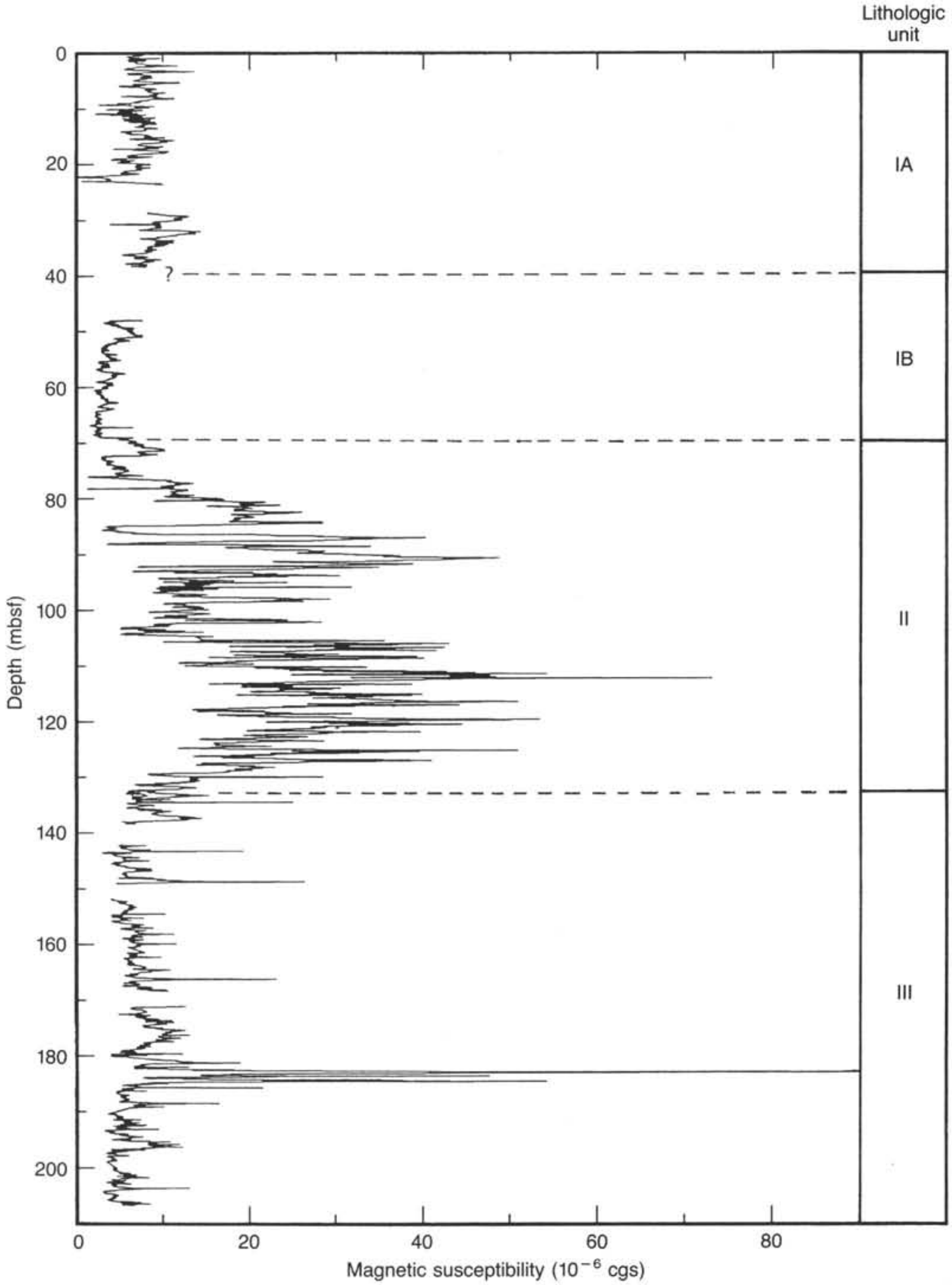

Figure 13. Whole-core magnetic susceptibility profile of Hole 710A. The lithologic units indicated in this figure are identical to those defined in the "Lithostratigraphy" section in this chapter. Unit I = clay-bearing nannofossil ooze (IA = oxidized, IB = reduced); Unit II = clayey nannofossil ooze and nannofossil clay; Unit III = nannofossil ooze and chalk (with volcanic-ash-rich horizons in various stages of alteration).

brief period during the middle Miocene when dissolution of carbonate constituents in the sediment was less severe than during early and late Miocene times.

4. Between 135 and 209 mbsf, the general level of background values of susceptibility falls to between 3 and 7×10^{-6} cgs, reflecting an increase in carbonate content and an improvement in the preservation of biogenic silica and carbonate constituents in the sediment. These features suggest that dissolution of biogenic components in this interval, which consists almost entirely of nannofossil ooze and chalk of Oligocene age (Unit III), is much lower than in the overlying Miocene sequence. However, a number of prominent peaks in susceptibility rise above background levels and correspond to volcanic-ash-rich horizons in varying stages of alteration (see "Lithostratigraphy" section). Volcanic-ash-rich horizons generally exhibit high susceptibility values because of the large amount of titanomagnetite they frequently contain (Kennett, 1981). The major peak in susceptibility (over 1×10^{-4} cgs) at 183 mbsf corresponds to a large, degraded volcanic-ash-rich horizon which can be correlated with similar horizons—also characterized by large peaks

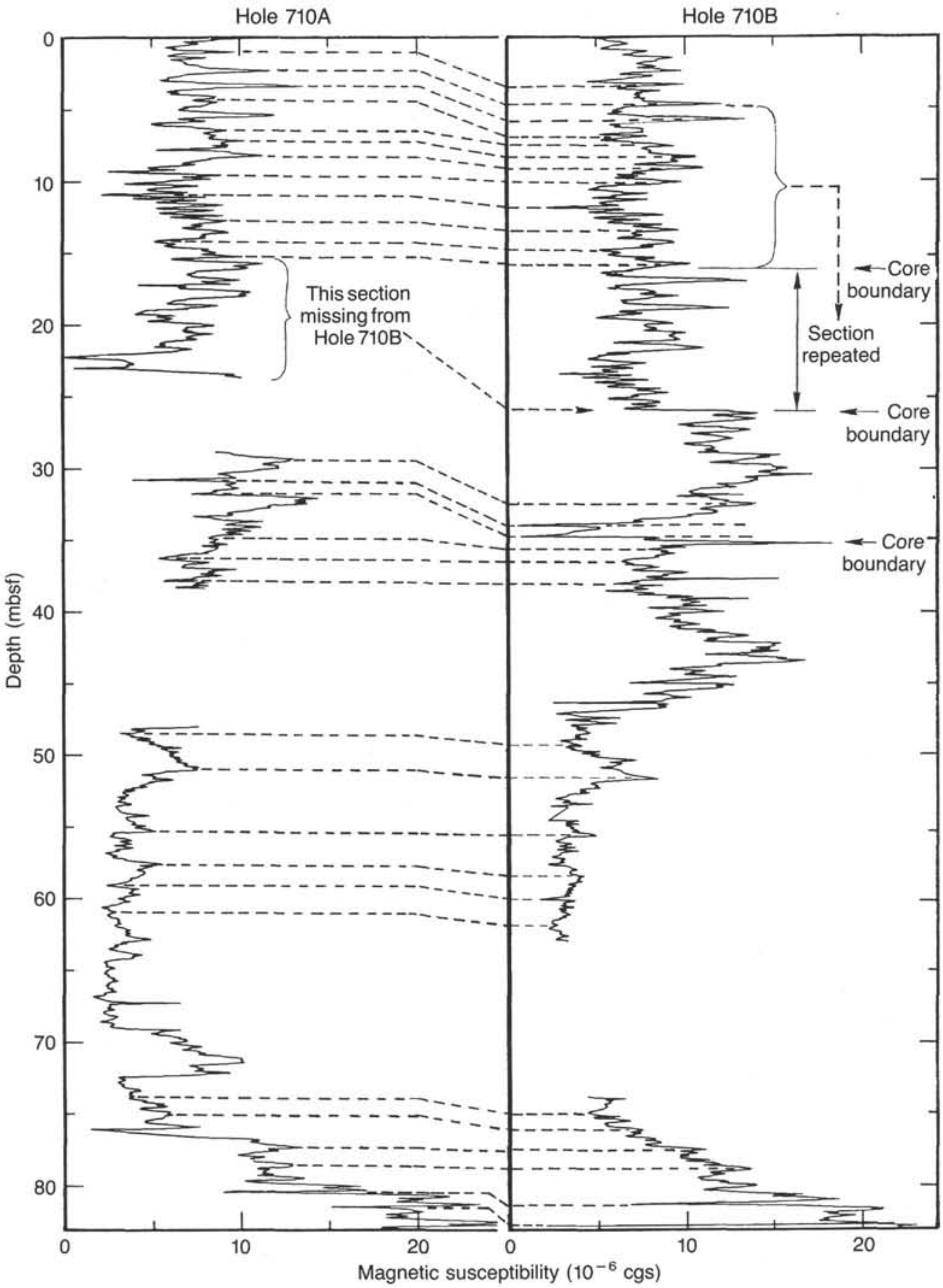

Figure 14. Suggested correlation between the whole-core susceptibility profiles of Holes 710A and 710B for the late Miocene to topmost Pleistocene interval between 0 and 83 mbsf.

in susceptibility—in Holes 709B (at 236 mbsf) and 708A (at 228 mbsf).

The clear lithologic control of susceptibility variations at Site 710 makes possible a detailed and reliable correlation between holes (see Fig. 14). This reveals the presence of various stratigraphic discontinuities, including (1) an hiatus, possibly due to winnowing, at the top of Hole 710A; (2) loss of sediment at the junction between adjacent cores (e.g., at 6.5 mbsf, 16.2 mbsf, 25.8 mbsf, and 35.3 mbsf in Hole 710B); and (3) the presence of a repeated sequence in Hole 710B, between 16.2 mbsf and 25.8 mbsf (corresponding exactly to Core 115-710B-3H), stratigraphically equivalent to the overlying sequence between 4.5 mbsf and 16.2 mbsf. The presence of a repeated sequence corresponding to Core 115-710B-3H is also indicated by the repetition of the Pleistocene nannofossil Subzone CN14A in this interval (see "Biostratigraphy" section, this chapter).

Figure 15 shows an expanded view of that section in Hole 710B in which most of the repeated sequence occurs and the stratigraphically equivalent horizons in Hole 710A. The repeated sequence in Hole 710B, corresponding to Core 115-710B-3H, is most probably the result of repenetration of the corer into the sequence previously recovered by Cores 115-710B-1H and -2H, possibly as a result of inadequate heave compensation during the swell. In Figure 15, the interval labeled "X" within the re-

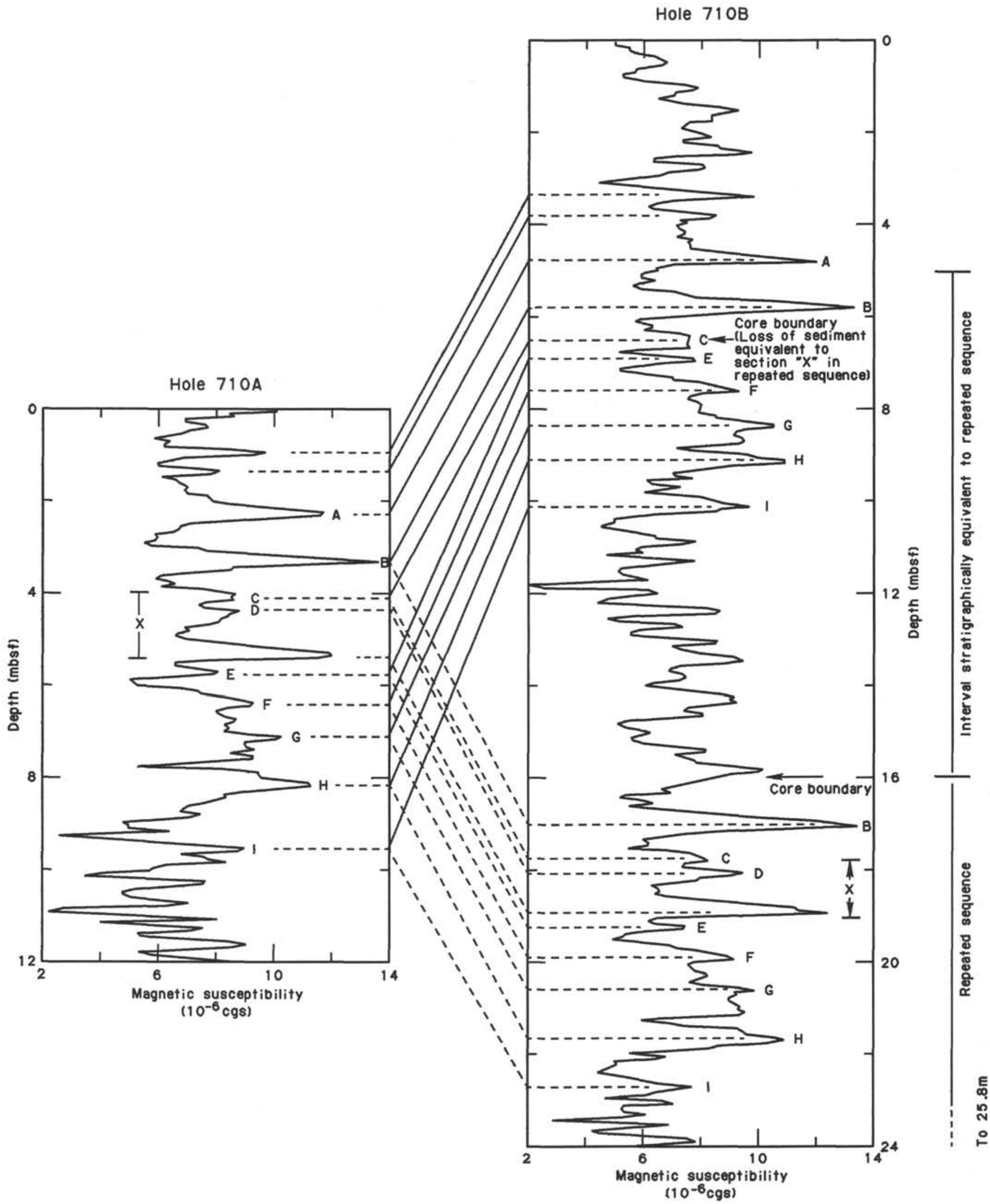

Figure 15. Whole-core magnetic susceptibility profiles of Holes 710A and 710B, showing the repetition of sequence in Hole 710B below 16.2 mbsf (repeated sequence corresponds exactly with Core 710B-3H), and a suggested correlation for the interval in which repetition occurs. Some of the more clearly correlatable peaks in the susceptibility profile of each hole (and within the repeated sequence) are letter coded to clarify identification. The section labeled "X," which is identifiable both in Hole 710A and in the repeated sequence of Hole 710B, is absent from the upper sequence of Hole 710B because of sediment loss at the junction between Cores 115-710B-1H and -2H.

peated sequence of Hole 710B is absent from the overlying, stratigraphically equivalent sequence because of sediment loss at the junction between Cores 115-710B-1H and -2H. Similarly, in Figure 14, the susceptibility profile of the sequence in Hole 710A between 15.5 mbsf and 23.6 mbsf, underlying the stratigraphic horizon which correlates with the base of Core 115-710B-2H (immediately overlying the recored sequence), does not appear to exhibit any obvious features which may be correlated with the susceptibility profile of Hole 710B below the repeated sequence. This stratigraphic interval, therefore, is probably absent from the sequence in Hole 710B and has been replaced by the repeated sequence recovered by Core 115-710B-3H.

A detailed account of the causes and effects of coring irregularities of this kind is given by Ruddiman et al. (1987), based on their analysis of HPC cores collected during DSDP Leg 94 (Sites 607 through 611).

SEDIMENTATION RATES

We computed sedimentation rates (based on biostratigraphic datums and magnetostratigraphic reversal boundaries) for the entire section at Site 710. These are shown in Figure 16 (see also Table 3). Plots of the magnetic reversal boundaries alone in the top 121.6 m of the section are shown in Figure 17. Despite the fact that the early through middle Miocene section is strongly condensed, there is no evidence of time-stratigraphic gaps. By combing data from Holes 710A and 710B, we observed two short hiatuses: one between 1.9 and 2.4 Ma, and the other between 2.7 and 3.0 Ma.

Sedimentation rates at Site 710 are low relative to those at other sites. Pronounced carbonate dissolution, which has removed a large portion of the foraminiferal carbonate and siliceous fossils below the upper Neogene, contributes to the compressed sediment section.

As at other sites, there is an upswing in sedimentation rates at approximately 10 Ma. Apparently the changing sedimentation regime in the late Miocene can be detected in very dissolved sediments and is clearly represented by nannofossil carbonate sedimentation. These enhanced rates are particularly impressive because siliceous fossils are largely absent from this interval. Nannofossil data suggest that redeposition may be partially responsible. The low middle Miocene rate coincides with marked decreases in carbonate content (see "Geochemistry" section, this chapter).

The low Oligocene rates are consistent with the high degree of carbonate dissolution evidenced in the floras and faunas. Coarse-fraction planktonic foraminifers and all solution-prone nannofossil species have been removed by dissolution.

Estimated sedimentation rates from Hole 710A are as follows:

Pleistocene: 9.3 m/m.y. (0–15.4 mbsf)
13.5 m/m.y. (15.4–18.5 mbsf)
Pliocene–Miocene: 10.8 m/m.y. (33.3–74.2 mbsf)
late Miocene: 5.7 m/m.y. (74.2–80.0 mbsf)
middle Miocene: 9.7 m/m.y. (102.3–105.2 mbsf)
early Miocene–Oligocene: 2.1–7.9 m/m.y. (105.2–181.6 mbsf)

GEOCHEMISTRY

Interstitial Water Studies

Data from interstitial water analyses are summarized in Table 4 and Figure 18.

Calcium and Magnesium

Calcium and magnesium exhibit downhole gradients of 0.009 and −0.0156 mmol/L/m, respectively, giving an overall $\Delta Ca^{2+}/Mg^{2+}$ relationship of −1.01 (Fig. 19). The calcium concentration increases from 11.14 mmol/L at 5.95 mbsf to 16.26 mmol/L at 204.25 mbsf, while the concentration of magnesium decreases from 54.16 to 48.36 mmol/L over the same interval. One interesting aspect of these data is the uniform nature of the calcium gradient compared with the abrupt changes in the magnesium concentrations. The gradual increase in calcium is what one might expect if the profile were controlled by diffusion from an underlying calcium source (i.e., basalt alteration). The magnesium profile, on the other hand, suggests that certain diagenetic reactions are also occurring within the sediments even though diffusion into an underlying magnesium sink also is present. Such reactions possibly involve the formation of magnesium-rich clay minerals via the alteration of existing silicates in the sediments. Although the calcium and magnesium gradients are among the steepest observed in any of the sites studied during Leg 115, they are still substantially lower than the average of 0.08 mmol/L/m estimated by Lawrence and Gieskes (1981) as a world average.

Sulfate, Ammonia, Alkalinity, and Silica

Sulfate decreases predictably from a surface-seawater value of 29.5 mmol/L to 23.8 mmol/L at 204.25 mbsf. Ammonia increases from 7.36 μmol/L at 5.95 mbsf to 35.85 μmol/L at 120 mbsf. The alkalinity, however, does not increase as might be expected if the reduction in sulfate were solely a result of the oxidation of organic material according to the stoichiometry of the following reaction:

$$53SO_4^{2-} + C_{106}H_{263}0_{110}N_{16}P = 106HCO_3^- + 16NH_4^+ + 53HS^- + 39H_2O + HPO_4^{2-}$$

Similarly, the rise in NH_4^+ is not as large as might be predicted from the sulfate loss. Hence, the small rise in alkalinity suggests that the decrease in sulfate content might also be a result of other processes, perhaps precipitation of $CaCO_3$ coupled with the adsorption of NH_4^+ onto clay particles.

The concentration of silica rises rapidly to concentrations between 700 and 900 μmol/L, similar to other sites investigated on this leg.

X-ray Mineralogy, Carbonate, and Organic Analyses

The mineralogy of the sediments from Hole 710A is dominated by low magnesium calcite, with quartz present at concentrations between 2 and 3 wt% in all the samples analyzed. The percentage of carbonate varies between 30 and 98 wt%, with an overall mean of 81.13% (± 11.59; Table 5 and Fig. 20). As at Sites 707, 708, and 709, there are systematic variations in the percentage of carbonate downcore (Fig. 21). The most obvious of these is the middle Miocene low that we previously identified at Sites 707, 708, and 709. Moving downhole from the characteristic late middle Miocene carbonate low, the carbonate content rises rapidly to a concentration of over 80 wt% and subsequently to a concentration of 92 wt% in Oligocene sediments.

The percentage of organic carbon varies between 0% and 0.15% (Table 6). The highest concentrations are found in the upper 30 mbsf, decreasing to below detection limits at 37.65 mbsf (Fig. 20).

PHYSICAL PROPERTIES

Introduction

Site 710 is located on the Madingley Rise, north of the Mascarene Plateau, about 50 km southeast of Site 709 at a water depth of 3812 m. We drilled two holes using APC- and XCB-drilling techniques. Nannofossil ooze containing varying amounts of carbonate and clay was recovered to 80 mbsf and subsequently carbonate-rich (>90%) nannofossil ooze with in-

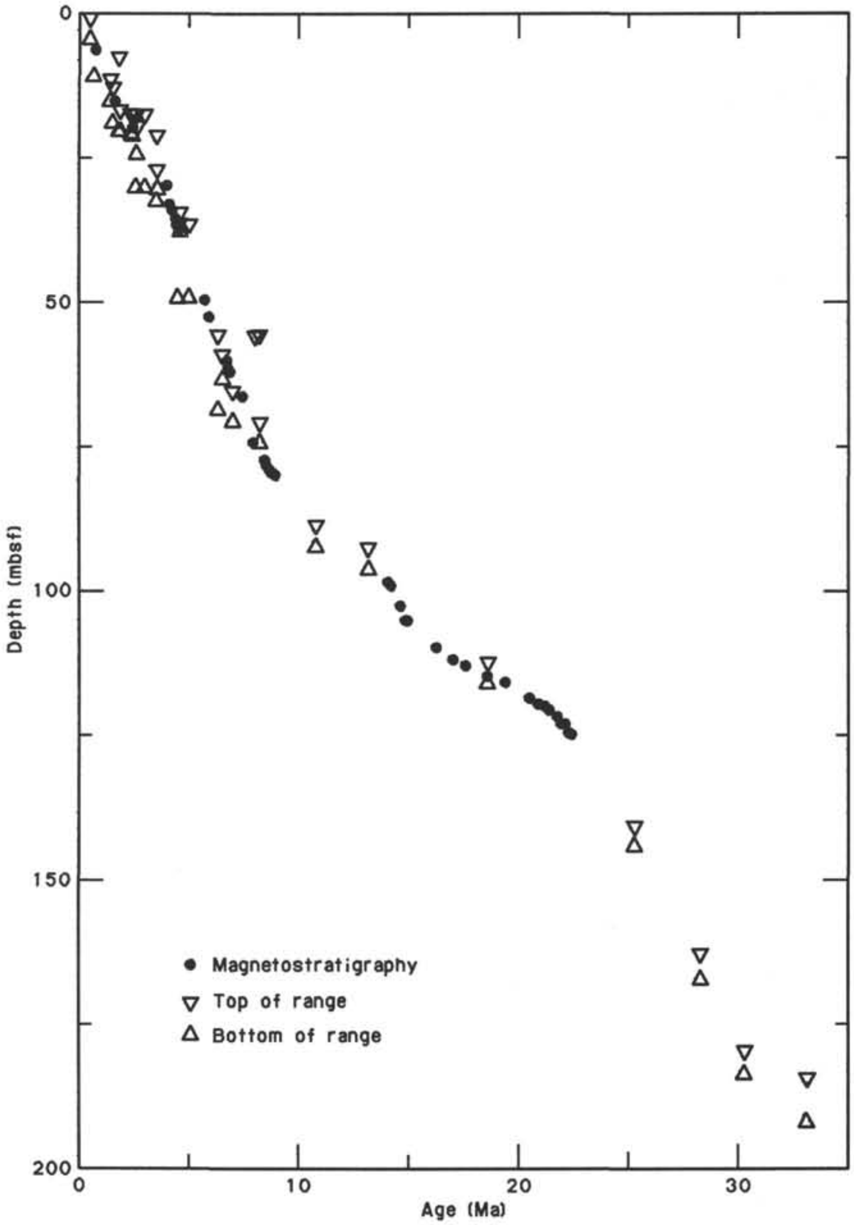

Figure 16. Sedimentation rates in Hole 710A based on the biostratigraphic datum levels listed in Table 3. Age-depth relationships for magnetostratigraphic reversal boundaries are listed in Table 2.

cipient chalk layers to the base of Hole 710A. There were a few thin turbidite horizons consisting of foraminiferal ooze. We noted drilling disturbance only within the lower ooze-chalk sequence.

This section presents the results of physical property measurements for index properties, compressional- and shear-wave velocities, shear strength, continuous compressional velocity (*P*-wave logger), and continuous wet-bulk density (GRAPE).

Index Properties

Figures 22 and 23 and Table 7 present the index properties for Site 710. Carbonate-content data are given in Table 7 and Figure 24. The index properties and carbonate content results from Hole 710A and Hole 710B are in good agreement.

Wet-bulk density increases with depth, indicating an increase in the consolidation of the sediment. Conversely, porosities and water content decrease with depth. These changes in the properties of the "homogeneous" nannofossil ooze are not evident from visual descriptions of the cores. Wet-bulk densities increase from 1.48 g/cm^3 at the seafloor to 1.63 g/cm^3 at 67 mbsf in the pure nannofossil ooze, followed by a drop to 1.51 g/cm^3 at 78 mbsf, which marks the onset of clay-bearing nannofossil ooze. Within the clay-bearing nannofossil ooze, there is a gradual increase of wet-bulk densities, associated with a decrease of porosity and water content. This indicates increasing consolidation with depth. The underlying nannofossil ooze with chalk layers (first encountered at 132 mbsf) is characterized by only a minor scatter in the index properties.

Grain densities are constant throughout Hole 710A, although the carbonate contents vary considerably with depth (Fig. 24). The continuous GRAPE record of the wet-bulk densities, shown in Figure 25, matches the measurements on the discrete samples.

Compressional-Wave Velocity and Acoustic Impedance

The results of the discrete V_p measurements from Site 710 are given in Table 8 and Figure 26. The data from Hole 710A are

Table 3. Biostratigraphic datum levels, Site 710.

	Species event	Depth (mbsf)	Age (Ma)
LO	*P. lacunosa* (N)	2.8-3.1	0.46
LO	*N. reinholdii* (D)	<9.5	0.65
LO	*C. macintyrei* (N)	13.4-13.8	1.45
LO	*P. prismatium* (R)	14.7-17.7	1.55
FO	*P. doliolus* (D)	9.5-19.2	1.8
LO	*D. brouweri* (N)	18.3-18.8	1.89
LO	*D. pentaradiatus* (N)	19.2-19.5	2.35
LO	*D. surculus* (N)	19.5-20.1	2.41
LO	*S. peregrina* (R)	21.4-23.1	2.60
LO	*N. jouseae* (D)	19.2-28.8	2.6
FO	*R. praebergonii* (D)	19.2-28.8	3.0
LO	*P. doliolus* (R)	23.1-31.0	3.53
LO	*R. pseudoumbilica* (N)	28.8-29.1	3.56
FO	*N. jouseae* (D)	38.3-47.9	4.5
FO	*C. rugosus* (N)	36.1-36.6	4.60
LO	*D. quinqueramus* (N)	38.3-47.9	5.0
FO	*A. tirimus* (N)	60.8-61.8	6.50
LO	*D. hughesi* (D)	67.1-69.3	7.00
FO	*N. reinholdii* (D)	>57.5	8.0
FO	*N. marina* (D)	>57.5	8.2
FO	*D. quinqueramus* (N)	72.5-72.5	8.20
FO	*C. coalitus* (N)	90.1-90.6	10.80
LO	*S. heteromorphus* (N)	94.0-94.6	13.20
FO	*S. heteromorphus* (N)	113.9-115.2	17.10
LO	*S. ciperoensis* (N)	142.1-142.4	25.20
LO	*S. distentus* (N)	164.2-165.53	28.20
FO	*S. ciperoensis* (N)	181.2-182.1	30.20
LO	*S. corona* (D)	57.5-67.1	6.30
FO	*D. ateuchus* (D)	186.0-190.4	33.00

Note: FO = first occurrence, LO = last occurrence, N = nannofossil, D = diatom, and R = radiolarian.

quite scattered around a mean value of 1500 m/s. There is an increase of velocity with depth within the clay-bearing nannofossil ooze which is not evident in the adjacent nannofossil oozes. The data from Hole 710B show less scatter around a mean of 1500 m/s. The measurement at 85 mbsf, which was obtained on a fractured sample, is included for comparative purposes. Other measurements below 1470 m/s are filtered.

There is a good correlation between the velocities measured on discrete samples and the *P*-wave logger measurements (Figs. 25 and 26). The match is best for the clay-bearing nannofossil ooze in the depth interval from 80 to 120 mbsf. This agreement gives confidence in the *P*-wave logger results for intervals in which we could obtain no discrete samples. We computed an impedance profile from the GRAPE wet-bulk density and the *P*-wave logger results (Fig. 27). It shows a major impedance contrast at the onset of the clay within the nannofossil ooze at 78 mbsf. The transition from the clay-bearing interval to the nannofossil ooze at 128 mbsf is gradual, except for one anomalously high velocity reading. The major low-frequency features of the continuous impedance profile can also be observed in the profile calculated from the discrete density and velocity measurements (Fig. 27 and Table 8).

Shear Strength

The experimental results for maximum shear strength at Site 710 are shown in Figure 28 and Table 9. There is a gradual increase in shear strength with depth in the nannofossil ooze. The transition from ooze to clay-bearing ooze shows a rapid increase in sediment cohesion. At 100 mbsf there is a reduction of shear strength; these measurements were taken in slumped beds and turbidites occurring within the clay-bearing nannofossil ooze. The shear strengths within the chalky nannofossil ooze (depths greater than 132 mbsf) show no depth dependence, although we can make a clear distinction between the chalk horizons and surrounding ooze: the "soft," semiconsolidated ooze has a shear

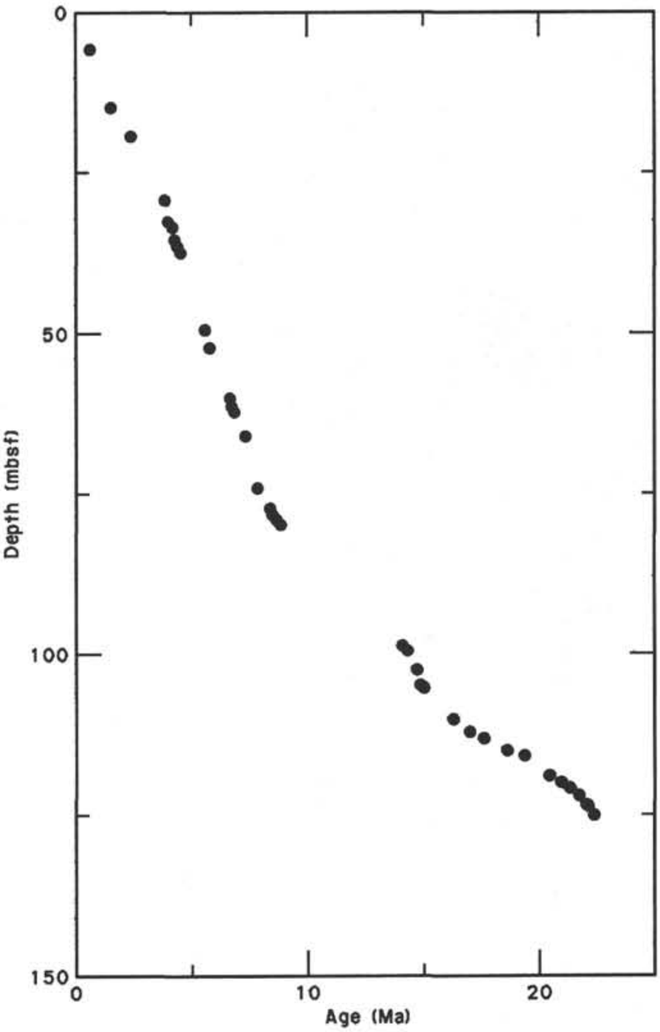

Figure 17. Sedimentation rates in Hole 710A based on magnetic reversal boundaries alone.

strength of below 50 kPa, while the "harder," more consolidated chalk chunks have twice the shear strength.

Thermal Conductivity

The results for thermal conductivity at Site 710 are shown in Table 10 and Figure 29. The thermal conductivity data for this site show little overall trend with depth. This hole shows extreme local variability in the partially consolidated sediments between the consolidated and unconsolidated intervals. We performed several detailed studies of a core to check small-scale variability. These showed fairly smooth variations within a core, with an overall average of about 1.2 $W \cdot m^{-1} \cdot K^{-1}$. The range in the values is from 0.75 to 1.4 $W \cdot m^{-1} \cdot K^{-1}$.

Summary

The sediments recovered at Site 710 were soft nannofossil and clay-bearing nannofossil oozes, and "pasty" nannofossil ooze containing fragments and chunks of hard nannofossil chalk. All physical properties measurements showed a fair amount of scatter in the nannofossil ooze. The shear strength was the only measurement showing a significant increase with depth. The transition to clay-bearing nannofossil ooze at 78 mbsf results in a marked drop in wet-bulk density, shear strength, and V_p measurements. There is an increase in all these measurements with

Table 4. Interstitial water analyses, Hole 710A.

Sample interval (cm)	Depth (mbsf)	Ca (mmol/L)	Mg (mmol/L)	Cl (mmol/L)	Al (mmol/L)	pH	Salinity (‰)	Si (μmol/L)	SO_4 (mmol/L)	NH_4 (μmol/L)
Seawater	0	10.38	54.16	554.33	2.62	8.44	34.8	1	29.54	0
115-710A-										
1H-4, 145–150	5.95	11.14	53.08	540.34	3.62	7.60	34.5	631	28.4	7.36
2H-4, 145–150	15.45	11.73	52.41	537.54	3.84	7.40	34.5	703	28.26	8.90
3H-2, 145–150	22.15	12.13	51.27	559.93	3.84	7.38	35.0	807	28.10	14.28
4H-4, 145–150	34.75	12.67	51.22	557.13	3.94	7.36	35.2	791	28.10	15.05
6H-4, 145–150	53.85	13.44	51.19	565.53	3.99	7.40	35.2	910	26.99	20.44
9H-5, 120–125	83.80	13.86	51.01	554.33	3.92	7.52	35.2	885	26.03	35.85
12H-5, 120–125	112.70	14.92	48.64	580.46	4.15	7.51	35.2	620	24.28	32.75
15X-3, 115–125	136.55	15.32	48.66	534.74	3.68	7.40	35.5	737	25.24	7.36
18X-3, 115–125	165.55	15.71	48.83	566.47	3.74	7.45	35.6	857	24.44	0.43
22X-3, 115–125	204.25	16.26	48.36	534.74	3.79	7.45	35.5	976	23.80	4.28

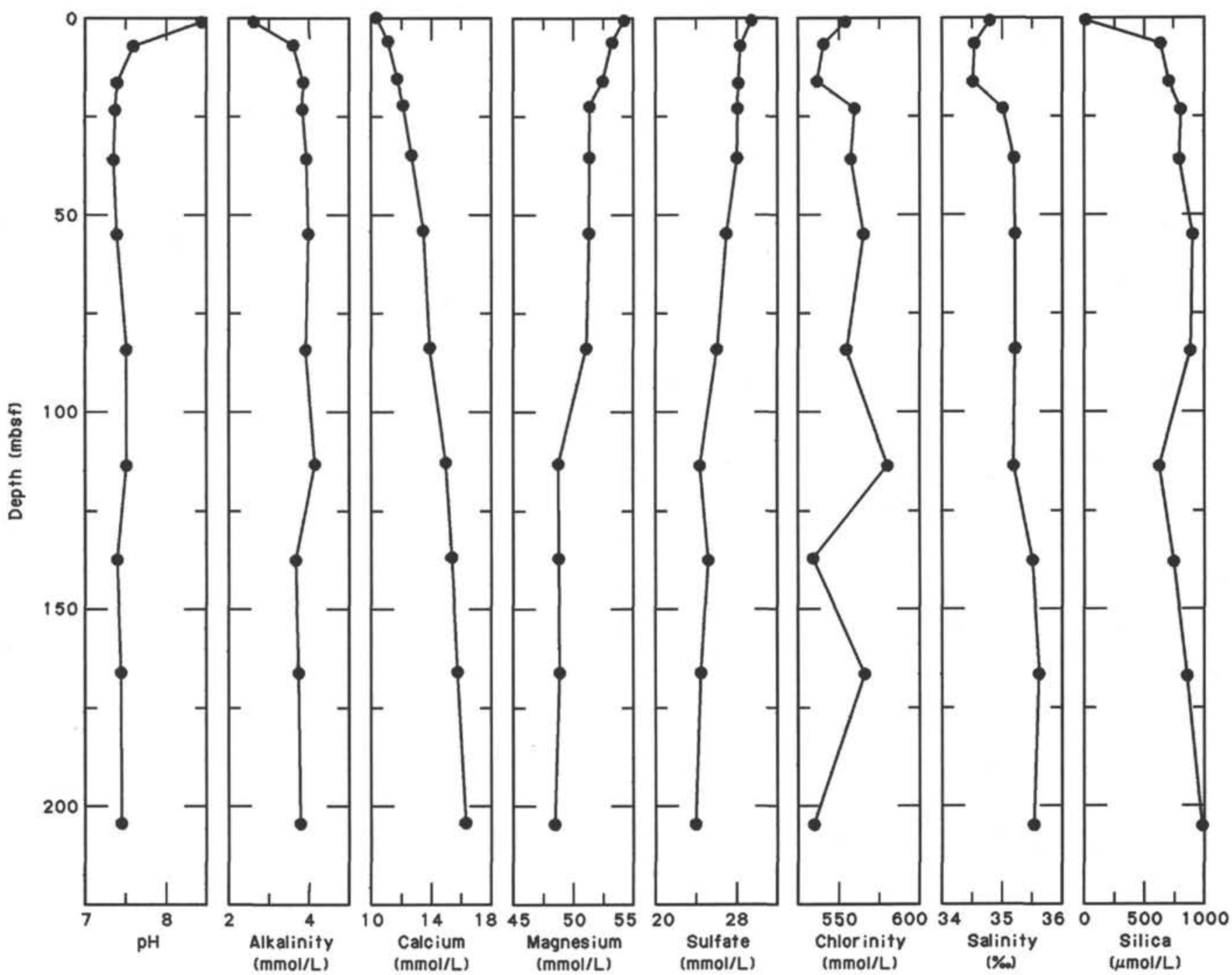

Figure 18. Summary of interstitial water analyses, Hole 710A, as a function of sub-bottom depth. Surface seawater is plotted at 0 mbsf.

increasing depth, which indicates greater consolidation within the clay-bearing nannofossil ooze.

At 132 mbsf, there is a second significant reduction in the wet-bulk density profile which is matched by a drop in V_p. This is related to the transition to nannofossil ooze showing an incipient chalk formation. The index properties, continuous GRAPE wet-bulk density, and *P*-wave velocity profiles remain remarkably constant through this sediment type to the base of Hole

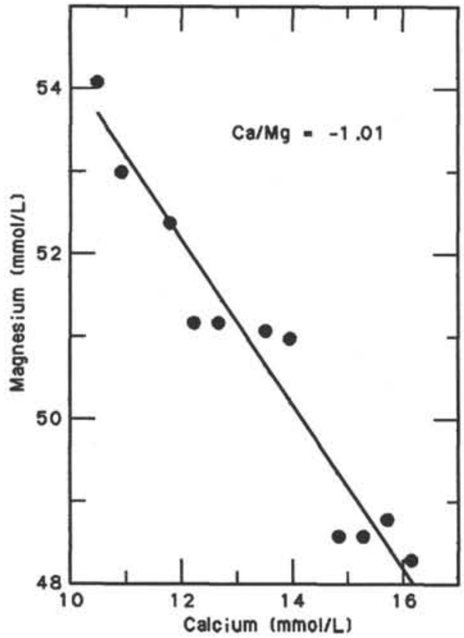

Figure 19. Concentration of calcium and magnesium in interstitial waters from Hole 710A. Note the overall conservative relationship of calcium and magnesium with some deviations, indicating that some diagenetic reactions involving magnesium are taking place in the sediments.

710A. The shear strength of the harder chalk chunks is twice that of the semiconsolidated ooze. There was visual evidence of disturbance within this ooze-chalk sequence.

SEISMIC STRATIGRAPHY

Some 30 nmi to the southeast and 800 m downslope of Site 709 lies Site 710. We planned this site as the third in a sequence of progressively deeper sites to investigate the history of carbonate dissolution in the equatorial water column and to study circulation in the northwestern Indian Ocean. Site 710 is at a water depth of 3812 m, on a flat plain in the center of the Madingley Rise (Fig. 30). The site was positioned on the V34-06 (9 August 1977) seismic reflection profile (Fig. 31). In the existing single-channel seismic (SCS) records, it is evident that some deformation of sediments has occurred, probably in the form of downslope movement from the high ground to the west.

Our approach with the *JOIDES Resolution* was from the northwest, where we could optimize the definition of any large-scale disturbance (slumps or faults). Our own survey employed 3.5- and 12-kHz depth recorders and a single-channel seismic, water-gun reflection profiler. The 3.5-kHz depth recorder showed parallel layering in the upper 75 m of the section, and the SCS profile revealed an area where the sediments appeared reasonably undisturbed down to the basement reflector (Fig. 32).

We recognized several distinct reflectors within the stratigraphic section at Site 710. Below the sediment-water interface is a fairly continuous reflector at about 0.13 s (two-way traveltime). Next is a strong reflector at 0.33 s, followed by the basement reflector at 0.52 s.

REFERENCES

Berger, W. H., 1973. Deep-sea carbonates: evidence for a coccolith lysocline. *Deep Sea Res.*, 20:917–921.

Canfield, D. E., and Berner, R. A., 1987. Dissolution and pyritization of magnetite in anoxic marine sediments. *Geochim. Cosmochim. Acta*, 51:645–659.

Fisher, R. L., Bunce, E. T., et al., 1974. *Init. Repts. DSDP*, 24: Washington (U.S. Govt. Printing Office).

Fisher, R. L., Sclater, J. G., and McKenzie, D. P., 1971. Evolution of the Central Indian Ridge, western Indian Ocean. *Geol. Soc. Am. Bull.*, 82:553–562.

Froelich, P. N., Klinkhammer, G. P., Bender, M. L., Luedtke, N. A., Heath, G. R., Cullen, D., Dauphin, P., Hartman, B., Hammond, D., and Maynard, V., 1979. Early oxidation of organic matter in pelagic sediments of the eastern Equatorial Atlantic: suboxic diagenesis. *Geochim. Cosmochim. Acta*, 43:1075–1090.

Karlin, R., and Levi, S., 1983. Diagenesis of magnetic minerals in recent hemipelagic sediments. *Nature*, 303:327–330.

________, 1985. Geochemical and sedimentological control of the magnetic properties of hemipelagic sediments. *J. Geophys. Res.*, 90: 10,373–10,392.

Karlin, R., Lyle, M., and Heath, G. R., 1987. Authigenic magnetite formation in suboxic marine sediments. *Nature*, 326:490–493.

Kennett, J. P., 1981. Marine tephrochronology. *In* Emiliani, C. (Ed.), *The Sea* (Vol. 7): New York (Wiley), 1373–1436.

Lawrence, J. R., and Gieskes, J. M., 1981. Constraints on water transport and alteration in the oceanic crust from the isotopic composition of pore water. *J. Geophys. Res.*, 86:7924–7927.

Lyle, M., 1983. The brown-green color transition in marine sediments: a marker of the Fe(III)–Fe(II) redox boundary. *Limnol. Oceanogr.*, 28:1026–1033.

Peterson, M.N.A., 1966. Calcite: rates of dissolution in a vertical profile in the central Pacific. *Science*, 154:1542–1544.

Roth, P. H., and Berger, W. H., 1975. Distribution and dissolution of coccoliths in the south and central Pacific. *In* Sliter, W. V., Bé, A.W.H., and Berger, W. H. (Eds.), *Dissolution of Deep-Sea Carbonates*. Spec. Publ. Cushman Found. Foram. Res., 13:87–113.

Ruddiman, W. F., Cameron, D., and Clement, B. M., 1987. Sediment disturbance and correlation of offset holes drilled with the hydraulic piston corer: Leg 94. *In* Ruddiman, W. F., Kidd, R. B., Thomas, E., et al., 1987. *Init. Repts. DSDP*, 94, Pt. 2: Washington (U.S. Govt. Printing Office): 615–634.

Schlich, R., 1982. The Indian Ocean: aseismic ridges, spreading centers, and oceanic basins. *In* Nairn, A.E.M., and Stehli, F. G. (Eds.), *The Ocean Basins and Margins* (Vol. 6): New York (Plenum), 51–148.

Takahashi, T., 1975. Carbonate chemistry of sea water and the calcite compensation depth in the oceans. *In* Sliter, W. V., Bé, A.W.H., and Berger, W. H. (Eds.), *Dissolution of Deep-Sea Carbonates*. Spec. Publ. Cushman Found. Foram. Res., 13:11–26.

Ms 115A-109

Table 5. Carbonate content of samples from Hole 710A.

Sample interval (cm)	Depth (mbsf)	Carbonate (wt%)
115-710A-		
1H-1, 25-26	0.25	84.58
1H-1, 135-136	1.35	84.91
1H-2, 25-26	1.75	81.02
1H-2, 135-136	2.85	81.41
1H-3, 25-26	3.25	76.25
1H-3, 135-136	4.35	82.39
1H-4, 25-26	4.75	82.42
1H-4, 52-55	5.02	81.49
1H-4, 135-136	5.85	85.3
1H-5, 25-26	6.25	79.94
1H-5, 135-136	7.35	75.72
1H-6, 25-26	7.75	83.00
1H-6, 58-60	8.08	70.40
1H-6, 135-136	8.85	82.85
2H-1, 25-26	9.75	75.55
2H-1, 135-136	10.85	92.03
2H-2, 25-26	11.25	98.04
2H-2, 60-63	11.60	78.91
2H-2, 135-136	12.35	74.75
2H-3, 25-26	12.75	78.77
2H-3, 135-136	13.85	84.19
2H-4, 25-26	14.25	85.63
2H-4, 60-63	14.60	85.01
2H-4, 135-136	15.35	85.51
2H-5, 25-26	15.75	79.50
2H-5, 135-136	16.85	78.99
2H-6, 25-26	17.25	86.25
2H-6, 60-63	17.60	79.28
2H-6, 135-136	18.35	86.82
2H-7, 25-26	18.75	83.34
3H-1, 25-26	19.45	82.59
3H-1, 60-63	19.80	80.61
3H-1, 135-136	20.55	79.77
3H-2, 25-26	20.95	78.49
3H-2, 119-120	21.89	79.31
3H-3, 25-26	22.45	70.93
3H-3, 60-63	22.80	74.95
3H-3, 135-136	23.55	74.29
4H-1, 25-26	29.05	74.99
4H-1, 135-136	30.15	67.85
4H-2, 25-26	30.55	72.93
4H-2, 60-63	30.90	75.34
4H-2, 135-136	31.65	77.60
4H-3, 25-26	32.05	65.21
4H-3, 135-136	33.15	76.35
4H-4, 25-26	33.55	75.15
4H-4, 60-63	33.90	76.61
4H-4, 135-136	34.65	77.25
4H-5, 25-26	35.05	77.19
4H-5, 135-136	36.15	82.27
4H-6, 25-26	36.55	75.12
4H-6, 60-63	36.90	76.85
4H-6, 135-136	37.65	78.80
4H-7, 25-26	38.05	82.51
6H-1, 25-26	48.15	81.84
6H-1, 135-136	49.25	76.71
6H-2, 14-15	49.54	72.4
6H-2, 60-63	50.00	71.37
6H-2, 124-125	50.64	68.62
6H-3, 14-15	51.04	79.93
6H-3, 124-125	52.14	74.24
6H-4, 0-1	52.40	78.56
6H-4, 60-63	53.00	83.50
6H-4, 95-96	53.35	78.31
6H-5, 14-15	54.04	76.14
6H-5, 124-125	55.14	75.11
6H-6, 14-15	55.54	85.93
6H-6, 60-63	56.00	88.70
6H-6, 124-125	56.64	83.27
6H-7, 14-15	57.04	81.34
7H-1, 25-26	57.75	70.95
7H-1, 135-136	58.85	81.88
7H-2, 25-26	59.25	79.35
7H-2, 60-63	59.60	80.65
7H-2, 135-136	60.35	80.49
7H-3, 25-26	60.75	85.21

Table 5 (continued).

Sample interval (cm)	Depth (mbsf)	Carbonate (wt%)
115-710A-		
7H-3, 135-136	61.85	80.94
7H-4, 25-26	62.25	78.11
7H-4, 60-63	62.60	80.48
7H-4, 135-136	63.35	85.31
7H-5, 25-26	63.75	81.57
7H-5, 32-35	63.82	83.16
7H-5, 135-136	64.85	85.65
7H-6, 25-26	65.25	85.38
7H-6, 60-63	65.60	88.02
7H-6, 135-136	66.35	86.58
8H-1, 25-26	67.35	88.66
8H-1, 60-63	67.70	86.66
8H-1, 135-136	68.45	86.58
8H-2, 25-26	68.85	78.76
8H-2, 60-63	69.20	74.91
8H-2, 135-136	69.95	69.01
8H-3, 25-26	70.35	74.01
8H-3, 135-136	71.45	61.89
8H-4, 25-26	71.85	50.22
8H-4, 135-136	72.95	82.54
8H-5, 25-26	73.35	79.34
8H-5, 135-136	74.45	69.85
8H-6, 25-26	74.85	68.96
8H-6, 60-63	75.20	70.64
8H-6, 135-136	75.95	74.70
9H-1, 25-26	76.85	70.35
9H-1, 135-136	77.95	72.22
9H-2, 25-26	78.35	68.88
9H-2, 60-63	78.70	71.15
9H-2, 135-136	79.45	66.44
9H-3, 25-26	79.85	63.21
9H-3, 135-136	80.95	45.57
9H-4, 25-26	81.35	53.19
9H-4, 135-136	82.45	46.35
9H-5, 25-26	82.85	62.46
9H-5, 63-66	83.23	51.68
9H-5, 112-114	83.72	58.08
9H-6, 25-26	84.35	33.79
9H-6, 120-123	85.30	83.34
9H-6, 135-136	85.45	84.37
9H-7, 25-26	85.85	71.90
10H-1, 25-26	86.45	59.10
10H-1, 135-136	87.55	42.96
10H-2, 25-26	87.95	86.32
10H-2, 60-63	88.30	69.96
10H-2, 135-136	89.05	68.68
10H-3, 25-26	89.45	48.95
10H-3, 135-136	90.55	40.22
10H-4, 25-26	90.95	30.04
10H-4, 63-66	91.33	64.77
10H-4, 135-136	92.05	69.74
10H-5, 25-26	92.45	56.62
10H-6, 25-26	93.95	66.60
10H-6, 60-63	94.30	87.89
10H-6, 135-136	95.05	66.75
10H-7, 25-26	95.45	83.84
11H-1, 25-26	96.05	87.59
11H-1, 135-136	97.15	81.54
11H-2, 25-26	97.55	84.70
11H-2, 135-136	98.65	81.55
11H-3, 25-26	99.05	83.28
11H-3, 58-61	99.38	74.57
11H-3, 135-136	100.15	87.37
11H-4, 25-26	100.55	81.82
11H-5, 25-26	102.05	66.10
11H-5, 135-136	103.15	89.26
11H-6, 25-26	103.55	89.23
11H-6, 90-93	104.20	90.40
11H-6, 135-136	104.65	77.89
11H-7, 25-26	105.05	76.24
12H-1, 25-26	105.75	79.24
12H-1, 135-136	106.85	61.60
12H-2, 25-26	107.25	51.42
12H-2, 60-63	107.60	73.37
12H-2, 135-136	108.35	64.32
12H-3, 25-26	108.75	57.21
12H-3, 135-136	109.85	82.71

Table 5 (continued).

Sample interval (cm)	Depth (mbsf)	Carbonate (wt%)
115-710A-		
12H-4, 25–26	110.25	60.00
12H-4, 60–63	110.60	71.57
12H-4, 135–136	111.35	61.20
12H-5, 25–26	111.75	54.60
12H-6, 25–26	113.25	82.32
12H-6, 60–63	113.60	76.88
12H-6, 135–136	114.35	67.14
12H-7, 25–26	114.75	73.29
12H, CC, 25–26	115.35	67.96
13H-1, 25–26	115.45	69.68
13H-2, 25–26	116.95	72.91
13H-2, 60–63	117.30	87.76
13H-2, 135–136	118.05	74.79
13H-3, 25–26	118.45	74.64
13H-3, 135–136	119.55	68.53
13H-4, 25–26	119.95	72.31
13H-4, 60–63	120.30	68.94
13H-4, 135–136	121.05	78.07
13H-5, 25–26	121.45	81.49
13H-5, 135–136	122.55	77.23
13H-6, 25–26	122.95	70.54
13H-6, 60–63	123.30	82.67
13H-6, 135–136	124.05	81.98
13H-7, 25–26	124.45	78.5
14X-1, 25–26	125.15	65.68
14X-1, 135–136	126.25	84.35
14X-2, 25–26	126.65	78.49
14X-2, 135–136	127.75	87.49
14X-3, 25–26	128.15	86.23
14X-3, 89–91	128.79	70.38
14X-3, 135–136	129.25	88.43
14X-4, 25–26	129.65	88.12
14X-4, 89–91	130.29	86.28
14X-4, 135–136	130.75	88.74
14X-5, 25–26	131.15	90.78
14X-5, 135–136	132.25	92.76
14X-6, 25–26	132.55	92.82
14X-6, 135–136	132.60	89.32
15X-1, 25–26	132.65	91.16
15X-1, 135–136	133.75	91.34
15X-2, 25–26	134.15	92.44
15X-2, 86–88	134.76	91.98
15X-2, 135–136	135.25	91.23
15X-3, 25–26	135.65	89.42
15X-3, 111–112	136.51	90.64
15X-4, 25–26	137.15	86.47
15X-4, 48–50	137.38	87.08
15X-4, 135–136	138.25	92.51
15X-5, 25–26	138.65	91.73
15X-5, 94–95	139.34	74.35
16X-1, 25–26	142.35	92.51
16X-1, 135–136	143.45	94.17
16X-2, 25–26	143.85	92.54
16X-2, 47–50	144.07	93.09
16X-2, 135–136	144.95	92.89
16X-3, 25–26	145.35	93.94
16X-3, 135–136	146.45	90.60
16X-4, 25–26	146.85	91.86
16X-4, 57–60	147.17	91.85
16X-4, 135–136	147.95	90.25
16X-5, 25–26	148.35	91.62
16X-5, 96–97	149.06	93.19
17X-1, 25–26	152.05	92.61
17X-1, 135–136	153.15	89.93
17X-2, 25–26	153.55	90.46
17X-2, 47–49	153.77	90.54
17X-2, 135–136	154.65	90.65
17X-3, 25–26	155.05	92.27
17X-3, 135–136	156.15	90.32
17X-4, 25–26	156.55	89.37
17X-4, 135–136	157.65	91.79
17X-5, 25–26	158.05	91.60
17X-5, 37–39	158.17	91.52
17X-5, 52–55	158.32	91.71
17X-5, 135–136	159.15	90.60
17X-6, 25–26	159.55	91.67
17X-6, 135–136	160.65	91.79

Table 5 (continued).

Sample interval (cm)	Depth (mbsf)	Carbonate (wt%)
115-710A-		
18X-1, 25–26	161.65	92.34
18X-1, 135–136	162.75	93.35
18X-2, 25–26	163.15	92.17
18X-2, 53–55	163.43	89.88
18X-2, 135–136	164.25	87.73
18X-3, 25–26	164.65	88.68
18X-4, 25–26	166.15	87.89
18X-4, 87–89	166.77	91.50
18X-4, 135–136	167.25	91.65
18X-5, 25–26	167.65	88.65
19X-1, 25–26	171.35	90.14
19X-1, 135–136	172.45	90.30
19X-2, 25–26	172.85	89.71
19X-2, 31–33	172.91	90.91
19X-2, 135–136	173.95	90.21
19X-3, 135–136	175.45	89.20
19X-4, 25–26	175.85	88.37
19X-4, 135–136	176.95	86.64
19X-5, 25–26	177.35	86.72
19X-5, 87–89	177.97	89.34
19X-5, 135–136	178.45	84.62
19X-6, 25–26	178.85	91.20
19X-6, 135–136	179.95	86.86
20X-1, 25–26	181.05	86.42
20X-1, 135–136	182.15	89.58
20X-2, 8–10	182.38	89.45
20X-2, 25–26	182.55	86.98
20X-2, 135–136	183.65	73.48
20X-3, 25–26	184.05	87.79
20X-3, 135–136	185.15	89.91
20X-4, 25–26	185.55	89.31
20X-4, 135–136	186.65	91.65
20X-5, 25–26	187.05	92.15
20X-5, 49–50	187.29	92.01
20X-5, 135–136	188.15	92.24
20X-6, 25–26	188.55	88.60
21X-1, 25–26	190.65	93.99
21X-1, 102–103	191.42	93.74
21X-2, 25–26	191.68	93.34
21X-2, 135–136	192.78	93.82
21X-3, 25–26	193.18	95.77
21X-3, 135–136	194.28	95.07
21X-4, 8–10	194.51	92.57
21X-4, 25–26	194.68	94.04
21X-4, 135–136	195.78	90.94
21X-5, 25–26	196.18	93.60
21X-5, 135–136	197.28	94.95
21X-6, 8–10	197.48	93.54
21X-6, 25–26	197.65	90.66
21X-6, 135–136	198.75	92.08
22X-1, 25–26	200.35	91.73
22X-1, 71–73	200.81	92.17
22X-1, 135–136	201.45	90.68
22X-2, 25–26	201.85	92.10
22X-2, 135–136	202.95	91.00
22X-3, 25–26	203.35	92.62
22X-3, 115–116	204.25	93.22
22X-4, 10–12	204.70	93.36
22X-4, 25–26	204.85	92.64
22X-4, 30–32	204.90	87.09
22X-4, 50–52	205.10	90.67
22X-4, 86–88	205.46	93.56
22X-4, 108–110	205.68	93.44
22X-4, 115–116	205.75	92.79
22X-5, 25–26	206.01	90.54

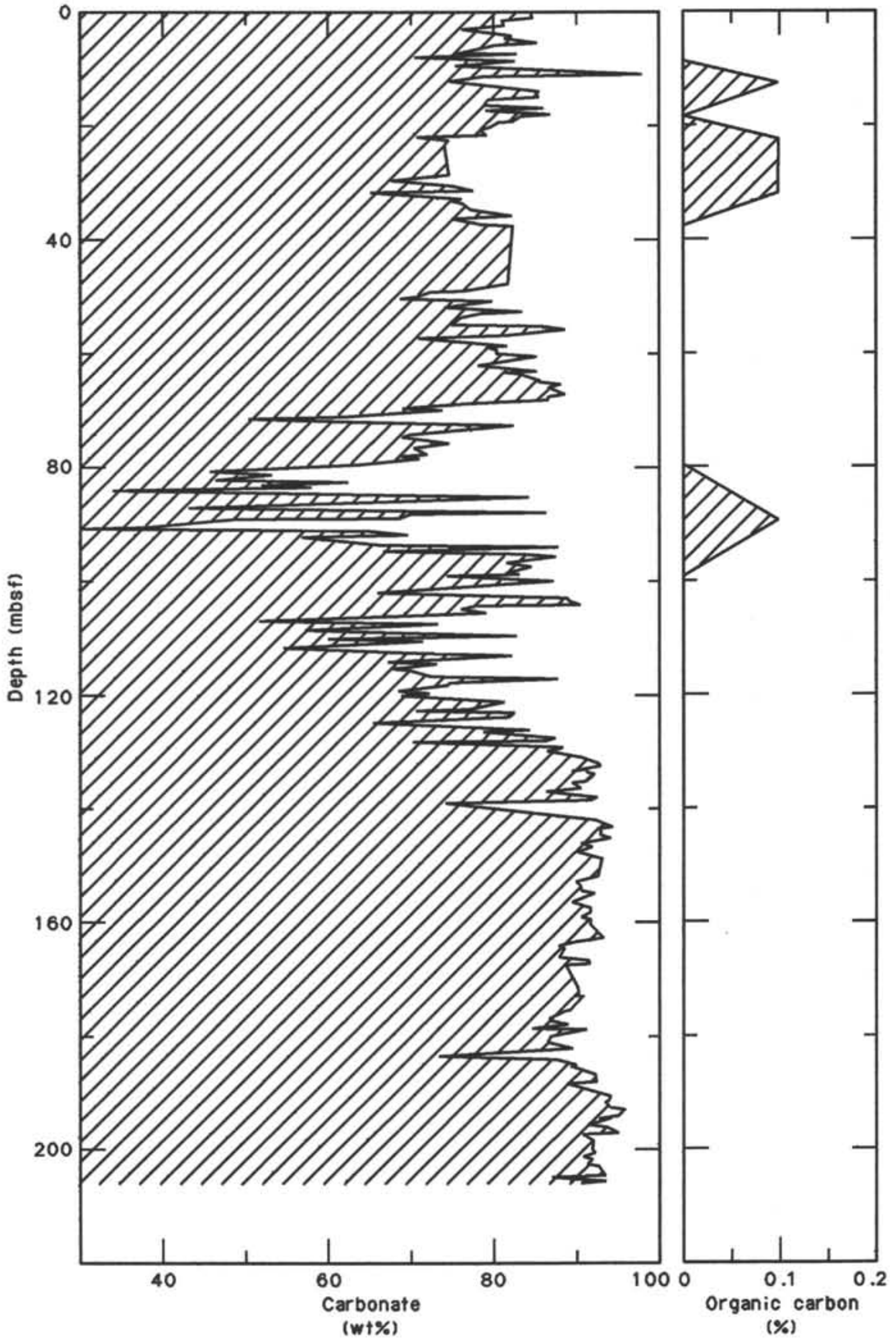

Figure 20. Carbonate and organic carbon content of samples from Hole 710A plotted against increasing depth below seafloor.

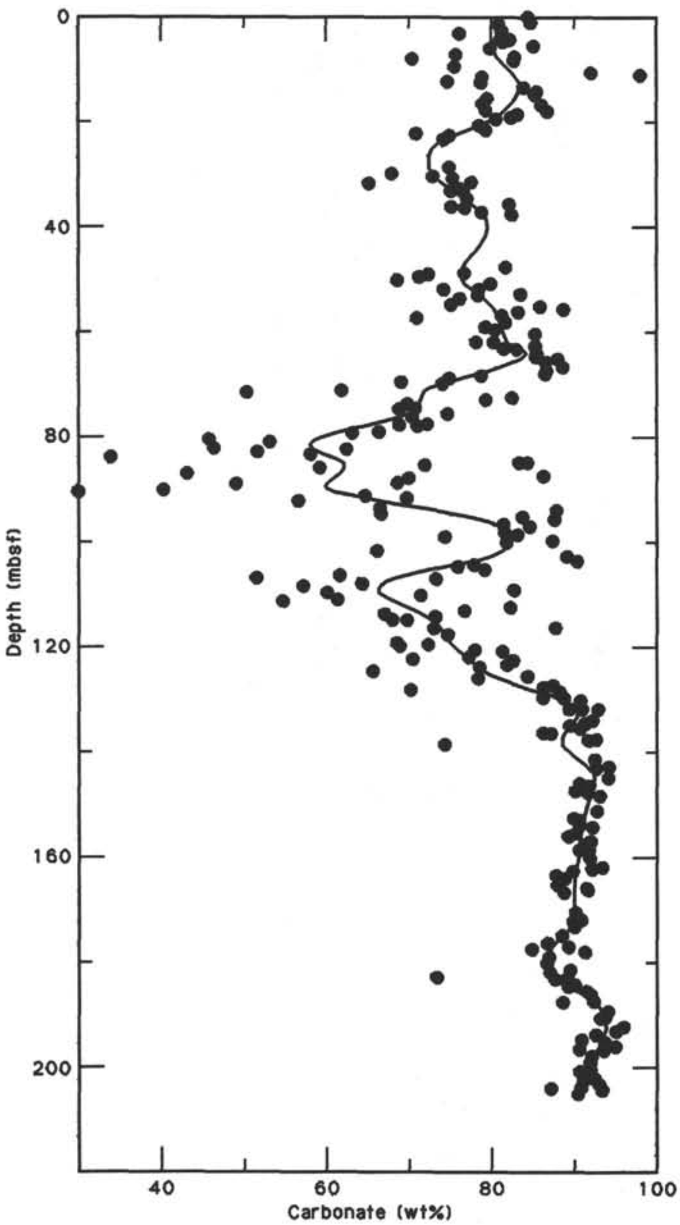

Figure 21. Low-resolution moving average calculated for carbonate values shown in Figure 20.

Table 6. Organic carbon analyses, Hole 710A.

Sample interval (cm)	Depth (mbsf)	Organic carbon (%)
115-710A-		
1H-3, 25-26	3.25	0.03
1H-6, 135-136	8.85	0.06
2H-3, 25-26	12.75	0.15
2H-6, 135-136	18.35	0.06
3H-3, 25-26	22.45	0.10
4H-3, 25-26	32.05	0.10
4H-6, 135-136	37.65	0.00
6H-3, 14-15	51.04	0.00
7H-3, 25-26	60.75	0.00
8H-3, 25-26	70.35	0.00
9H-3, 25-26	79.85	0.03
10H-3, 25-26	89.45	0.12
11H-3, 25-26	99.05	0.00
12H-3, 25-26	108.75	0.00
13H-3, 25-26	118.45	0.00
14X-3, 25-26	128.15	0.00
15X-3, 25-26	135.65	0.08
16X-3, 25-26	145.35	0.00
17X-3, 25-26	155.05	0.00
18X-3, 25-26	164.65	0.00
19X-3, 135-136	175.45	0.00
20X-3, 25-26	184.05	0.00
21X-3, 25-26	193.18	0.00
22X-3, 25-26	203.35	0.00

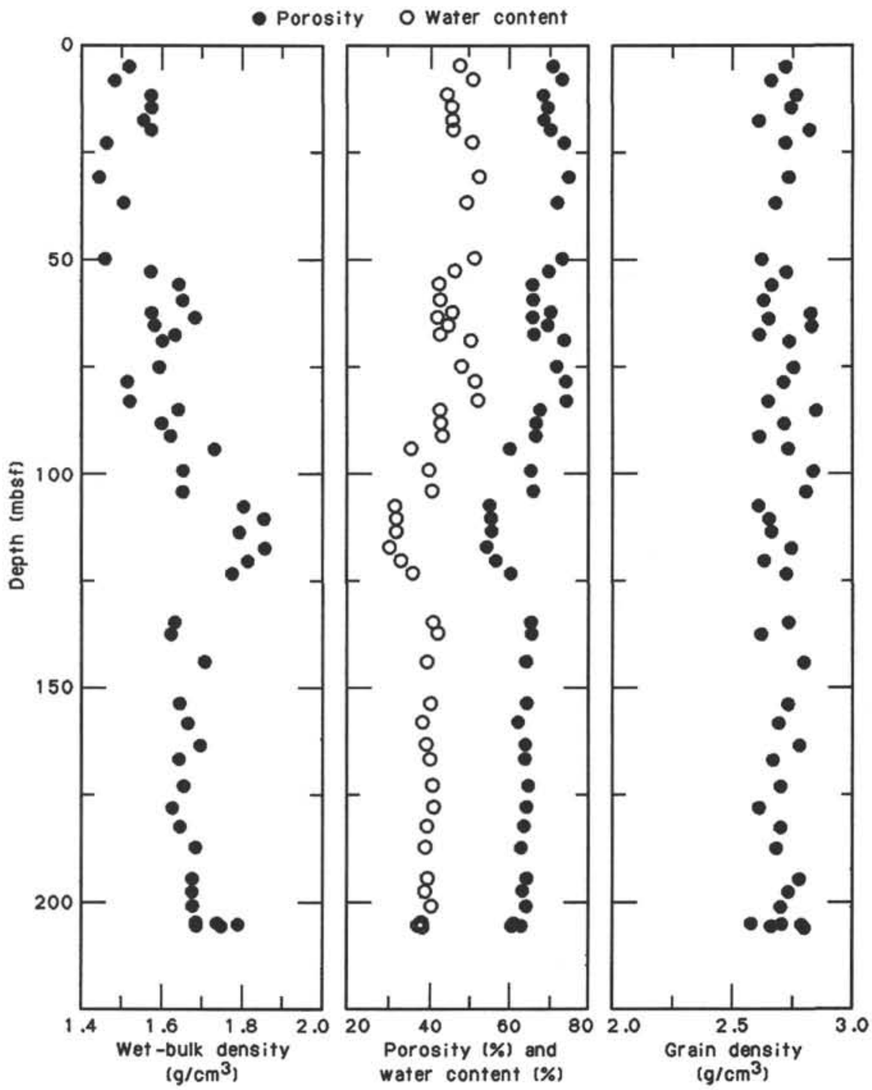

Figure 22. Index properties (wet-bulk density, water content, porosity, and grain density) at Hole 710A.

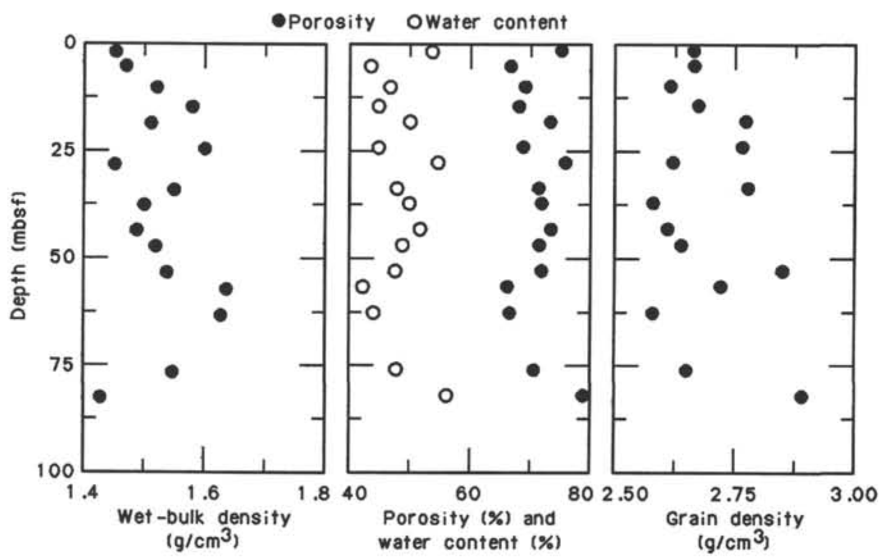

Figure 23. Index properties (wet-bulk density, water content, porosity, and grain density) at Hole 710B.

Table 7. Index-properties data, Site 710.

Section interval (cm)	Depth (mbsf)	Water content (%)	Porosity (%)	Wet-bulk density (g/cm^3)	Dry-bulk density (g/cm^3)	Grain density (g/cm^3)	Carbonate content (wt%)
115-710A-							
1H-4, 52	5.02	48.28	71.64	1.52	0.79	2.73	81.49
1H-6, 58	8.08	51.85	74.05	1.48	0.71	2.67	70.40
2H-2, 60	11.60	45.24	69.33	1.57	0.86	2.77	78.91
2H-4, 60	14.60	46.54	70.34	1.57	0.84	2.75	85.01
2H-6, 60	17.60	46.56	69.32	1.55	0.83	2.62	79.28
3H-1, 60	19.80	46.73	71.07	1.57	0.83	2.83	80.61
3H-3, 60	22.80	51.62	74.30	1.46	0.71	2.73	74.95
4H-2, 60	30.90	53.53	75.87	1.44	0.67	2.75	75.34
4H-6, 60	36.90	50.31	72.94	1.50	0.75	2.69	76.61
6H-2, 60	50.00	52.36	74.20	1.46	0.70	2.64	71.37
6H-4, 60	53.00	47.17	70.76	1.57	0.83	2.74	83.50
6H-6, 60	56.00	43.29	66.92	1.64	0.93	2.68	88.70
7H-2, 60	59.60	43.57	66.85	1.65	0.93	2.64	80.65
7H-4, 60	62.60	46.74	71.15	1.57	0.83	2.84	80.48
7H-5, 32	63.82	43.02	66.62	1.68	0.96	2.67	83.16
7H-6, 60	65.60	45.80	70.37	1.58	0.86	2.84	88.02
8H-1, 60	67.70	43.80	67.01	1.63	0.92	2.63	86.66
8H-2, 60	69.20	51.43	74.28	1.60	0.78	2.75	74.91
8H-6, 60	75.20	49.10	72.57	1.59	0.81	2.77	70.64
9H-2, 60	78.70	52.52	74.94	1.51	0.72	2.73	71.15
9H-5, 60	83.20	53.23	75.08	1.52	0.71	2.67	51.68
9H-6, 120	85.30	43.69	68.71	1.64	0.93	2.86	83.34
10H-2, 60	88.30	43.79	67.74	1.60	0.90	2.73	69.96
10H-4, 63	91.33	44.32	67.39	1.62	0.90	2.63	64.77
10H-6, 60	94.30	36.76	61.18	1.73	1.10	2.75	87.89
11H-3, 58	99.38	41.22	66.36	1.65	0.97	2.85	74.57
11H-6, 90	104.20	41.81	66.68	1.65	0.96	2.82	90.40
12H-2, 60	107.60	32.75	55.83	1.80	1.21	2.63	73.37
12H-4, 60	110.60	32.99	56.47	1.85	1.24	2.67	71.57
12H-6, 60	113.60	33.09	56.63	1.79	1.20	2.68	76.88
13H-2, 60	117.30	31.39	55.45	1.85	1.27	2.76	78.76
13H-4, 60	120.30	34.17	57.61	1.81	1.19	2.65	68.94
13H-6, 60	123.30	37.15	61.57	1.77	1.11	2.74	82.62
15X-2, 86	134.76	42.16	66.46	1.63	0.94	2.75	91.98
15X-4, 48	137.38	43.29	66.61	1.62	0.92	2.64	87.08
16X-2, 47	144.07	40.52	65.46	1.70	1.01	2.82	93.09
17X-2, 47	153.77	41.32	65.68	1.64	0.97	2.75	90.54
17X-5, 37	158.17	39.39	63.53	1.66	1.01	2.71	91.52
18X-2, 53	163.43	40.52	65.29	1.69	1.01	2.80	89.88
18X-4, 87	166.77	41.32	65.17	1.64	0.96	2.69	91.50
19X-2, 31	172.91	41.85	65.93	1.65	0.96	2.72	90.91
19X-5, 87	177.97	42.07	65.37	1.62	0.94	2.63	89.34
20X-2, 8	182.38	40.59	64.70	1.64	0.98	2.72	89.45
20X-5, 49	187.29	40.14	64.12	1.68	1.01	2.70	92.01
21X-4, 8	194.51	40.67	65.45	1.67	0.99	2.80	92.57
21X-6, 8	197.48	40.04	64.46	1.67	1.00	2.75	93.54
22X-1, 71	200.81	41.53	65.60	1.67	0.98	2.72	92.17
22X-4, 10	204.70	38.93	62.12	1.68	1.03	2.60	93.36
22X-4, 30	204.90	39.15	63.35	1.73	1.05	2.72	87.09
22X-4, 50	205.10	38.80	63.65	1.78	1.09	2.80	90.67
22X-4, 86	205.46	37.99	61.89	1.68	1.04	2.68	93.56
22X-4, 108	205.68	38.97	63.96	1.74	1.06	2.81	93.44
115-710B-							
1H-2, 49	1.99	53.88	75.49	1.45	0.67	2.66	77.21
1H-4, 84	5.34	43.51	66.98	1.47	0.83	2.66	83.71
2H-3, 78	10.28	46.77	69.45	1.52	0.85	2.61	82.70
2H-6, 63	14.63	45.03	68.36	1.58	0.87	2.67	81.02
3H-2, 60	18.30	50.27	73.51	1.51	0.75	2.77	82.00
3H-6, 60	24.30	45.01	69.05	1.60	0.88	2.76	86.99
4H-2, 60	27.90	55.06	76.08	1.45	0.65	2.62	89.09
4H-6, 60	33.90	48.13	71.76	1.55	0.80	2.77	68.43
5H-2, 60	37.40	50.28	72.10	1.50	0.75	2.58	76.47
5H-6, 60	43.40	52.06	73.78	1.49	0.72	2.61	69.21
6H-2, 60	47.00	49.05	71.57	1.52	0.78	2.64	78.56
6H-6, 60	53.00	47.83	72.13	1.54	0.81	2.85	82.87
7H-2, 60	56.60	42.60	66.61	1.64	0.94	2.72	85.66
7H-6, 60	62.60	44.53	67.17	1.63	0.90	2.58	80.75
9H-2, 60	75.90	48.32	71.07	1.55	0.80	2.65	76.01
9H-6, 60	81.90	56.78	79.02	1.43	0.62	2.89	52.49

Table 8. Compressional-wave velocity and acoustic impedance data, Site 710.

Section interval (cm)	Depth (mbsf)	V_p (m/s)	Acoustic impedance ($g/cm^2 \cdot s \cdot 10^4$)
115-710A-			
1H-4, 52	5.02	1510	22.95
1H-6, 58	8.08	1511	22.36
2H-2, 60	12.20	1499	23.53
2H-4, 60	15.20	1454	22.82
2H-6, 60	18.20	1491	23.11
3H-1, 60	20.30	1503	23.60
3H-3, 60	23.30	1502	21.93
4H-2, 60	31.50	1579	22.73
4H-6, 60	37.50	1494	22.41
6H-2, 60	50.80	1488	21.72
6H-4, 60	53.80	1494	23.45
6H-6, 60	56.80	1542	25.28
7H-2, 60	60.40	1526	25.17
9H-2, 60	79.70	1487	22.45
9H-6, 60	85.70	1493	22.69
10H-2, 60	89.40	1497	23.95
10H-6, 60	95.40	1526	26.39
11H-3, 58	100.48	1525	25.16
11H-6, 90	105.30	1575	25.98
12H-2, 60	108.70	1548	27.86
12H-4, 60	111.70	1561	28.87
12H-6, 60	114.70	1571	28.12
15X-4, 48	140.48	1520	24.62
16X-2, 47	147.17	1545	26.26
17X-5, 37	161.27	1533	25.44
19X-5, 87	177.67	1502	24.33
115-710B-			
1H-2, 49	1.99	1540	22.33
1H-4, 84	5.34	1490	21.90
2H-3, 78	13.28	1497	22.75
2H-6, 63	17.63	1497	23.65
3H-2, 60	21.30	1502	22.68
3H-5, 60	25.80	1504	24.06
4H-2, 60	30.90	1508	21.86
4H-6, 60	36.90	1526	23.65
5H-2, 60	40.40	1501	22.51
5H-6, 60	46.40	1502	22.38
6H-2, 60	50.00	1494	22.71
6H-6, 60	56.00	1508	23.22
7H-2, 60	59.60	1505	24.68
7H-6, 60	65.60	1533	24.98
9H-2, 60	78.70	1378	21.35
9H-6, 60	84.70	1402	20.04

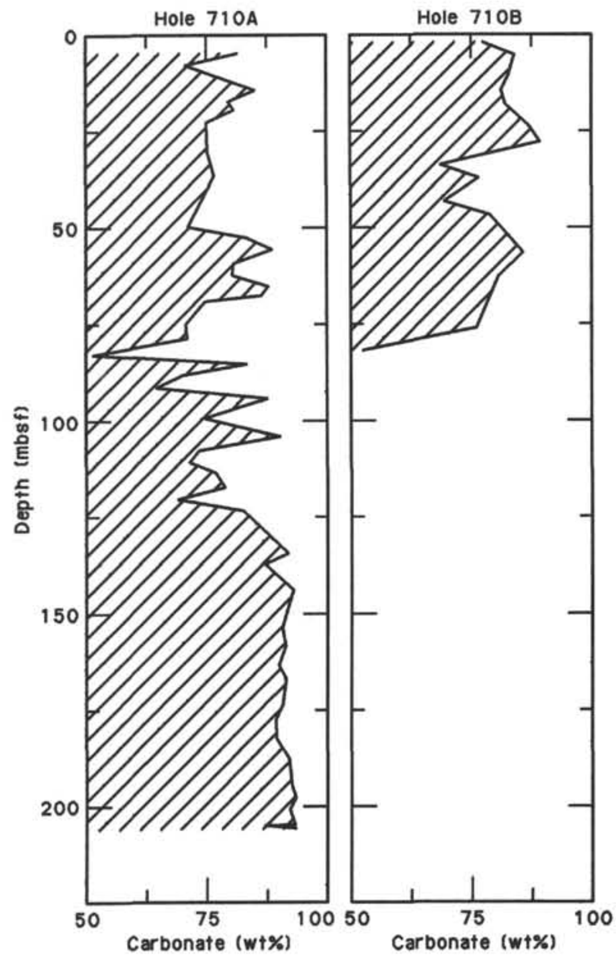

Figure 24. Carbonate content of samples for which the index properties were measured at Holes 710A and 710B.

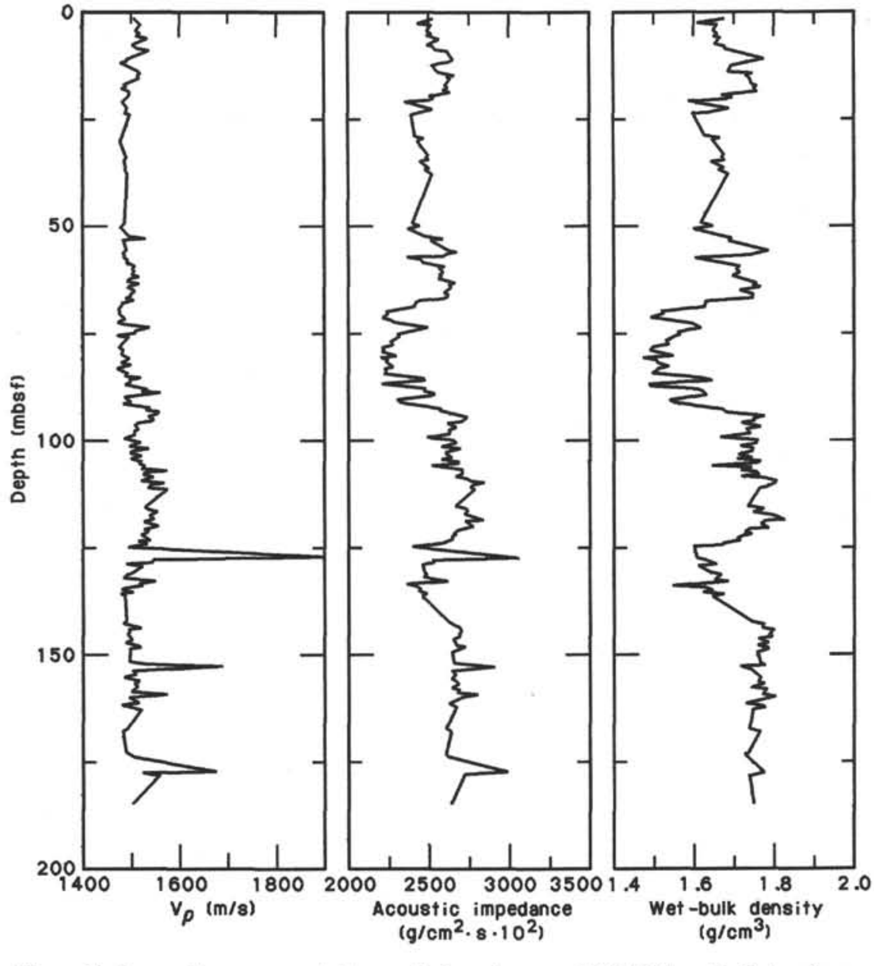

Figure 25. *P*-wave logger, computed acoustic impedance, and GRAPE wet-bulk density records (left to right) for Site 710.

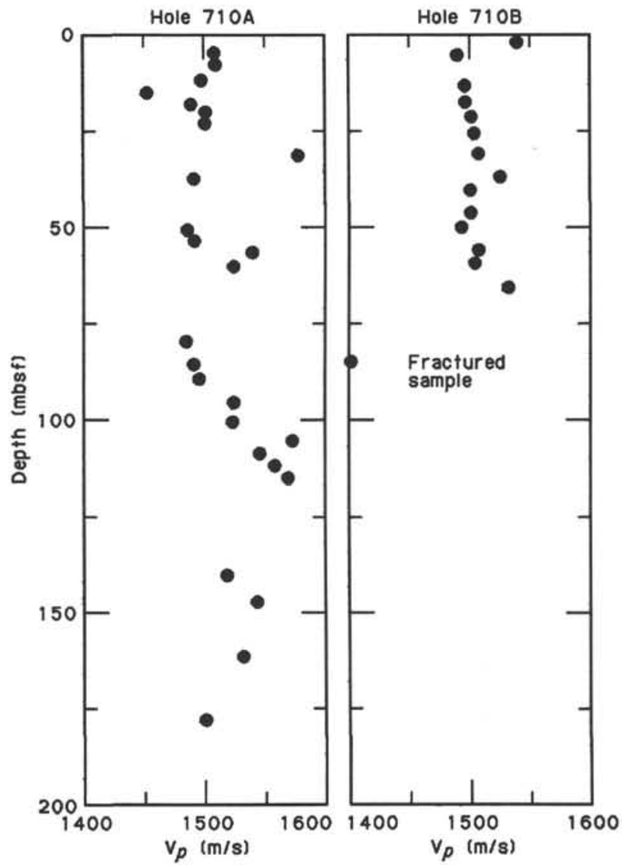

Figure 26. Compressional-wave velocity at Holes 710A and 710B.

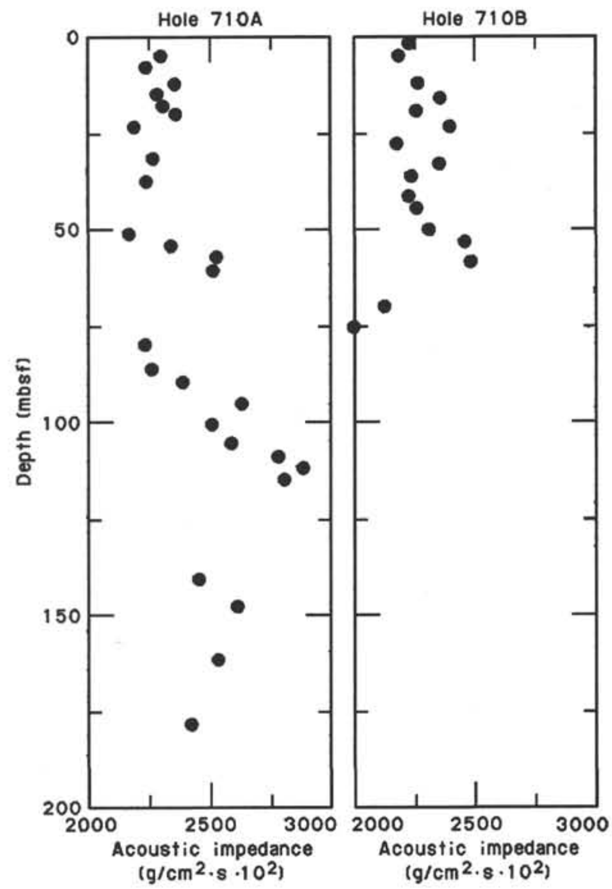

Figure 27. Acoustic impedance calculated from wet-bulk density and compressional-wave velocity of discrete samples at Holes 710A and 710B.

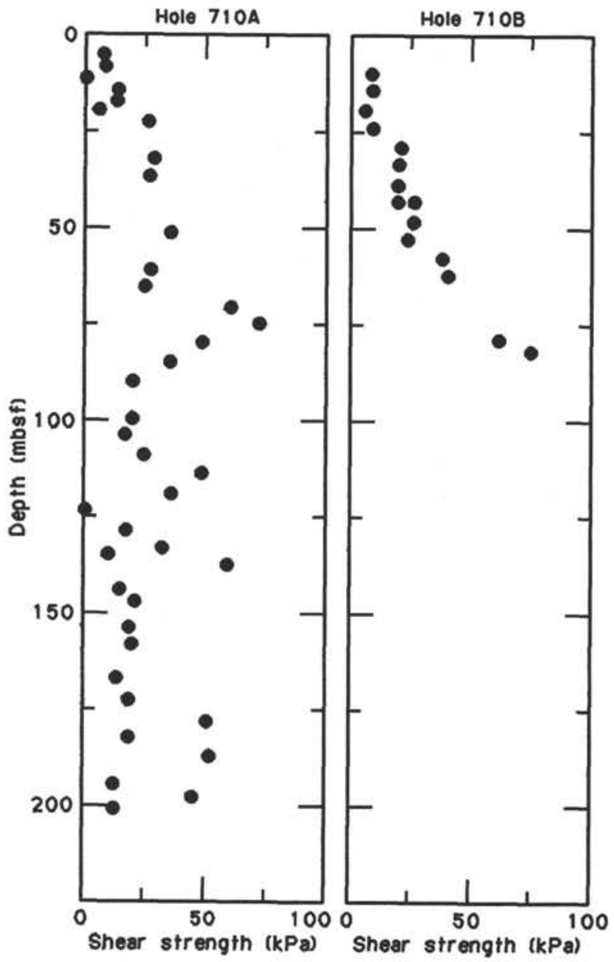

Figure 28. Measured shear strength on discrete samples from Holes 710A and 710B.

Table 9. Motorized shear strength data, Site 710.

Section interval (cm)	Depth (mbsf)	Peak (kPa)
115-710A-		
1H-4, 62	5.12	7.7
1H-6, 86	8.36	8.3
2H-2, 52	11.52	0.6
2H-4, 52	14.52	13.6
2H-6, 52	17.52	13.1
3H-1, 52	19.72	5.9
3H-3, 52	22.72	26.1
4H-3, 60	32.40	28.5
4H-6, 60	36.90	26.6
6H-3, 60	51.50	35.5
7H-3, 90	61.40	27.3
7H-6, 60	65.60	24.9
8H-3, 52	70.62	60.5
8H-6, 52	75.12	72.3
9H-3, 52	80.12	48.6
9H-6, 84	84.94	35.5
10H-3, 90	90.10	20.1
11H-3, 83	99.63	20.1
11H-6, 62	103.92	17.2
12H-3, 66	109.16	24.9
12H-6, 80	113.80	48.6
13H-3, 70	118.90	36.2
13H-6, 70	123.40	100.8
14X-3, 75	128.65	17.8
14X-6, 75	133.15	32.6
15X-2, 92	134.82	10.6
15X-4, 56	137.46	59.3
16X-2, 56	144.16	15.4
16X-4, 54	147.14	21.4
17X-2, 53	153.83	19.0
17X-5, 56	158.36	20.1
18X-4, 95	166.85	14.2
19X-2, 37	172.97	19.0
19X-5, 94	178.04	51.0
20X-2, 15	182.45	19.0
20X-5, 55	187.35	52.2
21X-4, 19	194.62	13.1
21X-6, 17	197.57	45.0
22X-1, 73	200.83	13.1
115-710B-		
2H-3, 50	10.00	8.3
2H-6, 48	14.48	8.8
3H-3, 50	19.70	5.9
3H-6, 50	24.20	8.9
4H-3, 50	29.30	20.8
4H-6, 50	33.80	20.1
5H-3, 65	38.95	19.5
5H-6, 65	43.45	19.5
5H-6, 65	43.45	26.1
6H-3, 65	48.55	26.0
6H-6, 43	52.83	23.7
7H-3, 40	57.90	38.0
7H-6, 40	62.40	40.3
9H-4, 65	78.95	61.7
9H-6, 45	81.75	74.7

Table 10. Thermal conductivity data, Site 710.

Section interval (cm)	Depth (mbsf)	Thermal conductivity $(W \cdot m^{-1} \cdot K^{-1})$
115-710A-		
1H-1, 80	0.80	1.030
1H-2, 80	2.30	0.988
1H-3, 80	3.80	1.134
1H-4, 70	5.20	1.206
1H-4, 80	5.30	1.094
1H-5, 70	6.70	1.141
1H-5, 80	6.80	1.052
2H-1, 80	10.30	0.917
2H-2, 70	11.70	1.762
2H-2, 80	11.80	1.246
2H-3, 70	13.20	1.249
2H-3, 80	13.30	1.126
3H-1, 80	20.00	1.235
3H-2, 80	21.50	1.223
3H-3, 70	22.90	1.136
4H-1, 80	29.60	1.079
4H-3, 80	32.60	1.043
4H-4, 80	34.10	1.042
4H-5, 80	35.60	1.165
4H-6, 80	37.10	1.129
4H-7, 40	38.20	1.193
6H-1, 80	48.70	1.222
6H-2, 80	50.20	0.950
6H-3, 80	51.70	1.118
6H-4, 80	53.20	1.172
6H-5, 80	54.70	1.141
6H-6, 80	56.20	1.139
6H-7, 20	57.10	1.309
7H-1, 80	58.30	1.153
7H-2, 80	59.80	1.242
7H-3, 80	61.30	1.001
7H-4, 80	62.80	1.199
7H-5, 20	63.70	1.146
7H-5, 30	63.80	1.323
7H-5, 40	63.90	1.400
7H-5, 50	64.00	1.364
7H-5, 60	64.10	1.435
7H-5, 70	64.20	1.212
7H-5, 80	64.30	1.386
7H-5, 90	64.40	1.285
7H-5, 100	64.50	1.365
7H-5, 110	64.60	1.255
7H-5, 130	64.80	1.206
7H-5, 140	64.90	1.299
7H-6, 80	65.80	1.235
7H-7, 20	66.68	1.291
8H-1, 80	67.90	1.252
8H-2, 80	69.40	0.964
8H-3, 80	70.90	1.118
8H-4, 80	72.40	1.237
8H-5, 90	74.00	1.247
8H-6, 80	75.40	1.279
9H-2, 80	78.90	1.115
9H-3, 80	80.40	1.235
9H-4, 80	81.90	1.070
9H-5, 10	82.70	1.603
9H-5, 20	82.80	1.128
9H-5, 30	82.90	1.132
9H-5, 40	83.00	1.053
9H-5, 50	83.10	1.059
9H-5, 60	83.20	0.814
9H-5, 70	83.30	1.083
9H-5, 80	83.40	1.049
9H-5, 90	83.50	1.175
9H-5, 100	83.60	1.135
9H-5, 110	83.70	1.068
9H-6, 80	84.90	1.147
9H-7, 40	86.00	1.175
10H-1, 80	87.00	1.024
10H-2, 80	88.50	1.232
10H-3, 80	90.00	1.191
10H-4, 80	91.50	1.188
10H-5, 80	93.00	1.322
10H-7, 40	95.60	1.394

Table 10 (continued).

Section interval (cm)	Depth (mbsf)	Thermal conductivity $(W \cdot m^{-1} \cdot K^{-1})$
115-710A-		
11H-1, 80	96.60	1.392
11H-2, 80	98.10	1.343
11H-3, 80	99.60	1.402
11H-4, 80	101.10	1.388
11H-5, 80	102.60	1.378
11H-6, 80	104.10	1.272
11H-7, 30	105.10	0.918
12H-1, 80	106.30	1.234
12H-2, 80	107.80	1.371
12H-3, 80	109.30	1.517
12H-4, 80	110.80	1.379
12H-5, 80	112.30	0.865
12H-6, 80	113.80	1.517
12H-7, 40	114.90	1.379
13H-1, 80	116.00	1.068
13H-2, 80	117.50	1.391
13H-3, 80	119.00	1.667
13H-4, 80	120.50	1.369
13H-5, 80	122.00	1.446
13H-6, 10	122.80	1.107
13H-6, 20	122.90	1.253
13H-6, 30	123.00	1.061
13H-6, 40	123.10	1.362
13H-6, 50	123.20	1.109
13H-6, 60	123.30	1.220
13H-6, 70	123.40	1.260
13H-6, 80	123.50	0.961
13H-6, 90	123.60	0.708
13H-6, 100	123.70	1.342
13H-6, 110	123.80	1.382
13H-6, 120	123.90	1.400
13H-6, 130	124.00	1.305
13H-6, 140	124.10	1.065
13H-7, 30	124.50	1.324
14X-1, 80	125.70	1.067
14X-2, 80	127.20	1.276
14X-3, 80	128.70	1.334
14X-4, 80	130.20	1.205
14X-5, 80	131.70	1.359
14X-6, 80	132.50	1.013
15X-1, 80	133.20	1.339
15X-2, 80	134.70	1.012
15X-3, 80	136.20	1.384
15X-4, 80	137.70	1.305
15X-5, 80	139.20	0.756
16X-1, 80	142.90	1.323
16X-2, 80	144.40	1.115
16X-3, 80	145.90	1.284
16X-4, 80	147.40	1.408
16X-5, 80	148.90	1.133
17X-1, 80	152.60	1.100
17X-2, 80	154.10	1.257
17X-3, 95	155.75	1.024
17X-4, 80	157.10	1.242
17X-5, 80	158.60	1.328
17X-6, 80	160.10	0.953
18X-1, 80	162.20	1.368
18X-2, 80	163.70	0.779
18X-3, 80	165.20	1.343
18X-4, 80	166.70	1.375
18X-5, 80	168.20	0.961
19X-1, 80	171.90	1.205
19X-3, 80	174.90	1.032
19X-4, 80	176.40	1.322
19X-5, 80	177.90	1.179
19X-6, 95	179.55	1.388
20X-1, 80	181.60	0.803
20X-2, 90	183.20	1.277
20X-3, 80	184.60	0.953
20X-4, 80	186.10	1.248
20X-5, 80	187.60	1.401
20X-6, 80	189.10	1.110
21X-1, 80	191.20	1.341
21X-2, 80	192.23	1.514
21X-3, 80	193.73	1.344

Table 10 (continued).

Section interval (cm)	Depth (mbsf)	Thermal conductivity ($W \cdot ^{-1} \cdot K^{-1}$)
115-710A-		
21X-4, 80	195.23	1.521
21X-5, 80	196.73	0.952
21X-6, 80	198.20	1.343
22X-1, 80	200.90	0.940
22X-2, 80	202.40	1.292
22X-3, 80	203.90	1.413
22X-4, 10	204.70	0.960
22X-4, 20	204.80	1.326
22X-4, 30	204.90	1.144
22X-4, 40	205.00	1.312
22X-4, 50	205.10	1.247
22X-4, 60	205.20	0.895
22X-4, 70	205.30	1.414
22X-4, 80	205.40	0.711
22X-4, 90	205.50	1.402
22X-4, 100	205.60	1.375
22X-4, 110	205.70	1.239
22X-5, 25	206.01	1.376

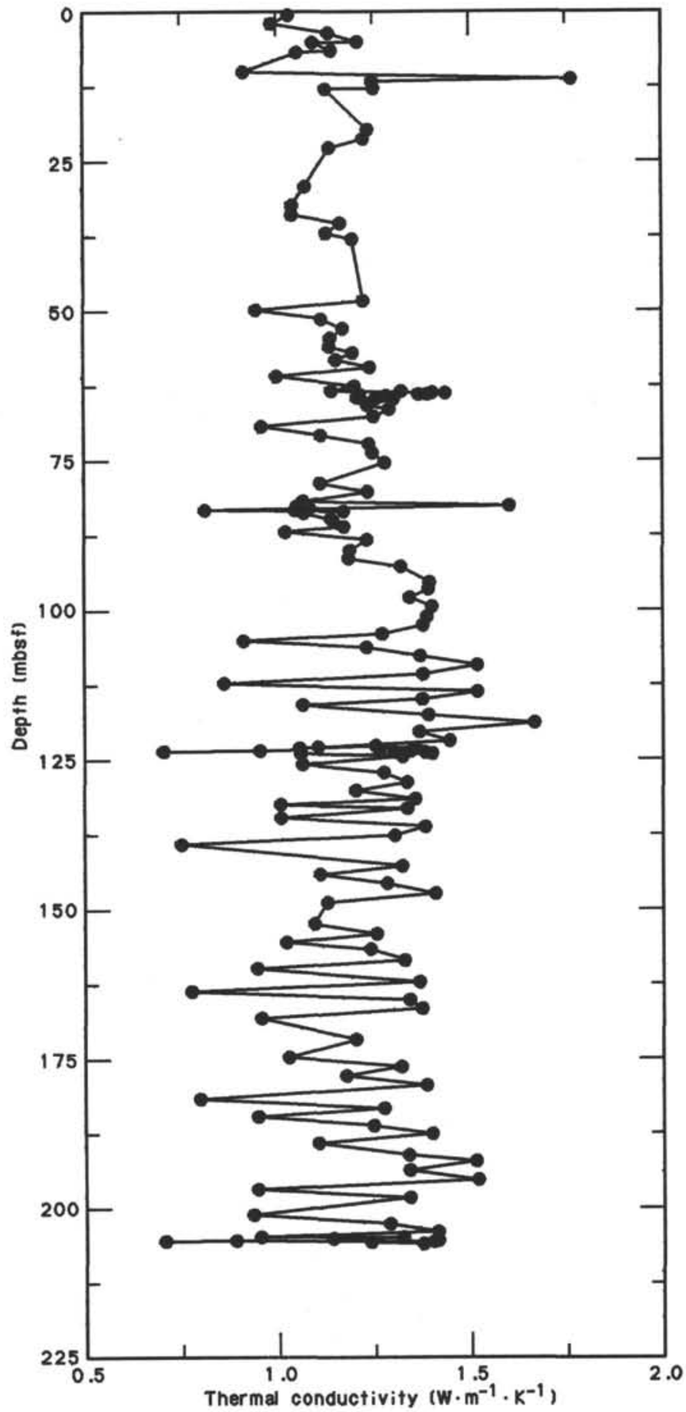

Figure 29. Thermal conductivity at Site 710.

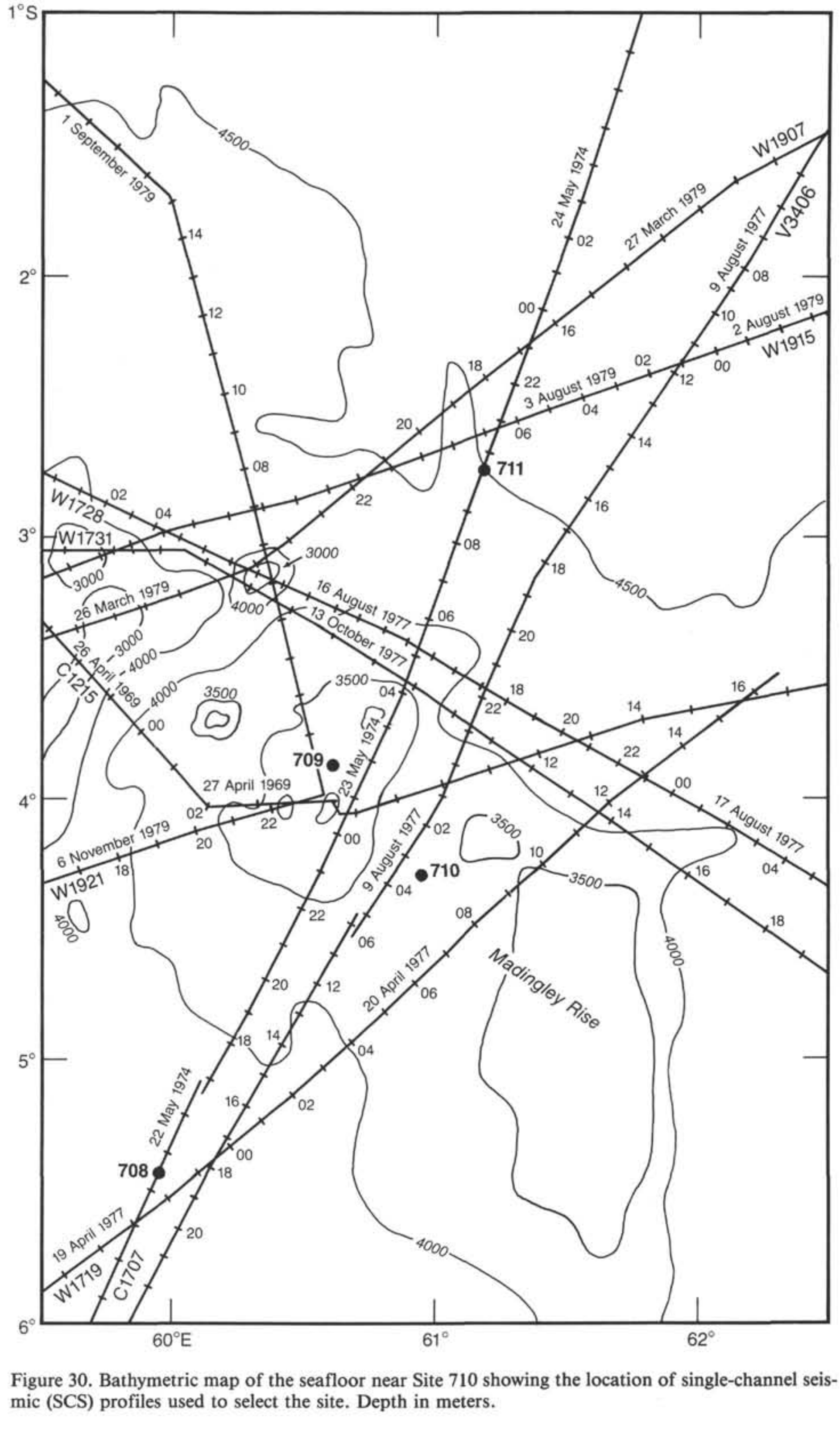

Figure 30. Bathymetric map of the seafloor near Site 710 showing the location of single-channel seismic (SCS) profiles used to select the site. Depth in meters.

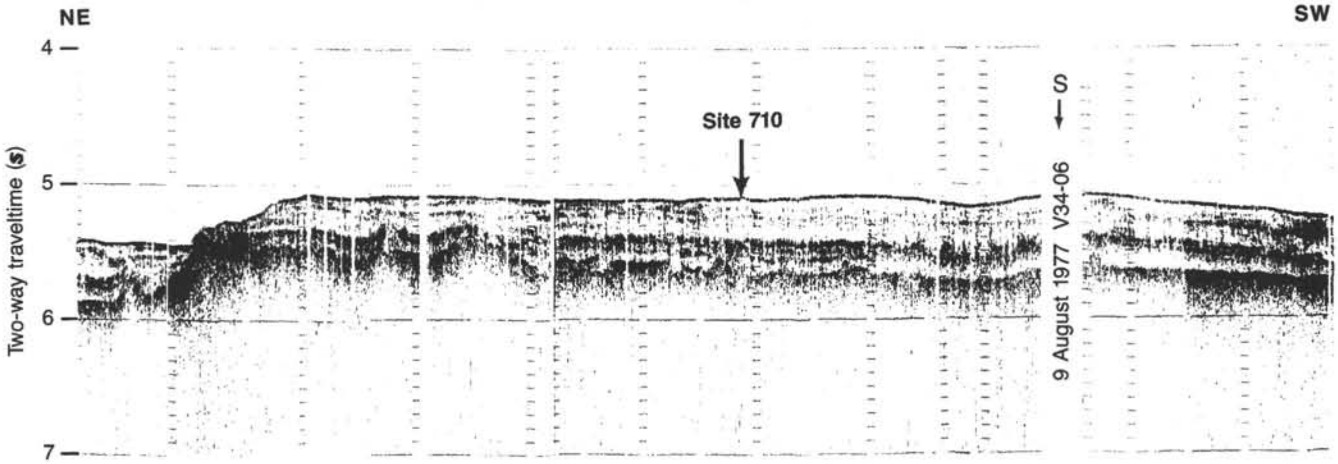

Figure 31. The V34-06 cruise SCS line (9 August 1977) on which we located Site 710. The basement is an irregular surface, probably ocean crust. A prominent reflector occurs at about 0.32 s below the sediment surface and may be a chert horizon, similar to those encountered at Site 707.

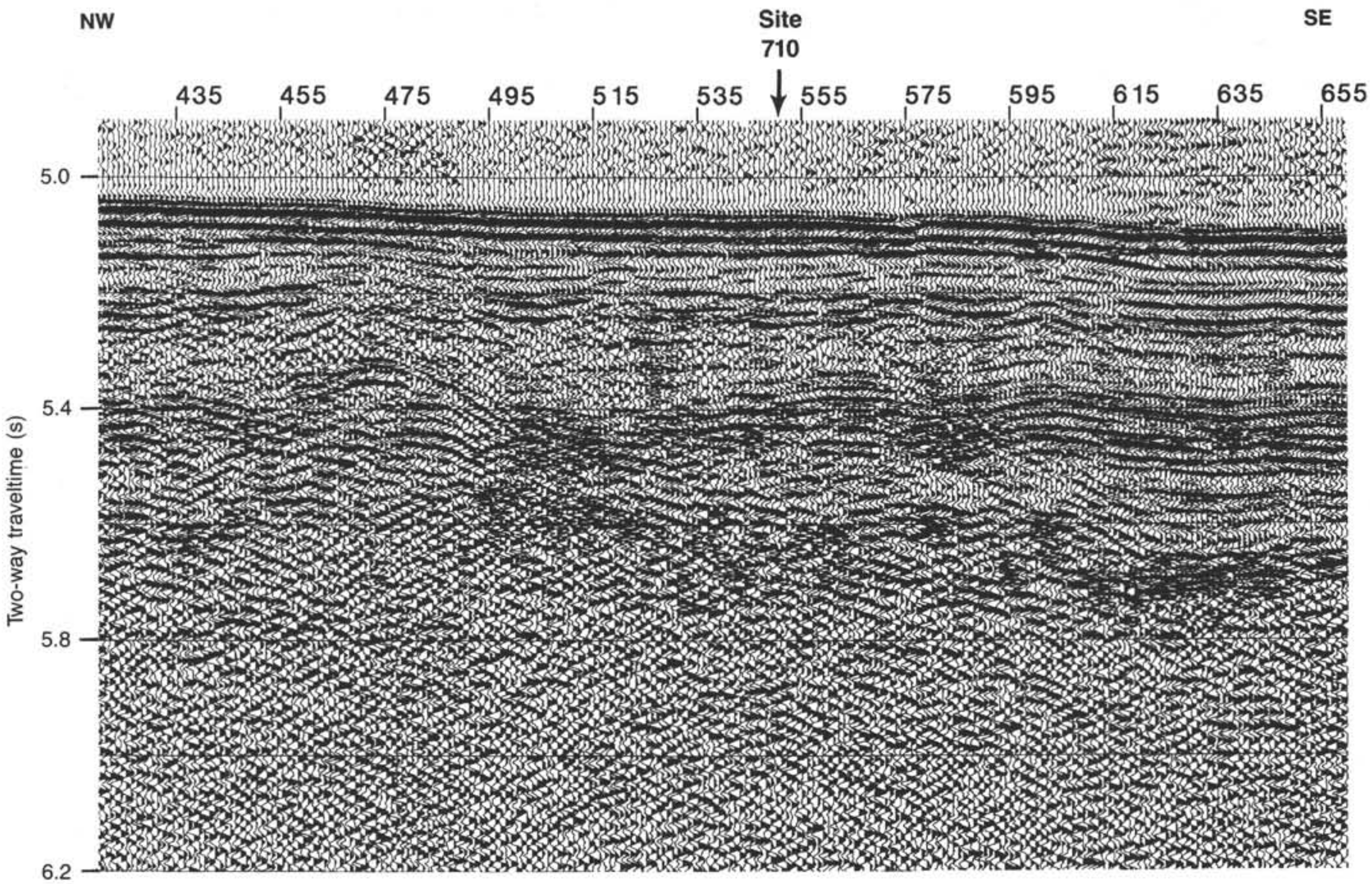

Figure 32. The *JOIDES Resolution* single-channel seismic (SCS), water-gun reflection profile recorded 8 June 1987 over Site 710.

SITE 710 HOLE A CORE 1H CORED INTERVAL 3812.0-3822.0 mbsl; 0.0-9.5 mbsf

TIME-ROCK UNIT | BIOSTRAT. ZONE/FOSSIL CHARACTER: FORAMINIFERS, NANNOFOSSILS, RADIOLARIANS, DIATOMS | PALEOMAGNETICS | PHYS. PROPERTIES | CHEMISTRY | SECTION | METERS | GRAPHIC LITHOLOGY | DRILLING DISTURB. | SED. STRUCTURES | SAMPLES | LITHOLOGIC DESCRIPTION

Time-rock unit: PLEISTOCENE

Foraminifers: N 21; AM

Nannofossils: CN 14b (NN 20); CN 14a (NN 19); AM

Radiolarians: *Collosphaera tuberosa*; *Amphirhopalum ypsilon*; CM

Diatoms: *P. doliolus*; RM; *N. reinholdii*; CM

Sections: 1, 2, 3, 4, 5, 6, 7, CC

Meters: 0.5, 1.0

Samples: IW

CLAY-BEARING NANNOFOSSIL OOZE

Major lithology: Clay-bearing nannofossil ooze, very pale brown (10YR 7/3), light gray (10YR 7/2), light brownish gray (10YR 6/2), and white (10YR 8/2); numerous color changes with gradational and indistinct contacts. Mottling and bioturbation common. Oxidized.

Minor lithology: Turbidites, foraminifer-nannofossil ooze, white (10YR 9/2), sharp basal contacts, gradational upper contacts, grading from fine sand at base to silt at top. Section 2, 108-110 cm, and Section 7, 21 cm, to CC, 4 cm.

29 color changes and 2 turbidites.

SMEAR SLIDE SUMMARY (%):

	1, 111 D	3, 31 D	5, 98 D
TEXTURE:			
Silt	10	5	5
Clay	90	95	95
COMPOSITION:			
Feldspar	Tr	—	—
Clay	—	5	5
Foraminifers	3	1	2
Nannofossils	80	82	83
Diatoms	6	4	4
Radiolarians	6	4	4
Sponge spicules	4	3	2
Silicoflagellates	1	1	Tr

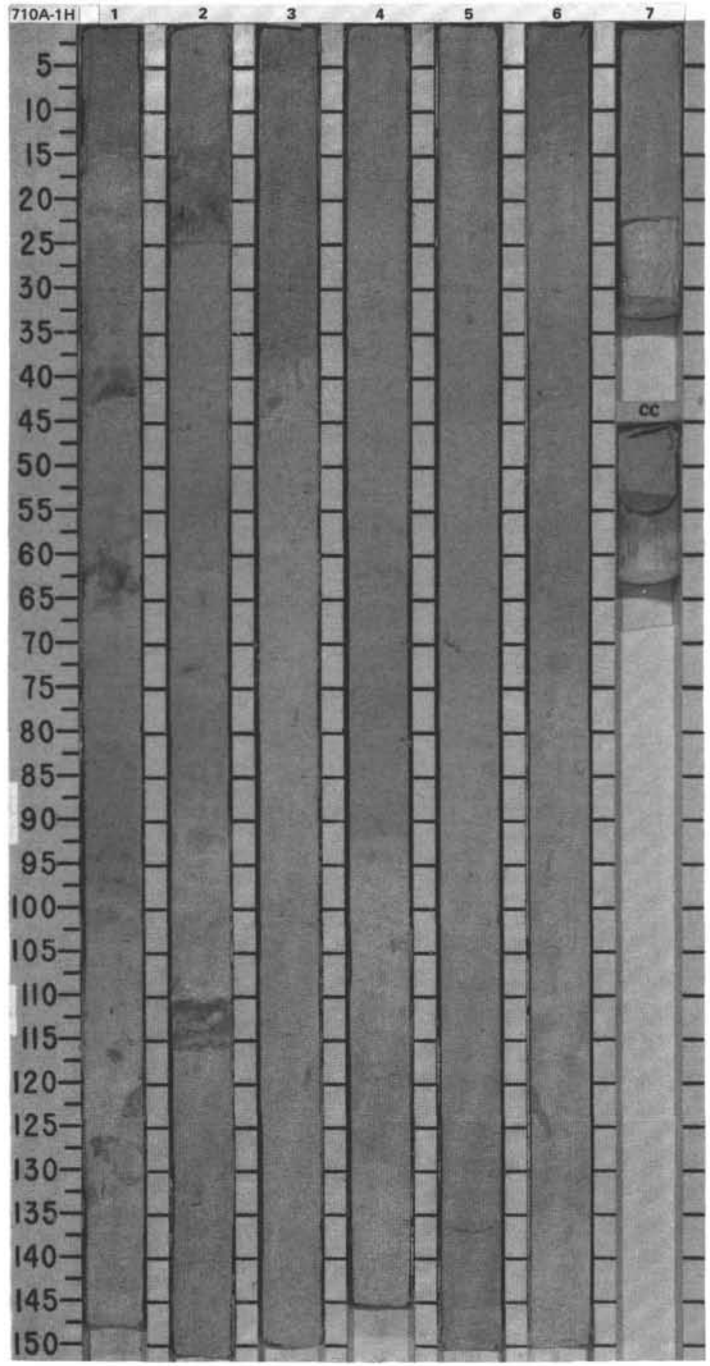

SITE 710 HOLE A CORE 2H CORED INTERVAL 3822.0-3831.7 mbsl; 9.5-19.2 mbsf

TIME-ROCK UNIT	FORAMINIFERS	NANNOFOSSILS	RADIOLARIANS	DIATOMS	PALEOMAGNETICS	PHYS. PROPERTIES	CHEMISTRY	SECTION	METERS	GRAPHIC LITHOLOGY	DRILLING DISTURB.	SED. STRUCTURES	SAMPLES
PLEISTOCENE	N 21	CN 13 - CN 14a (NN 19)	*Anthocyrtidium angulare*	*N. reinholdii* / AM				1	0.5, 1.0				*
								2					*
								3					
								4					IW
UPPER PLIOCENE				*R. praebergonii*				5					
			P. prismatium					6					
	AP	AG CN 12d	CG	FP				7, CC					

LITHOLOGIC DESCRIPTION

CLAY-BEARING NANNOFOSSIL OOZE

Major lithology: Clay-bearing nannofossil ooze, white (10YR 8/2) with slightly darker layers of very light gray (10YR 7.5/2); color alterations are assumed to be carbonate cycles. Bioturbated throughout, oxidized.

Minor lithology: Turbidites, foraminifer-nannofossil ooze, white (10YR 9/2), sharp basal contacts, gradational upper contacts, normally graded. Section 1, 57-61 and 128-144 cm; Section 2, 14-20 cm; Section 6, 20-25 cm; and CC, 4-5 and 8-9 cm.

37 color changes and 6 turbidites.

SMEAR SLIDE SUMMARY (%):

	1, 80 D	2, 19 M
TEXTURE:		
Sand	5	25
Silt	15	5
Clay	80	65
COMPOSITION:		
Quartz	—	Tr
Dolomite	Tr	Tr
Foraminifers	4	30
Nannofossils	82	65
Diatoms	5	1
Radiolarians	5	4
Sponge spicules	2	Tr
Silicoflagellates	2	—
Fish remains	—	Tr

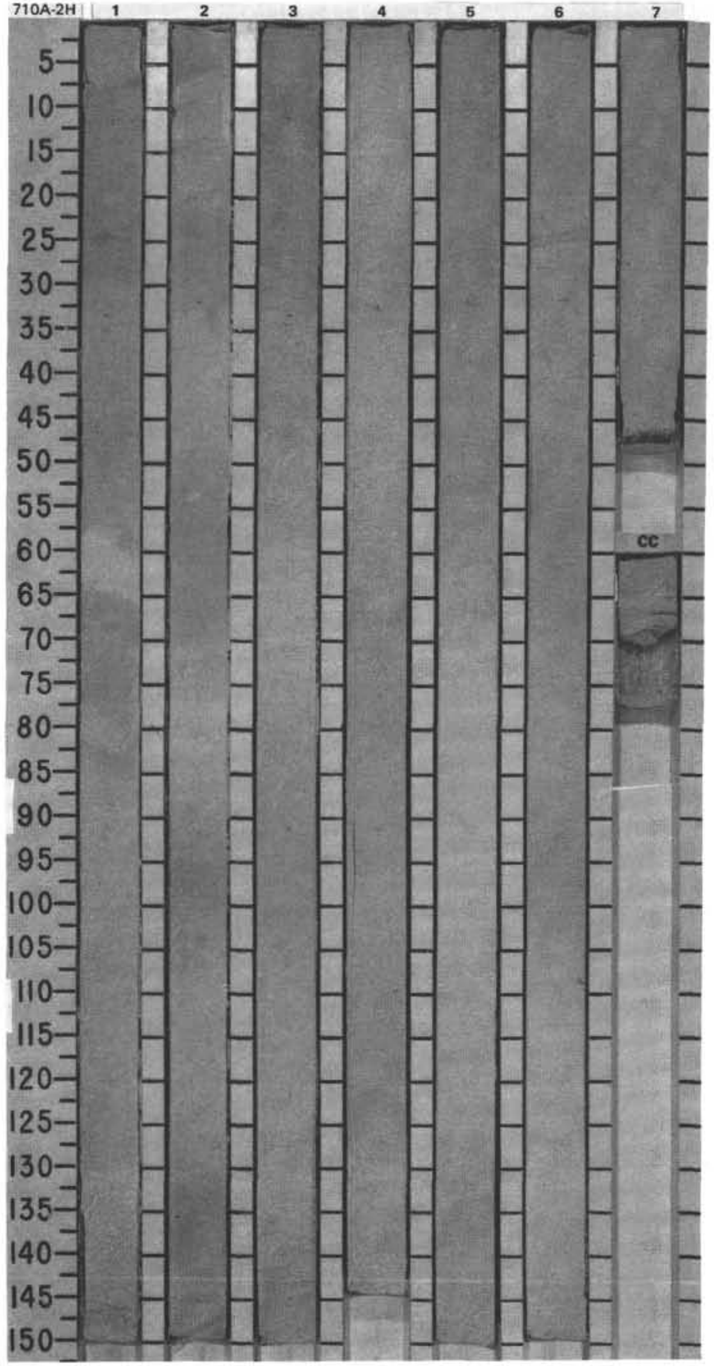

SITE 710 HOLE A CORE 3H CORED INTERVAL 3831.7-3841.3 mbsl; 19.2-28.8 mbsf

TIME-ROCK UNIT	FORAMINIFERS	NANNOFOSSILS	RADIOLARIANS	DIATOMS	PALEOMAGNETICS	PHYS. PROPERTIES	CHEMISTRY	SECTION	METERS	GRAPHIC LITHOLOGY	DRILLING DISTURB.	SED. STRUCTURES	SAMPLES
UPPER PLIOCENE	CP N 19 - N 18	AM CN 12a+b+c (NN 16 - NN 17)	CG *S. pentas* / *P. prismatium*	CM *N. jouseae* / *R. praebergonii* FP				1, 2, 3, CC	0.5, 1.0				*, IW, OG

(BIOSTRAT. ZONE/ FOSSIL CHARACTER)

LITHOLOGIC DESCRIPTION

CLAY-BEARING NANNOFOSSIL OOZE

Major lithology: Clay-bearing nannofossil ooze, white (10YR 8/2) and very light gray (10YR 7.5/2), interbedded with subtle contacts. Often bioturbated, oxidized. Section 1, 56-79 cm, contains many large benthic foraminifers.

Minor lithology: Foraminifer-nannofossil ooze, turbidite, white (10YR 9/2), sharp basal contact, gradational upper contact, normally graded. Section 3, 80-85 cm.

14 color changes and 1 turbidite.

SMEAR SLIDE SUMMARY (%):

	1, 87 D
TEXTURE:	
Sand	5
Silt	15
Clay	80
COMPOSITION:	
Quartz	Tr
Feldspar	Tr
Dolomite	Tr
Foraminifers	3
Nannofossils	81
Diatoms	5
Radiolarians	8
Sponge spicules	2
Silicoflagellates	1

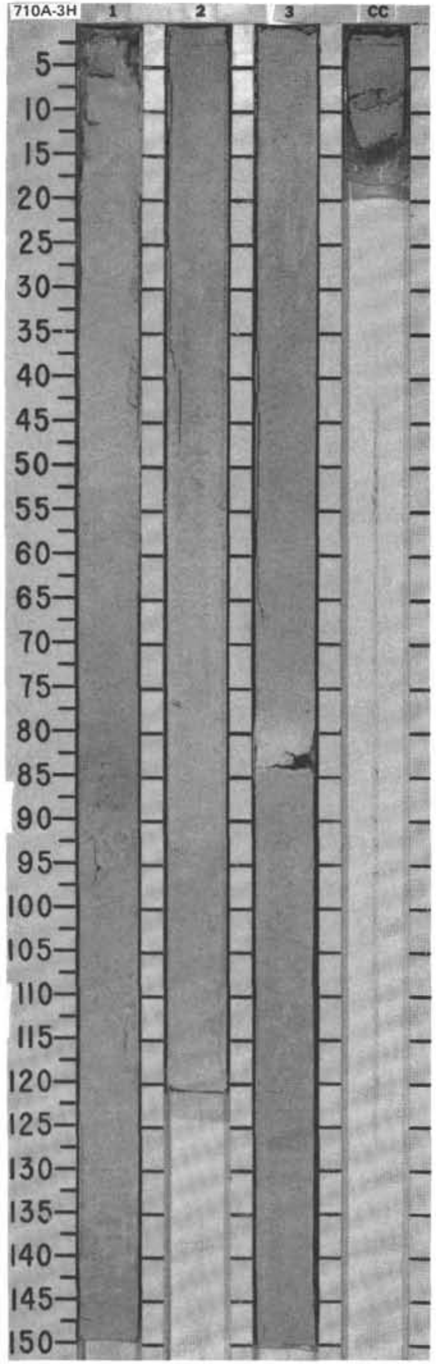

SITE 710 HOLE A CORE 4H CORED INTERVAL 3841.3-3850.8 mbsl; 28.8-38.3 mbsf

TIME-ROCK UNIT	FORAMINIFERS	NANNOFOSSILS	RADIOLARIANS	DIATOMS	PALEOMAGNETICS	PHYS. PROPERTIES	CHEMISTRY	SECTION	METERS	GRAPHIC LITHOLOGY	DRILLING DISTURB.	SED. STRUCTURES	SAMPLES
LOWER PLIOCENE	N 19 - N 18 (CP)	CN 10c - CN 11 (NN 13 - NN 15)	*Spongaster pentas* (CG)	*N. jouseae* (CM)				1, 2, 3, 4, 5, 6, 7, CC	0.5, 1.0				* (Section 1); IW (Section 4)

BIOSTRAT. ZONE/ FOSSIL CHARACTER

LITHOLOGIC DESCRIPTION

CLAY-BEARING NANNOFOSSIL OOZE

Major lithology: Clay-bearing nannofossil ooze, white (10YR 8/2) and light gray (10YR 7/2), interbedded with subtle contacts. Bioturbated throughout, oxidized.

Minor lithology: Foraminifer-nannofossil ooze, turbidite, white (10YR 9/2), sharp basal contact, gradational upper contact, normally graded. Section 2, 41-46 cm.

38 color changes and 1 turbidite.

SMEAR SLIDE SUMMARY (%):

	1, 80 D
TEXTURE:	
Sand	10
Silt	10
Clay	80
COMPOSITION:	
Quartz	Tr
Clay	1
Foraminifers	3
Nannofossils	80
Diatoms	5
Radiolarians	8
Sponge spicules	2
Silicoflagellates	1

710 A 5H NO RECOVERY

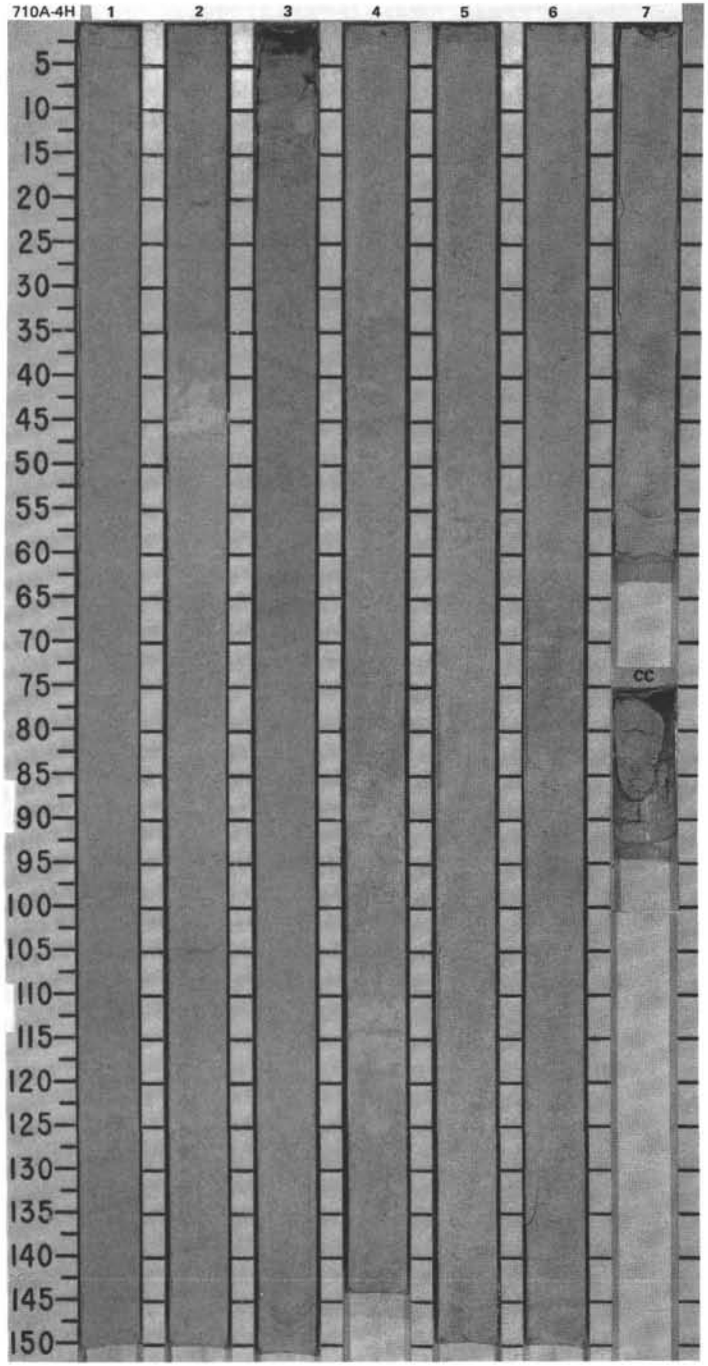

SITE 710 HOLE A CORE 6H CORED INTERVAL 3860.4-3870.0 mbsl; 47.9-57.5 mbsf

TIME-ROCK UNIT	FORAMINIFERS	NANNOFOSSILS	RADIOLARIANS	DIATOMS	PALEOMAGNETICS	PHYS. PROPERTIES	CHEMISTRY	SECTION	METERS	GRAPHIC LITHOLOGY	DRILLING DISTURB.	SED. STRUCTURES	SAMPLES
UPPER MIOCENE	N 17 / CP	CN 9b (NN 11) / AM	*Stichocorys peregrina* / FM	*T. convexa* / FM; *N. miocenica* / RP				1, 2, 3, 4, 5, 6, 7, CC	0.5, 1.0				* (Section 1); IW OG (Section 4)

BIOSTRAT. ZONE/FOSSIL CHARACTER

LITHOLOGIC DESCRIPTION

CLAY-BEARING NANNOFOSSIL OOZE

Major lithology: Clay-bearing nannofossil ooze, light greenish gray (5GY 7/1, 8/1), interbedded with subtle contacts, bioturbated. Some pyrite staining, reduced.

Minor lithology: Clay-bearing nannofossil ooze, pale green (5G 8/2) lamina. May be an altered ash. Section 3, 48 cm.

34 color changes and 0 turbidites.

SMEAR SLIDE SUMMARY (%):

	1, 80 D
TEXTURE:	
Sand	2
Silt	8
Clay	90
COMPOSITION:	
Feldspar	Tr
Dolomite	Tr
Foraminifers	1
Nannofossils	90
Diatoms	2
Radiolarians	5
Sponge spicules	1
Silicoflagellates	1

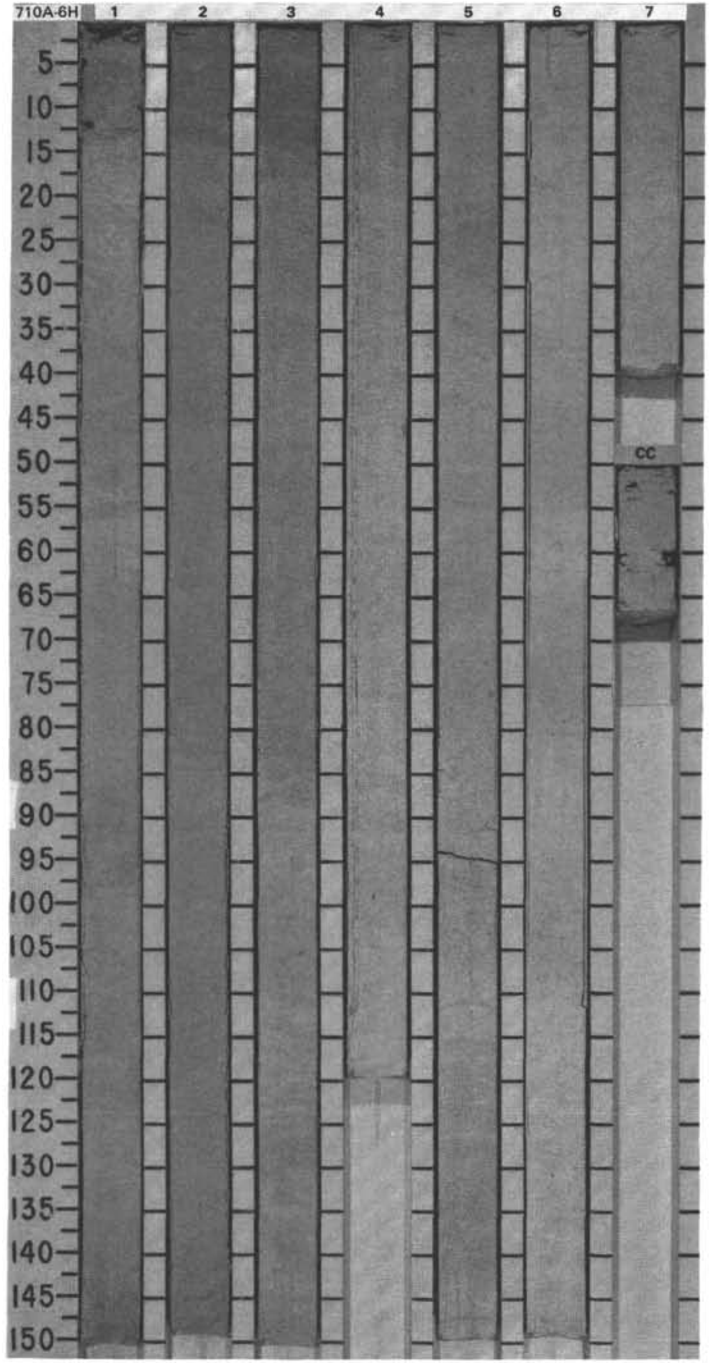

SITE 710 HOLE A CORE 7H CORED INTERVAL 3870.0-3879.6 mbsl; 57.5-67.1 mbsf

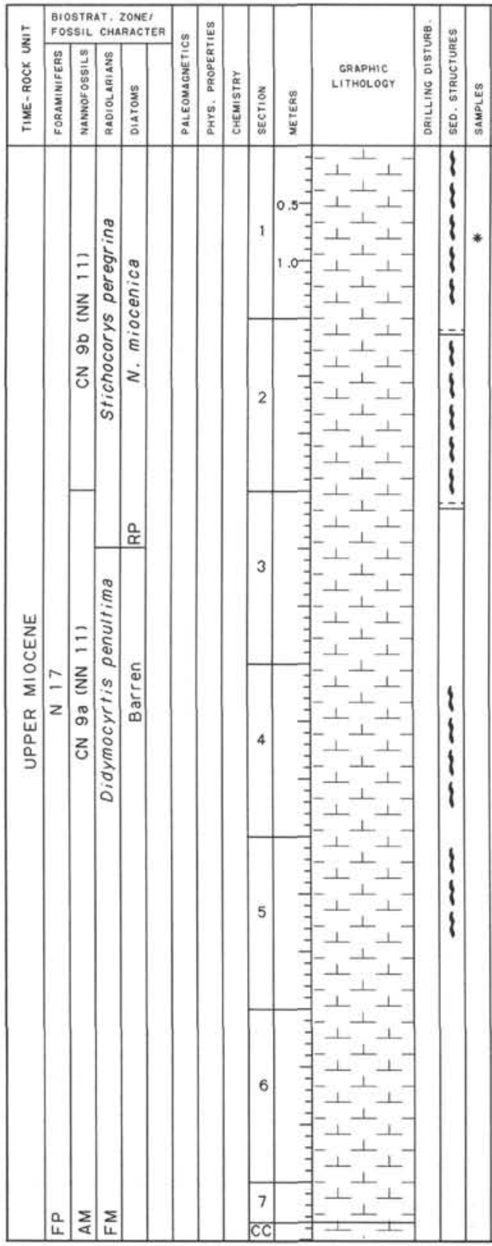

LITHOLOGIC DESCRIPTION

CLAY-BEARING NANNOFOSSIL OOZE

Major lithology: Clay-bearing nannofossil ooze, light greenish gray (5G 8/1, 7.5/1), subtle color variations throughout, some bioturbation. Pyrite-stained, reduced.

Minor lithology: Pyrite-stained clay-bearing nannofossil ooze, gray (N6), sharp basal contact, gradational upper contact. Section 2, 10-12.5 cm, and Section 3, 12-14 cm.

11 color changes in Sections 1-2; 4 color changes in Sections 3-CC; 0 color changes in Sections 5-CC; and 0 turbidites.

SMEAR SLIDE SUMMARY (%):

	1, 80
	D
TEXTURE:	
Sand	3
Silt	7
Clay	90
COMPOSITION:	
Quartz	Tr
Clay	Tr
Foraminifers	2
Nannofossils	91
Diatoms	Tr
Radiolarians	5
Sponge spicules	2
Silicoflagellates	Tr
Fish remains	Tr

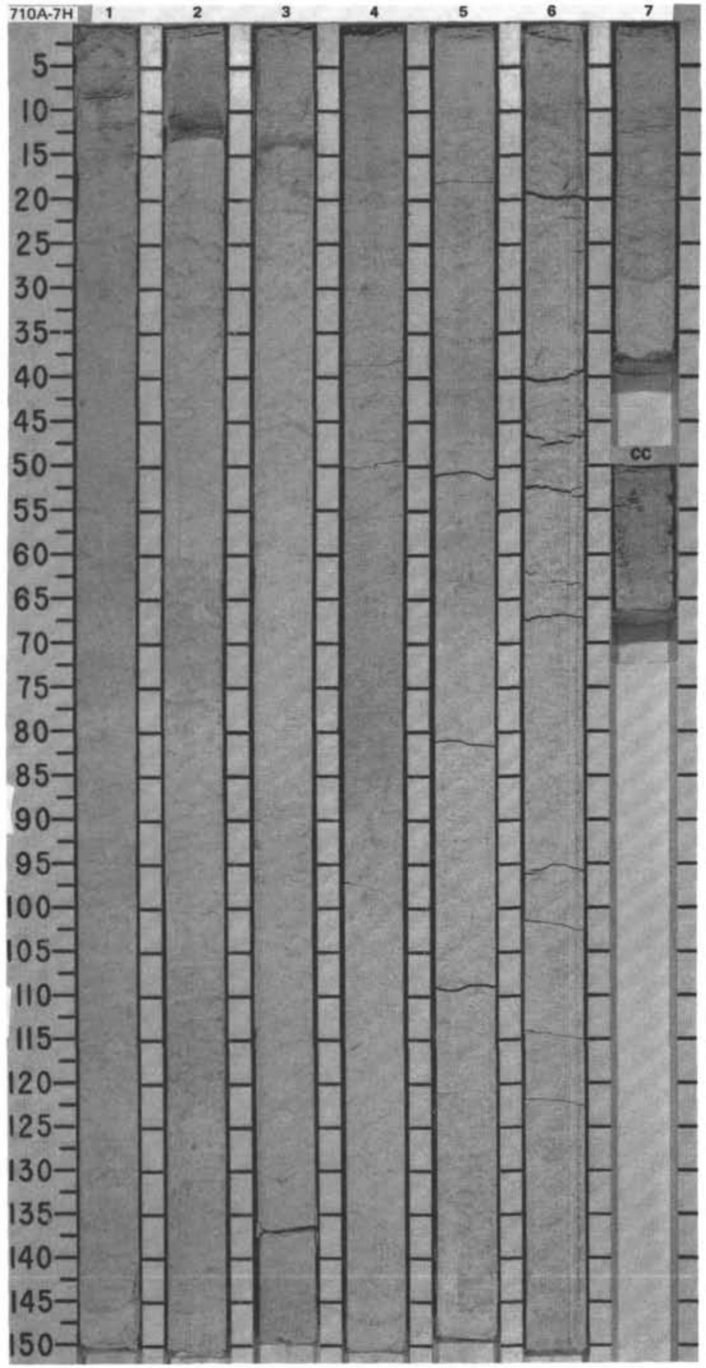

SITE 710 HOLE A CORE 8H CORED INTERVAL 3879.6-3889.1 mbsl; 67.1-76.6 mbsf

TIME-ROCK UNIT	FORAMINIFERS	NANNOFOSSILS	RADIOLARIANS	DIATOMS	PALEOMAGNETICS	PHYS. PROPERTIES	CHEMISTRY	SECTION	METERS	GRAPHIC LITHOLOGY	DRILLING DISTURB.	SED. STRUCTURES	SAMPLES
UPPER MIOCENE	RP	CN 9a (NN 11) / CN 8 (NN 10) CG	*Didymocyrtis antepenultima* CG	Barren				1, 2, 3, 4, 5, 6, CC	0.5, 1.0				* *

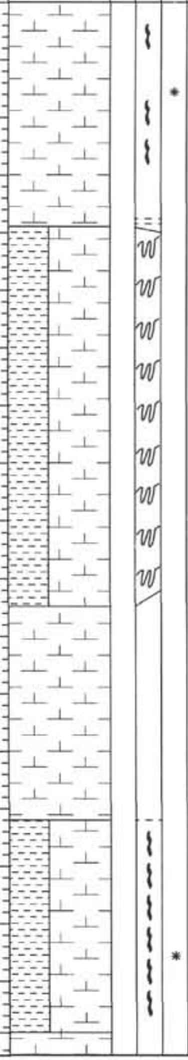

LITHOLOGIC DESCRIPTION

CLAY-BEARING NANNOFOSSIL OOZE and CLAY-NANNOFOSSIL OOZE

Major lithology: Clay-bearing nannofossil ooze, white (5G 9/1), pyrite-stained and reduced in Sections 1 and 2. Clay-nannofossil ooze, light gray (5Y 7/1) below Section 2, 47 cm; this interval is interpreted as a slump, oxidized. Below Section 4, 75 cm, becomes clay-bearing nannofossil ooze, light greenish gray (5G 8/1, 9/1), reduced. Becomes clay-nannofossil ooze, light gray (5Y 7/1) oxidized, below Section 5, 110 cm, to the bottom of the core.

Minor lithology: Pyrite-stained clay-bearing nannofossil ooze, gray (N6), Section 2, 44-45 cm.

2 color changes in Sections 1-4; 8 color changes in Sections 5-CC; and 0 turbidites.

SMEAR SLIDE SUMMARY (%):

	1, 80 D	6, 75 D
TEXTURE:		
Sand	2	3
Silt	3	7
Clay	95	90
COMPOSITION:		
Quartz	—	Tr
Dolomite	Tr	—
Foraminifers	2	3
Nannofossils	95	91
Radiolarians	2	4
Sponge spicules	1	2
Silicoflagellates	Tr	Tr
Fish remains	—	Tr

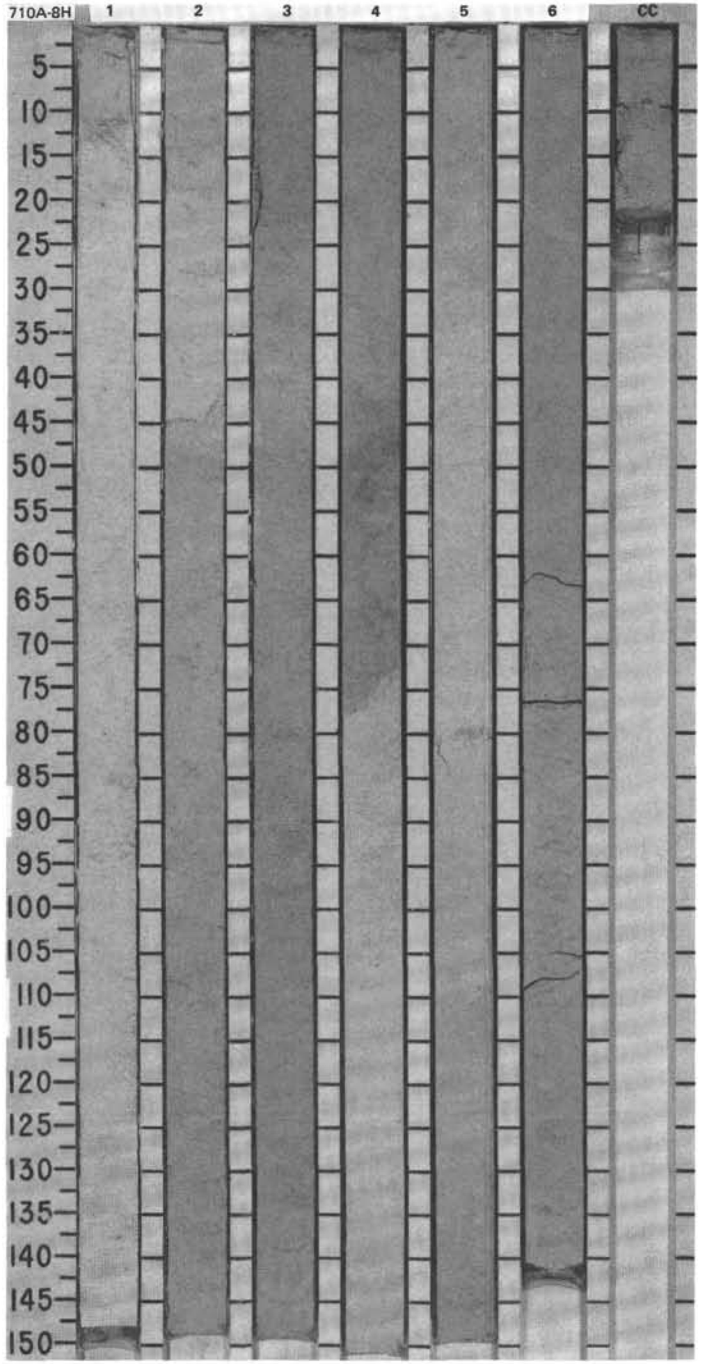

SITE 710 HOLE A CORE 9H CORED INTERVAL 38891.1-3898.7 mbsl; 76.6-86.2 mbsf

TIME-ROCK UNIT	FORAMINIFERS	NANNOFOSSILS	RADIOLARIANS	DIATOMS	PALEOMAGNETICS	PHYS. PROPERTIES	CHEMISTRY	SECTION	METERS	GRAPHIC LITHOLOGY	DRILLING DISTURB.	SED. STRUCTURES	SAMPLES
UPPER MIOCENE	RP	CN 8 (NN 10); CN 7 (NN 9); CN 6 (NN 8); RP	*D. pettersonni*; CM	Barren; FP				1, 2, 3, 4, 5, 6, 7, CC	0.5, 1.0				*, *, IW OG

BIOSTRAT. ZONE/ FOSSIL CHARACTER

LITHOLOGIC DESCRIPTION

CLAY-NANNOFOSSIL OOZE

Major lithology: Clay-nannofossil ooze, white (10YR 8/2) and very pale brown (10YR 7/3, 7/4). Subtle color variations due to variable amounts of clay. Bioturbated and oxidized. Becomes white (5G 8/1) and light gray (5Y 7/1), reduced, below Section 6, 86 cm.

Minor lithologies:

a. Nannofossil clay, light yellowish brown (10YR 6/4) and light brownish gray (2.5Y 6/2). Section 4, 10-21 and 127-148 cm; Section 5, 35-80 and 93-100 cm; and Section 6, 15-31 cm.
b. Foraminifer-bearing nannofossil ooze, possible turbidite, white (10YR 9/2) and very pale brown (10YR 8/3). Section 3, 73-82 cm, and Section 4, 33-35 cm.

1 color change in Sections 1-2; 31 color changes in Sections 3-CC; and 2 turbidites.

SMEAR SLIDE SUMMARY (%):

	1, 80 D	4, 80 D
TEXTURE:		
Sand	2	3
Silt	8	7
Clay	90	90
COMPOSITION:		
Feldspar	Tr	—
Clay	—	15
Foraminifers	2	2
Nannofossils	94	78
Radiolarians	3	4
Sponge spicules	1	1
Silicoflagellates	Tr	Tr

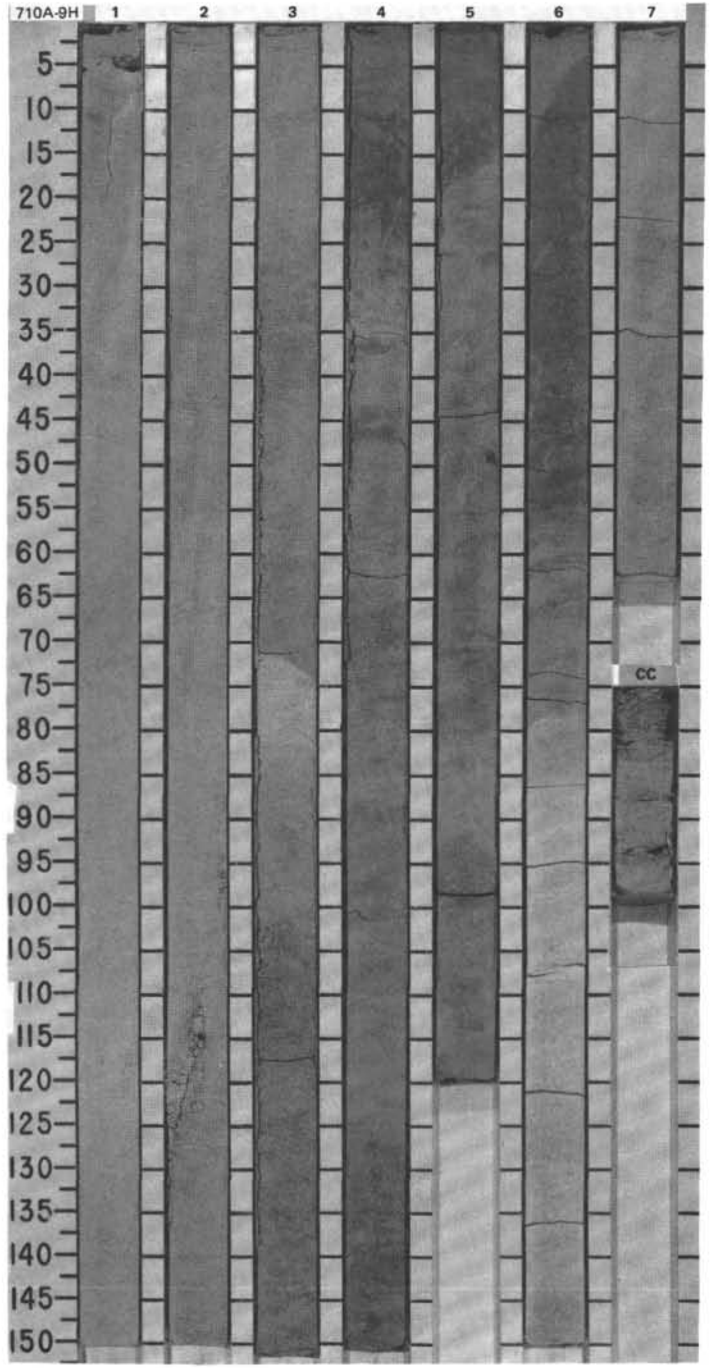

SITE 710 HOLE A CORE 10H CORED INTERVAL 3898.7-3908.3 mbsl; 86.2-95.8 mbsf

TIME-ROCK UNIT	FORAMINIFERS	NANNOFOSSILS	RADIOLARIANS	DIATOMS	PALEOMAGNETICS	PHYS. PROPERTIES	CHEMISTRY	SECTION	METERS	GRAPHIC LITHOLOGY	DRILLING DISTURB.	SED. STRUCTURES	SAMPLES
UPPER MIOCENE		CN 6 (NN 8)						1, 2, 3	0.5, 1.0				* *
LOWER-MIDDLE MIOCENE		CN 5 (NN 6 - NN 7)	Barren	Barren				4, 5, 6					
		CN 4 (NN 5)						7					
	RP	CM						CC					

LITHOLOGIC DESCRIPTION

CLAY-NANNOFOSSIL OOZE and RADIOLARIAN-BEARING NANNOFOSSIL CLAY

Major lithology: Clay-nannofossil ooze and radiolarian-bearing nannofossil clay, reduced above Section 1, 49 cm, light gray (2.5Y 7/2) and light brownish gray (2.5Y 6/2). Oxidized below Section 1, 49 cm, pale yellow (2.5Y 7/4), light yellowish brown (2.5Y 6/4, 10YR 6/4), yellowish brown (10YR 5/4), very pale brown (10YR 7/3), and white (10YR 8/2). Many color variations due to clay content variations.

Minor lithology: Foraminifer-nannofossil ooze, turbidite, white (10YR 9/2). Section 2, 35-50 cm; Section 4, 59-61 cm; Section 4, 144 cm, to Section 5, 10 cm; Section 6, 17-19, 45-55, and 124-130 cm; and CC, 0-10 cm.

Slumped intervals between Section 5, 60-130 cm, and Section 6, 25-102 cm.

Microfault at Section 5, 110-140 cm.

30 color changes and 9 turbidites.

SMEAR SLIDE SUMMARY (%):

	1, 90 M	2, 50 M
TEXTURE:		
Sand	5	40
Silt	25	10
Clay	70	50
COMPOSITION:		
Quartz	1	—
Clay	63	6
Volcanic glass	5	—
Foraminifers	Tr	40
Nannofossils	15	50
Radiolarians	10	3
Sponge spicules	5	1
Silicoflagellates	1	—

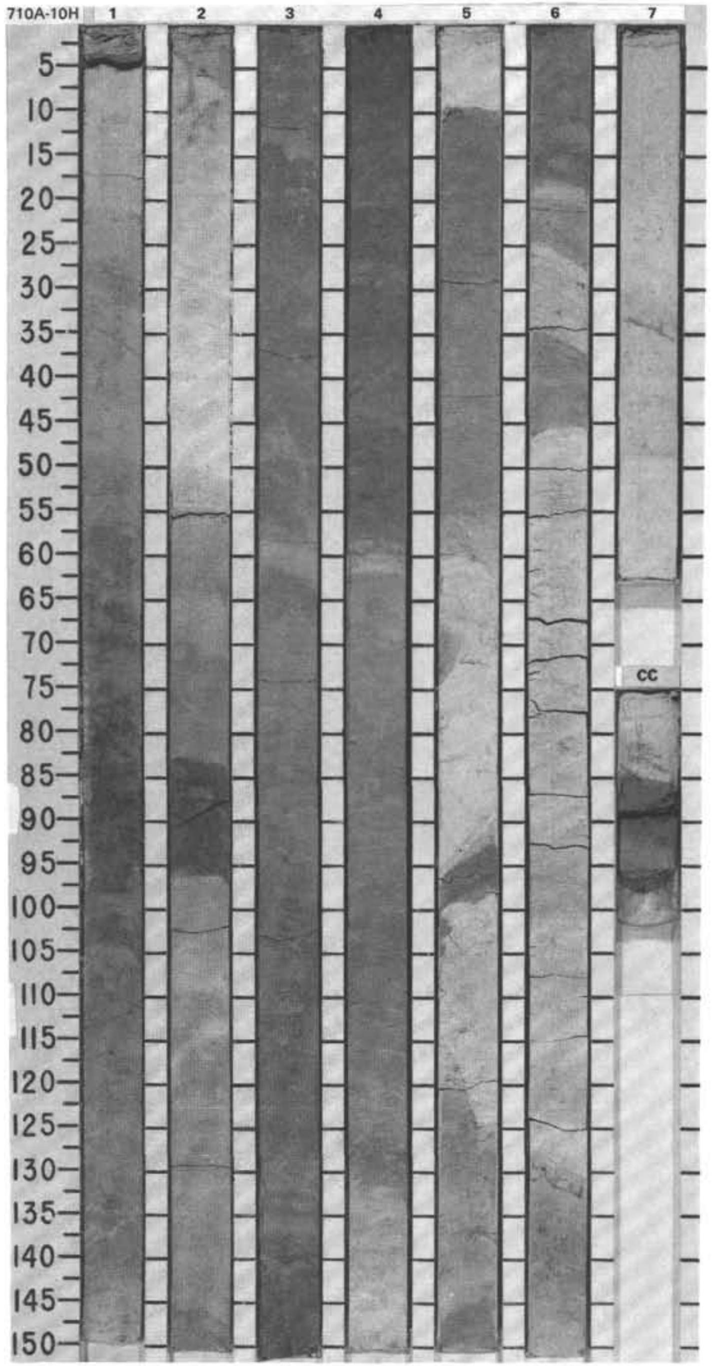

SITE 710 HOLE A CORE 11H CORED INTERVAL 3908.3-3918.0 mbsl; 95.8-105.5 mbsf

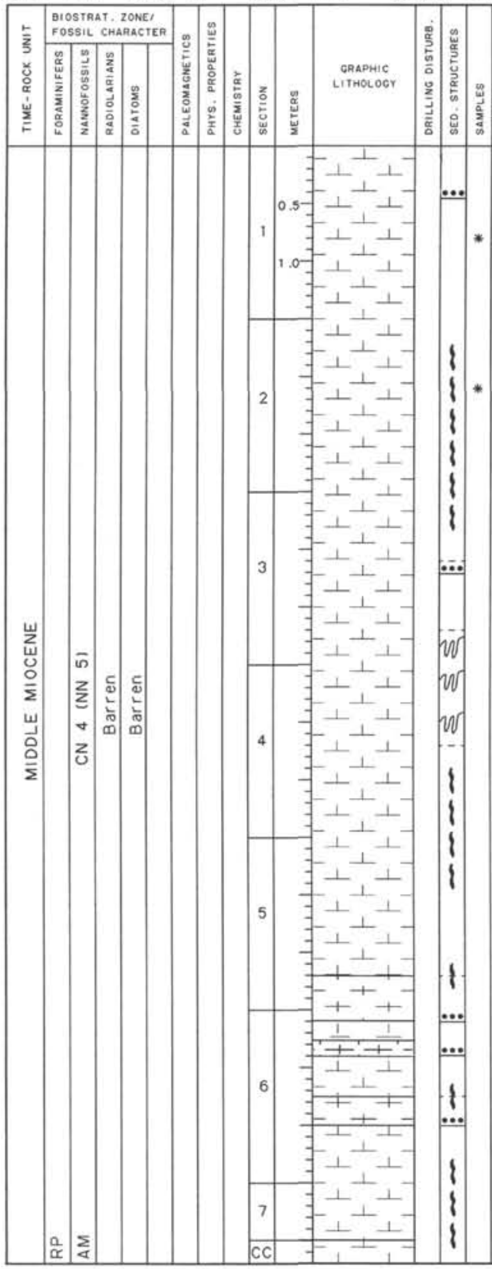

LITHOLOGIC DESCRIPTION

CLAY-BEARING NANNOFOSSIL OOZE

Major lithology: Clay-bearing nannofossil ooze, very pale brown (10YR 8/3, 7/3), light yellowish brown (10YR 6/4), and white (10YR 8/2, 9/2). Oxidized. Black speckles of possible MnO_2 are common. Mottling common.

Minor lithology: Foraminifer-nannofossil ooze, turbidites, white (10YR 9/2) and very pale brown (10YR 8/3). Usually sharp bottom and gradational upper contacts, and normally graded. Section 1, 41-46; Section 3, 64-69 cm; Section 5, 120 cm, to Section 6, 8 cm; and Section 6, 25-40 and 75-98 cm.

Slumped interval of contorted beds from Section 3, 130 cm(?), to Section 4, 70 cm(?).

About 25 color changes and 5 turbidites.

SMEAR SLIDE SUMMARY (%):

	1, 80 D	2, 60 D
TEXTURE:		
Sand	5	3
Silt	5	2
Clay	90	95
COMPOSITION:		
Quartz	1	2
Clay	2	5
Dolomite	Tr	—
Foraminifers	2	2
Nannofossils	90	90
Radiolarians	3	1
Sponge spicules	2	Tr

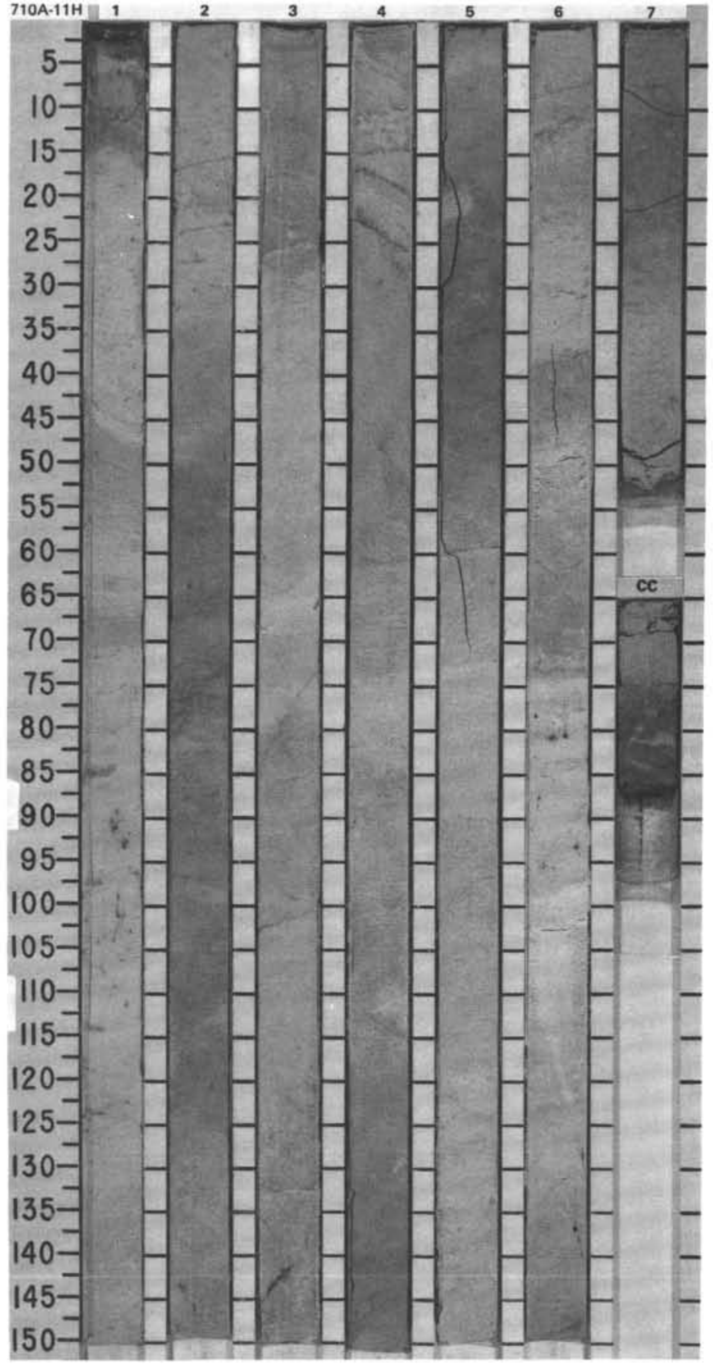

SITE 710 HOLE A CORE 12H CORED INTERVAL 3918.0-3927.7 mbsl; 105.5-115.2 mbsf

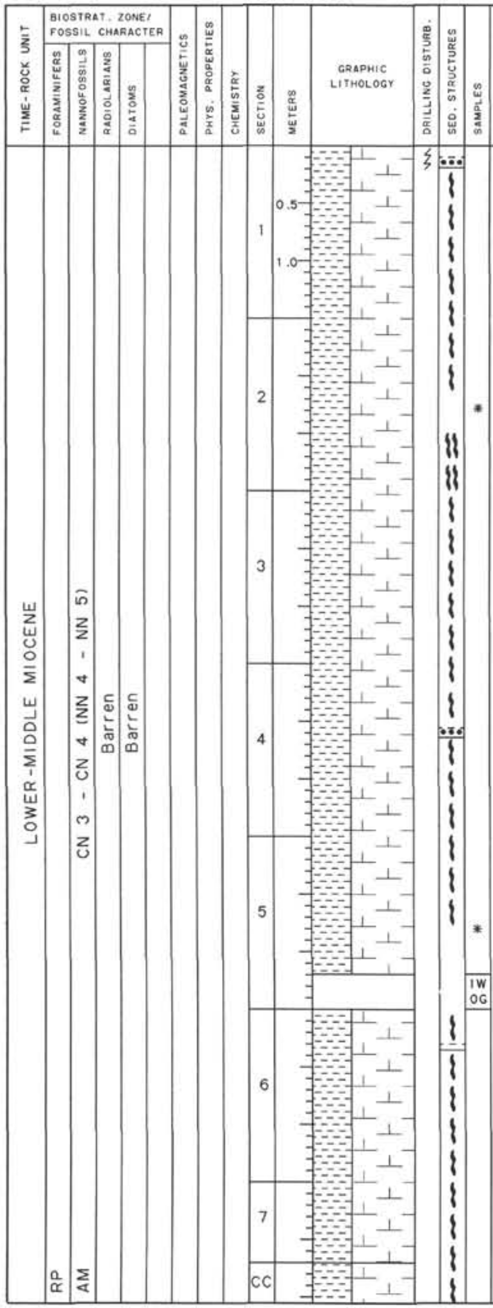

LITHOLOGIC DESCRIPTION

CLAY-NANNOFOSSIL OOZE

Major lithology: Clay-nannofossil ooze, brown (10YR 5/3), pale brown (10YR 6/3), very pale brown (10YR 7/3, 8/3, 7/4), and light yellowish brown (10YR 6/4). Distinct color cycles. Extensive bioturbation.

Minor lithology: Foraminifer-nannofossil ooze, turbidites, white (10YR 8/2) and very pale brown (10YR 8/3). Section 1, 12-18 cm; Section 4, 56-60 cm; and Section 6, 28-32 cm.

43 color changes and 3 turbidites.

SMEAR SLIDE SUMMARY (%):

	2, 80 D	5, 85 D
TEXTURE:		
Silt	—	20
Clay	100	80
COMPOSITION:		
Quartz	Tr	—
Clay	—	65
Volcanic glass	Tr	10
Dolomite	Tr	—
Accessory minerals	Tr	10
Foraminifers	Tr	—
Nannofossils	100	15
Sponge spicules	Tr	—

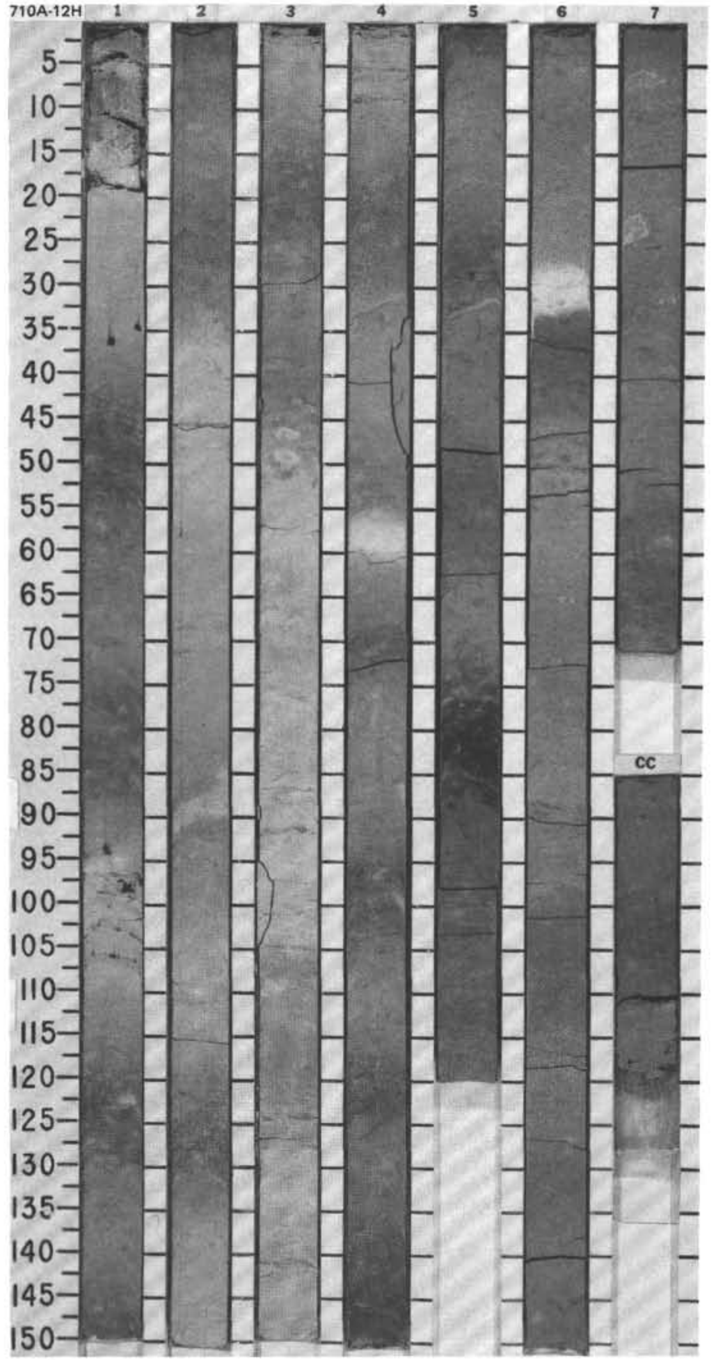

SITE 710 HOLE A CORE 13H CORED INTERVAL 3927.7-3937.4 mbsl; 115.2-124.9 mbsf

TIME-ROCK UNIT	FORAMINIFERS	NANNOFOSSILS	RADIOLARIANS	DIATOMS	PALEOMAGNETICS	PHYS. PROPERTIES	CHEMISTRY	SECTION	METERS	GRAPHIC LITHOLOGY	DRILLING DISTURB.	SED. STRUCTURES	SAMPLES
LOWER MIOCENE	RP	NN 2 (CN 1c - CN 2?) AM	Barren	Barren				1	0.5, 1.0				
								2					*
								3					
								4					
								5					
								6					*
								7					
								CC					

LITHOLOGIC DESCRIPTION

CLAY-BEARING NANNOFOSSIL OOZE

Major lithology: Clay-bearing nannofossil ooze, brown (10YR 5/3), light yellowish brown (10YR 6/4), very pale brown (10YR 7/3), pale brown (10YR 6/3), yellowish brown (10YR 5/4), and white (10YR 8/3). Mottled, gradational color contacts.

24 color changes and 0 turbidites.

SMEAR SLIDE SUMMARY (%):

	2, 80 D	6, 10 D
TEXTURE:		
Clay	100	100
COMPOSITION:		
Feldspar	—	Tr
Clay	15	20
Volcanic glass	Tr	2
Dolomite	—	Tr
Foraminifers	Tr	—
Nannofossils	85	78
Sponge spicules	Tr	Tr

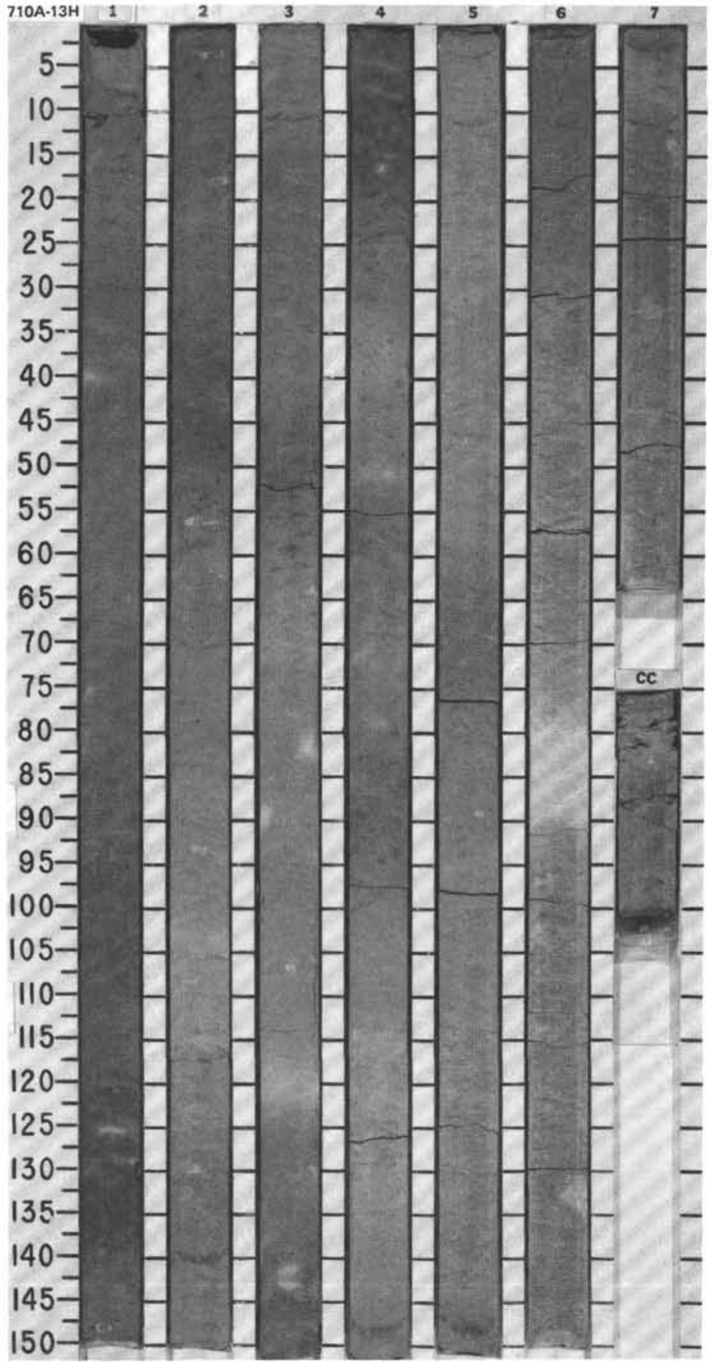

SITE 710 HOLE A CORE 14X CORED INTERVAL 3937.4-3944.9 mbsl; 124.9-132.4 mbsf

TIME-ROCK UNIT	BIOSTRAT. ZONE/FOSSIL CHARACTER: FORAMINIFERS	NANNOFOSSILS	RADIOLARIANS	DIATOMS	PALEOMAGNETICS	PHYS. PROPERTIES	CHEMISTRY	SECTION	METERS	GRAPHIC LITHOLOGY	DRILLING DISTURB.	SED. STRUCTURES	SAMPLES
LOWER MIOCENE	RP	NN 2 (CN 1c + CN 2?) AM	*C. tetrapera* RP	Barren				1, 2, 3, 4, 5, 6, 7	0.5, 1.0				* (Section 2), * (Section 5)

CLAY-BEARING NANNOFOSSIL OOZE

Major lithology: Clay-bearing nannofossil ooze, light yellowish brown (10YR 6/4), very pale brown (10YR 7/3), and pale brown (10YR 6/3). Mottled.

Minor lithologies:
a. Clay-nannofossil ooze, brown (10YR 5/3). Section 2, 50-78 cm.
b. Nannofossil ooze, possible turbidite, white (10YR 8/2). Sharp basal contact, gradational upper contact. Section 4, 10-96 cm.

12 color changes and 1 turbidite(?).

SMEAR SLIDE SUMMARY (%):

	2, 70	5, 70
	D	D
TEXTURE:		
Clay	100	100
COMPOSITION:		
Clay	30	15
Foraminifers	Tr	5
Nannofossils	70	80
Radiolarians	—	Tr
Sponge spicules	Tr	Tr

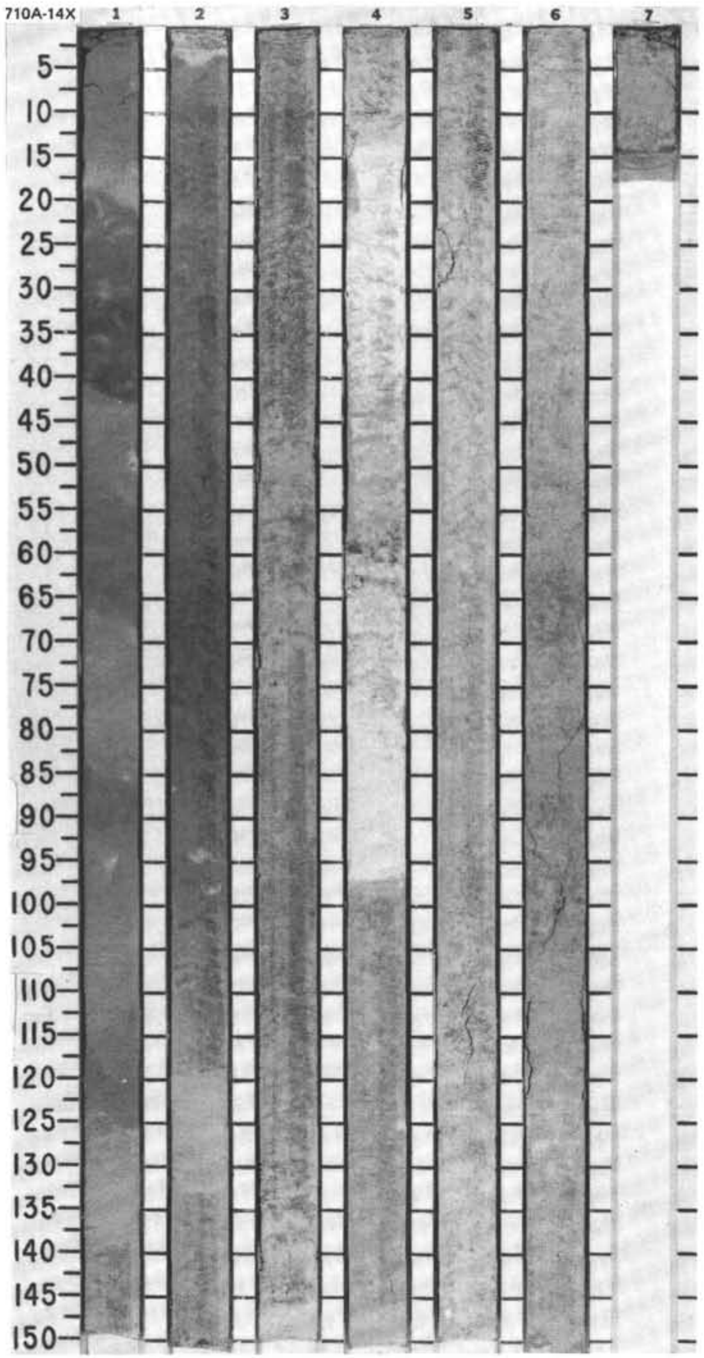

SITE 710 HOLE A CORE 15X CORED INTERVAL 3944.9-3954.6 mbsl; 132.4-142.1 mbsf

TIME-ROCK UNIT	BIOSTRAT. ZONE/ FOSSIL CHARACTER: FORAMINIFERS	NANNOFOSSILS	RADIOLARIANS	DIATOMS	PALEOMAGNETICS	PHYS. PROPERTIES	CHEMISTRY	SECTION	METERS	GRAPHIC LITHOLOGY	DRILLING DISTURB.	SED. STRUCTURES	SAMPLES
LOWER MIOCENE	RP	NN 1 (CN 1a+b) AM	*C. tetrapera* RP	Barren				1	0.5, 1.0				
								2					*
								3					IW OG
								4					*
								5					
								CC					

LITHOLOGIC DESCRIPTION

NANNOFOSSIL OOZE and NANNOFOSSIL CHALK

Major lithology: Nannofossil ooze, white (10YR 8/2), light gray (10YR 7/2), homogeneous. Interspersed harder nannofossil chalk horizons.

2 color changes and 0 turbidites.

SMEAR SLIDE SUMMARY (%):

	2, 67 D	4, 67 D
TEXTURE:		
Sand	2	—
Silt	20	20
Clay	78	80
COMPOSITION:		
Clay	5	5
Foraminifers	2	—
Nannofossils	93	95

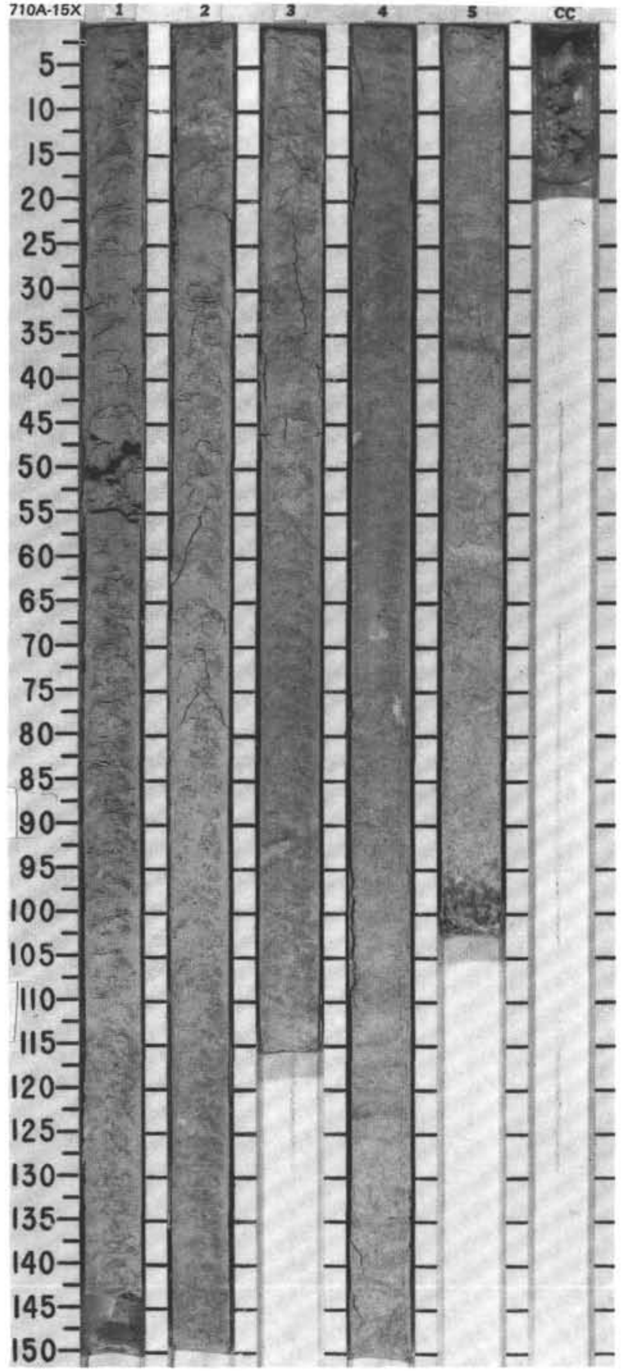

SITE 710 HOLE A CORE 16X CORED INTERVAL 3954.6-3964.3 mbsl; 142.1-151.8 mbsf

TIME-ROCK UNIT	BIOSTRAT. ZONE/ FOSSIL CHARACTER				PALEOMAGNETICS	PHYS. PROPERTIES	CHEMISTRY	SECTION	METERS	GRAPHIC LITHOLOGY	DRILLING DISTURB.	SED. STRUCTURES	SAMPLES
	FORAMINIFERS	NANNOFOSSILS	RADIOLARIANS	DIATOMS									
UPPER OLIGOCENE	RP	CP 19b (NP 25) AG	*Dorcadospyris ateuchus* FM	Barren				1	0.5 1.0				
								2					*
								3					
								4					*
								5					
								CC					

NANNOFOSSIL OOZE and NANNOFOSSIL CHALK

Major lithology: Nannofossil ooze, white (10YR 8/2), homogeneous. Interspersed horizons of harder nannofossil chalk.

0 color changes and 0 turbidites.

SMEAR SLIDE SUMMARY (%):

	2, 80 D	4, 80 D
TEXTURE:		
Silt	20	20
Clay	80	80
COMPOSITION:		
Quartz	—	Tr
Clay	5	5
Foraminifers	Tr	—
Nannofossils	95	95

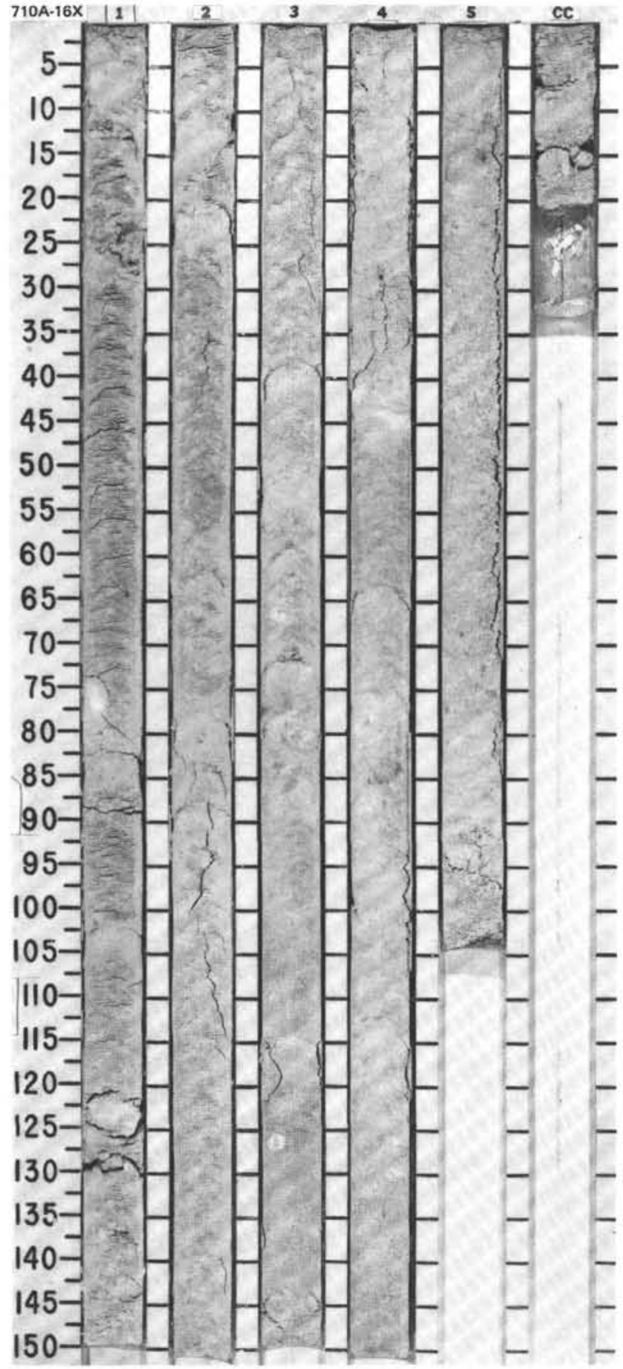

SITE 710 HOLE A CORE 17X CORED INTERVAL 3964.3-3973.9 mbsl; 151.8-161.4 mbsf

TIME-ROCK UNIT	BIOSTRAT. ZONE/ FOSSIL CHARACTER: FORAMINIFERS	NANNOFOSSILS	RADIOLARIANS	DIATOMS	PALEOMAGNETICS	PHYS. PROPERTIES	CHEMISTRY	SECTION	METERS	GRAPHIC LITHOLOGY	DRILLING DISTURB.	SED. STRUCTURES	SAMPLES
UPPER OLIGOCENE	RP	CP 19b (NP 25) AG	*Dorcadospyris ateuchus* FM	Barren				1	0.5, 1.0				
								2					*
								3					
								4					* *
								5					
								6					
								CC					

LITHOLOGIC DESCRIPTION

NANNOFOSSIL OOZE and NANNOFOSSIL CHALK

Major lithology: Nannofossil ooze, white (10YR 8/2), homogeneous. Interspersed horizons of harder nannofossil chalk, occasional black patches of manganese oxide(?).

5 color changes and 0 turbidites.

SMEAR SLIDE SUMMARY (%):

	2, 80 D	4, 80 D	4, 127 M
TEXTURE:			
Sand	1	3	—
Silt	30	20	30
Clay	69	77	70
COMPOSITION:			
Quartz	1	—	—
Clay	9	9	15
Accessory minerals	—	—	10
Foraminifers	1	5	Tr
Nannofossils	89	86	75
Radiolarians	—	Tr	—

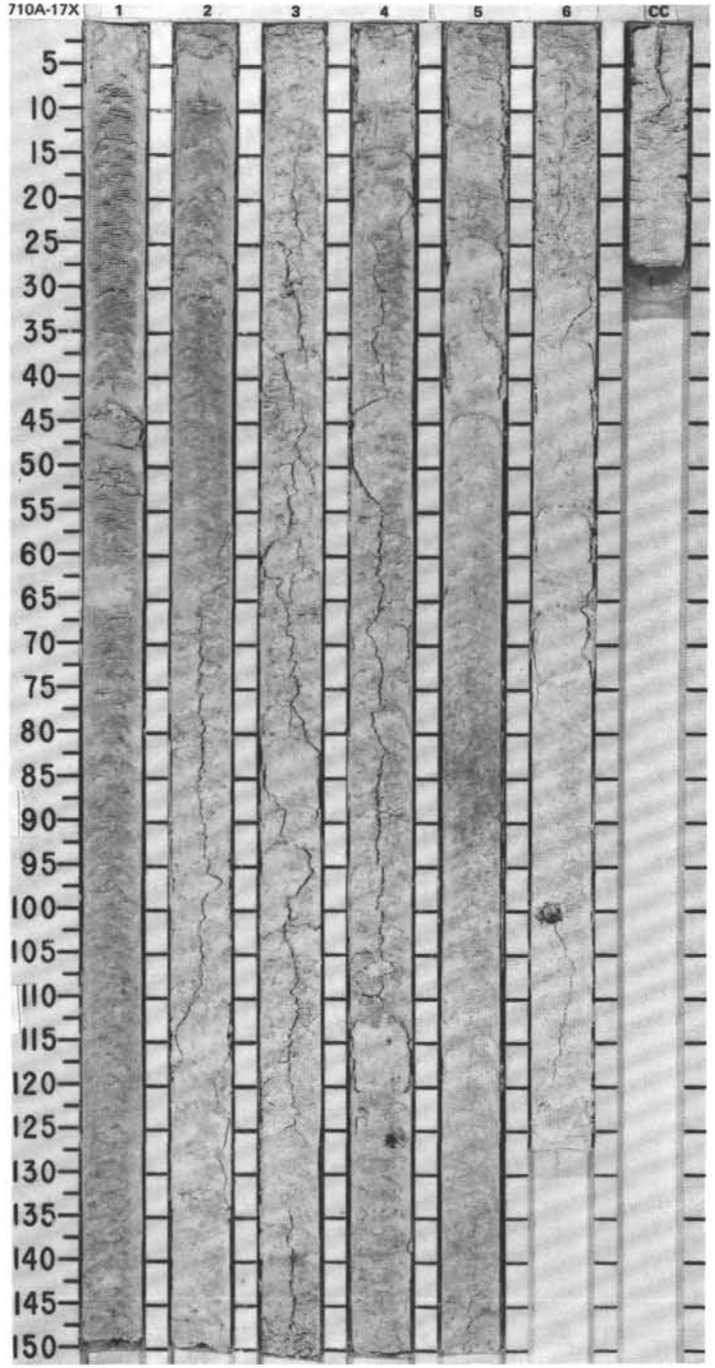

SITE 710 HOLE A CORE 18X CORED INTERVAL 3973.9-3983.6 mbsl; 161.4-171.1 mbsf

TIME-ROCK UNIT	BIOSTRAT. ZONE/FOSSIL CHARACTER: FORAMINIFERS	NANNOFOSSILS	RADIOLARIANS	DIATOMS	PALEOMAGNETICS	PHYS. PROPERTIES	CHEMISTRY	SECTION	METERS	GRAPHIC LITHOLOGY	DRILLING DISTURB.	SED. STRUCTURES	SAMPLES
UPPER OLIGOCENE	RP	CP 19b (NP25); CP 19a (NP 24); AG	*Dorcadospyris ateuchus*; FP	Barren				1	0.5, 1.0				
								2					*
								3					IW OG
								4					*
								5					
								CC					

LITHOLOGIC DESCRIPTION

NANNOFOSSIL OOZE and NANNOFOSSIL CHALK

Major lithology: Nannofossil ooze, white (N9, 10YR 8/2), and about 50% hard nannofossil chalk, otherwise homogeneous.

5 color changes and 0 turbidites.

SMEAR SLIDE SUMMARY (%):

	2, 80 D	4, 70 D
TEXTURE:		
Silt	30	20
Clay	70	80
COMPOSITION:		
Clay	5	2
Foraminifers	Tr	2
Nannofossils	95	96

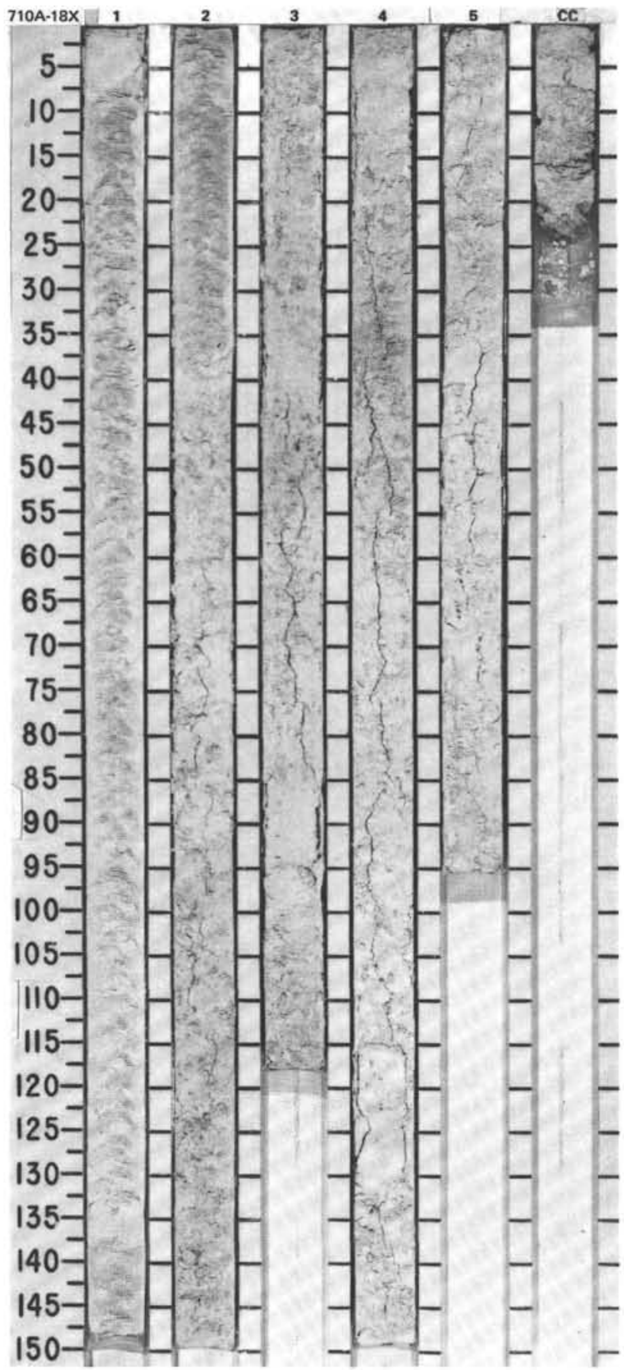

SITE 710 HOLE A CORE 19X CORED INTERVAL 3983.6-3993.3 mbsl; 171.1-180.8 mbsf

TIME-ROCK UNIT	FORAMINIFERS	NANNOFOSSILS	RADIOLARIANS	DIATOMS	PALEOMAGNETICS	PHYS. PROPERTIES	CHEMISTRY	SECTION	METERS	GRAPHIC LITHOLOGY	DRILLING DISTURB.	SED. STRUCTURES	SAMPLES
UPPER OLIGOCENE		CP 19a (NP 24)	*Dorcadospyris ateuchus*	Barren				1	0.5, 1.0				
								2					*
								3					
								4					*
								5					
								6					
	RP	AG	RP					CC					

(BIOSTRAT. ZONE/ FOSSIL CHARACTER: FORAMINIFERS, NANNOFOSSILS, RADIOLARIANS, DIATOMS)

LITHOLOGIC DESCRIPTION

NANNOFOSSIL CHALK and NANNOFOSSIL OOZE

Major lithology: Nannofossil chalk and nannofossil ooze, chalk varies from 0 to 90% of total in different sections, white (N9), homogeneous and featureless.

0 color changes and 0 turbidites.

SMEAR SLIDE SUMMARY (%):

	2, 80 D	4, 80 D
TEXTURE:		
Sand	1	1
Silt	30	30
Clay	69	69
COMPOSITION:		
Quartz	Tr	—
Clay	5	9
Volcanic glass	Tr	—
Accessory minerals	—	Tr
Foraminifers	Tr	Tr
Nannofossils	94	91
Sponge spicules	1	Tr

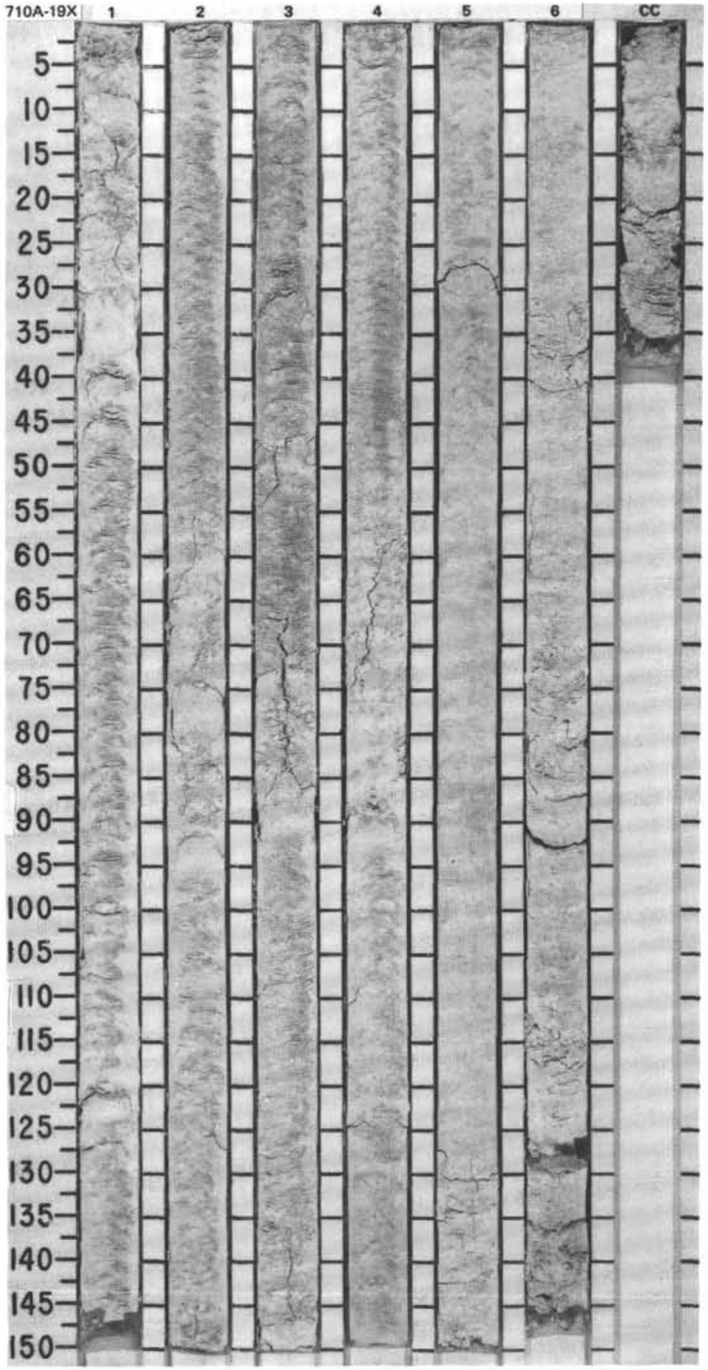

SITE 710 HOLE A CORE 20X CORED INTERVAL 3993.3-4002.9 mbsl; 180.8-190.4 mbsf

TIME-ROCK UNIT	FORAMINIFERS	NANNOFOSSILS	RADIOLARIANS	DIATOMS	SECTION	METERS	LITHOLOGIC DESCRIPTION
LOWER OLIGOCENE	RP	AG: CP 19a (NN 24); CP 17 - CP 18 (NP 23)	FP: *Dercadospyris ateuchus*; *Theocyrtis tuberosa*	Barren	1, 2, 3, 4, 5, 6, CC	0.5, 1.0	See below

Column headings: BIOSTRAT. ZONE/ FOSSIL CHARACTER; PALEOMAGNETICS; PHYS. PROPERTIES; CHEMISTRY; GRAPHIC LITHOLOGY; DRILLING DISTURB.; SED. STRUCTURES; SAMPLES

NANNOFOSSIL OOZE and NANNOFOSSIL CHALK

Major lithology: Nannofossil ooze and nannofossil chalk, white (N9), chalk varies from 0-90% of total in different sections.

Minor lithology: Clay-bearing nannofossil ooze and chalk, very pale brown (10YR 8/3), light gray (10YR 7/2), white (10YR 8/2), and light brownish gray (10YR 6/2). Probably dispersed ash layers, gradational color contacts. Section 2, 40-100 cm, and Section 3, 45-60 and 77-90 cm.

10 color changes and 0 turbidites.

SMEAR SLIDE SUMMARY (%):

	1, 80 D	3, 80 D
TEXTURE:		
Sand	—	2
Silt	15	30
Clay	85	68
COMPOSITION:		
Quartz	Tr	—
Clay	8	5
Volcanic glass	—	2
Foraminifers	Tr	Tr
Nannofossils	92	88
Radiolarians	Tr	5
Sponge spicules	Tr	—

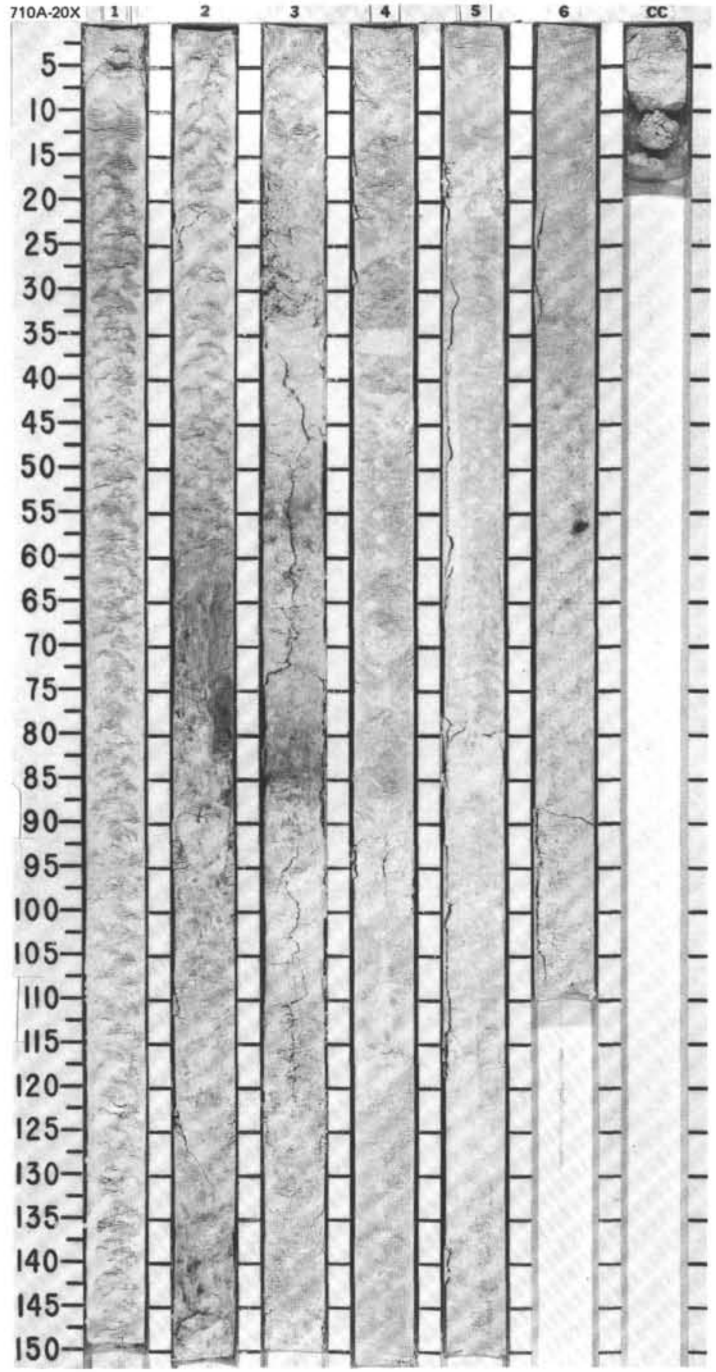

SITE 710 HOLE A CORE 21X CORED INTERVAL 4002.9-4012.6 mbsl; 190.4-200.1 mbsf

TIME-ROCK UNIT	FORAMINIFERS	NANNOFOSSILS	RADIOLARIANS	DIATOMS	PALEOMAGNETICS	PHYS. PROPERTIES	CHEMISTRY	SECTION	METERS	GRAPHIC LITHOLOGY	DRILLING DISTURB.	SED. STRUCTURES	SAMPLES
LOWER OLIGOCENE	P21a	CP 17 - CP 18 (NP 23)	*Theocyrtis tuberosa*	Barren				1	0.5, 1.0	VOID (see description)			
								2					*
								3					
								4					
								5					*
								6					
	RP	AG	FM					CC					

BIOSTRAT. ZONE/ FOSSIL CHARACTER

LITHOLOGIC DESCRIPTION

NANNOFOSSIL OOZE and NANNOFOSSIL CHALK

Major lithology: Nannofossil ooze and nannofossil chalk, white (N9), minor mottling varies from 0-70% of total in different sections.

2 color changes and 0 turbidites.

Note: In Section 1, from 103 to 150 cm, there is no void. Sections were cut to odd lengths.

SMEAR SLIDE SUMMARY (%):

	2, 80 D	5, 80 D
TEXTURE:		
Sand	1	2
Silt	20	30
Clay	79	68
COMPOSITION:		
Quartz	—	Tr
Clay	5	—
Volcanic glass	—	Tr
Foraminifers	1	2
Nannofossils	94	93
Radiolarians	Tr	5

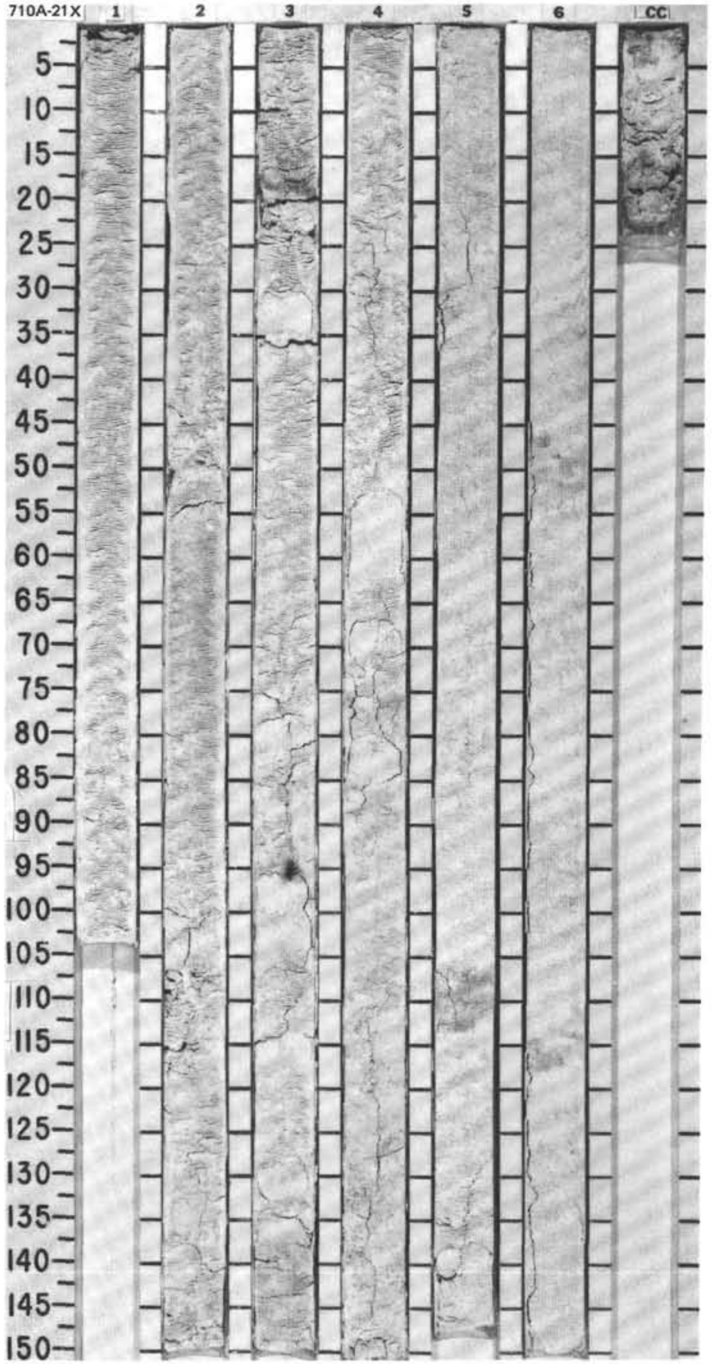

SITE 710 HOLE A CORE 22X CORED INTERVAL 4012.6-4022.2 mbsl; 200.1-209.7 mbsf

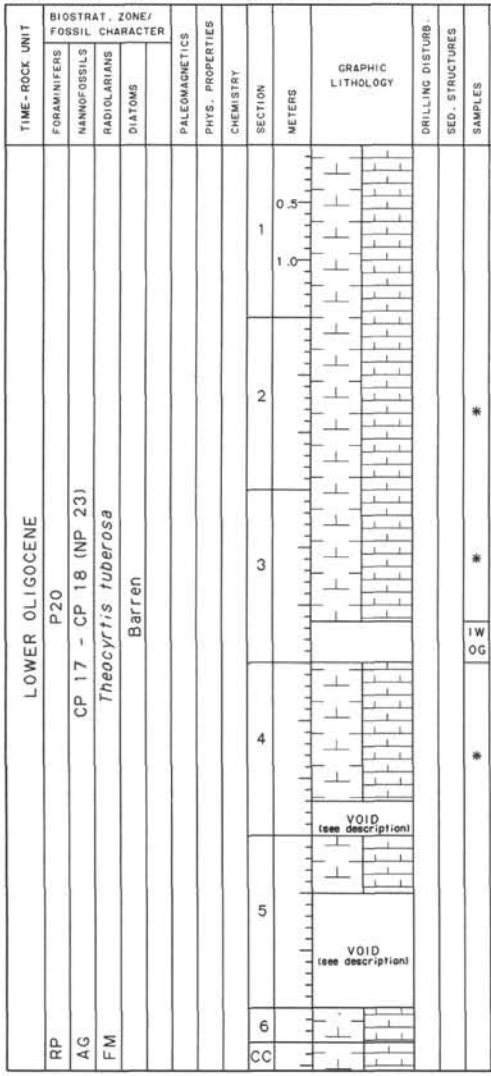

LITHOLOGIC DESCRIPTION

NANNOFOSSIL OOZE and NANNOFOSSIL CHALK

Major lithology: Nannofossil ooze and nannofossil chalk, white (N9) and very pale brown (10YR 8/3), some mottling.

Note: From Section 4, 117 cm, to Section 5, 0 cm, and from Section 5, 49 cm, to Section 6, 0 cm, there are no voids. Sections were cut to odd lengths.

4 color changes and 0 turbidites.

SMEAR SLIDE SUMMARY (%):

	2, 80 D	3, 60 M	4, 80 D
TEXTURE:			
Sand	5	—	2
Silt	25	30	30
Clay	70	70	68
COMPOSITION:			
Clay	5	5	—
Accessory minerals	—	2	—
Foraminifers	8	Tr	5
Nannofossils	80	93	90
Radiolarians	5	Tr	3
Sponge spicules	2	—	2

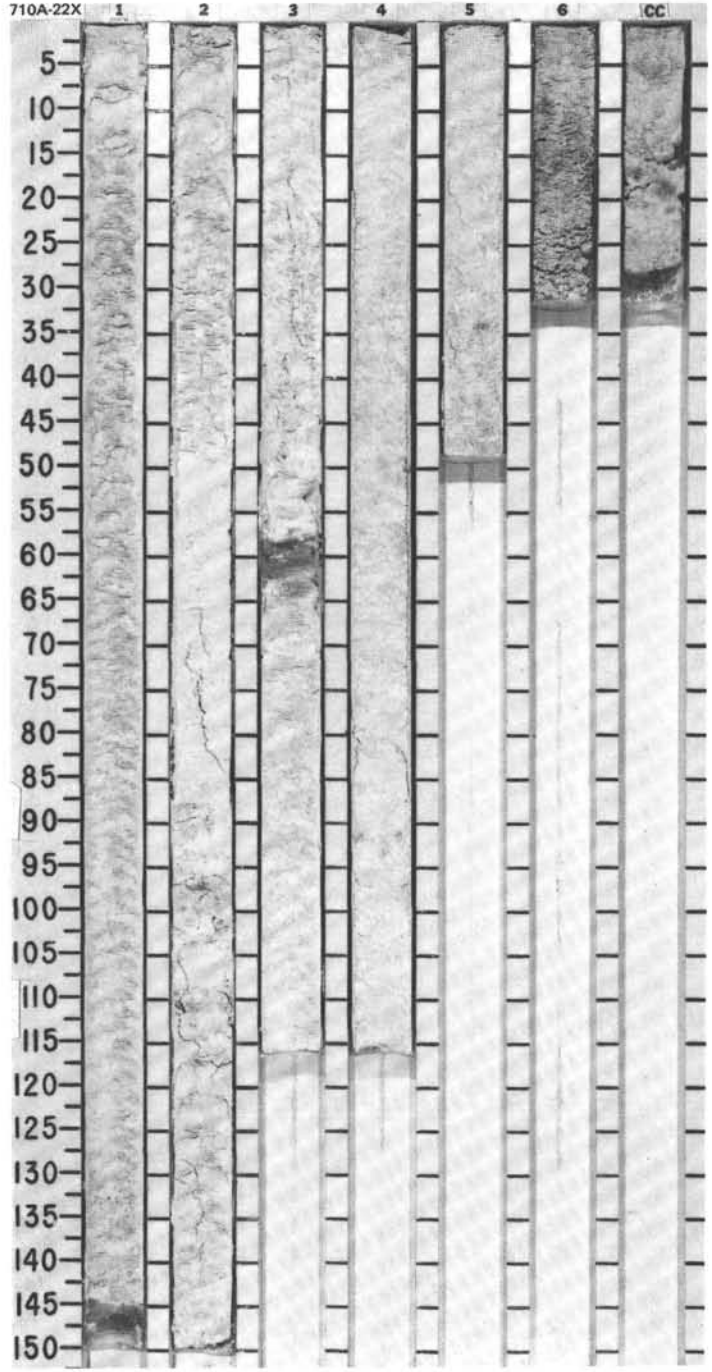

SITE 710 HOLE B CORE 1H CORED INTERVAL 3810.5-3817.0 mbsl; 0.0-6.5 mbsf

TIME-ROCK UNIT	FORAMINIFERS	NANNOFOSSILS	RADIOLARIANS	DIATOMS	PALEOMAGNETICS	PHYS. PROPERTIES	CHEMISTRY	SECTION	METERS	GRAPHIC LITHOLOGY	DRILLING DISTURB.	SED. STRUCTURES	SAMPLES
PLEISTOCENE	AM	CN 15 (NN 21); CN 14b (NN 20); CN 14a		*N. reinholdii*; CM				1, 2, 3, 4, 5, CC	0.5, 1.0				* * *

LITHOLOGIC DESCRIPTION

CLAY-BEARING NANNOFOSSIL OOZE

Major lithology: Clay-bearing nannofossil ooze, very pale brown (10YR 7/3), pale brown (10YR 6/3), light gray (10YR 7/2), light brownish gray (10YR 6/2), and white (10YR 8/2); gradational color changes. Mottling and bioturbation common. Oxidized.

Minor lithology: Turbidites, foraminifer-bearing nannofossil ooze, light gray (10YR 7/2) and white (10YR 8/2). Sharp basal contacts, gradational upper contacts, normally graded. Section 3, 15-22 cm, and Section 4, 35-45 cm.

23 color changes and 2 turbidites.

SMEAR SLIDE SUMMARY (%):

	1, 80 D	3, 21 M	4, 80 D
TEXTURE:			
Sand	4	25	5
Silt	30	20	15
Clay	66	55	80
COMPOSITION:			
Foraminifers	3	30	3
Nannofossils	85	66	93
Diatoms	5	—	Tr
Radiolarians	5	3	3
Sponge spicules	2	1	1

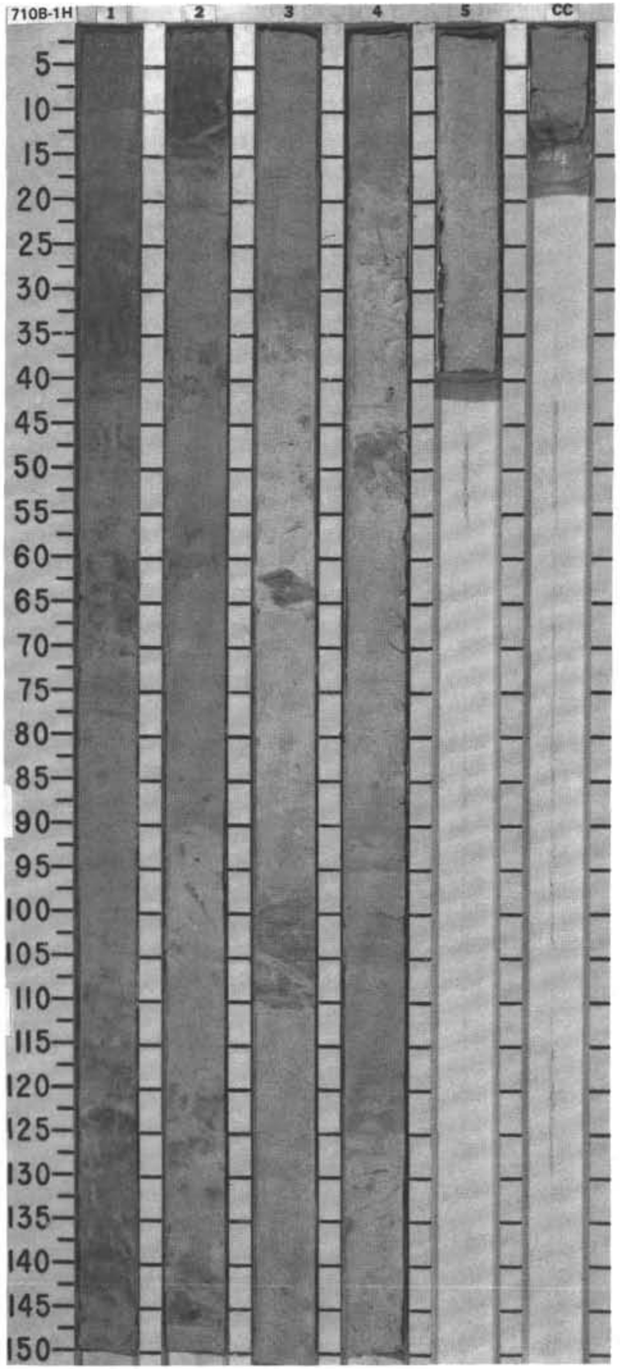

SITE 710 HOLE B CORE 2H CORED INTERVAL 3817.0-3826.7 mbsl; 6.5-16.2 mbsf

TIME-ROCK UNIT	BIOSTRAT. ZONE/FOSSIL CHARACTER: FORAMINIFERS	NANNOFOSSILS	RADIOLARIANS	DIATOMS	PALEOMAGNETICS	PHYS. PROPERTIES	CHEMISTRY	SECTION	METERS	GRAPHIC LITHOLOGY	DRILLING DISTURB.	SED. STRUCTURES	SAMPLES
PLEISTOCENE		CN 14a (NN 19)		N. reinholdii				1	0.5 / 1.0				*
								2					
								3					
								4					
								5					
		CN 13 (NN 19)						6					
		AM		CM				7					
								CC					

LITHOLOGIC DESCRIPTION

CLAY-BEARING, FORAMINIFER-BEARING NANNOFOSSIL OOZE

Major lithology: Clay-bearing, foraminifer-bearing nannofossil ooze, white (10YR 8/2) and very pale brown (10YR 8/3). Numerous minor color variations. Bioturbated and mottled. Oxidized.

Minor lithology: Turbidites, foraminifer-nannofossil ooze, white (10YR 9/2). Sharp basal contacts, gradational upper contacts, normally graded. Section 2, 137-141 cm, and Section 4, 18-20 and 76-89 cm.

32 color changes and 3 turbidites.

SMEAR SLIDE SUMMARY (%):

	1, 80 D
TEXTURE:	
Sand	15
Silt	10
Clay	75
COMPOSITION:	
Volcanic glass	Tr
Foraminifers	12
Nannofossils	76
Diatoms	3
Radiolarians	6
Sponge spicules	3
Silicoflagellates	Tr

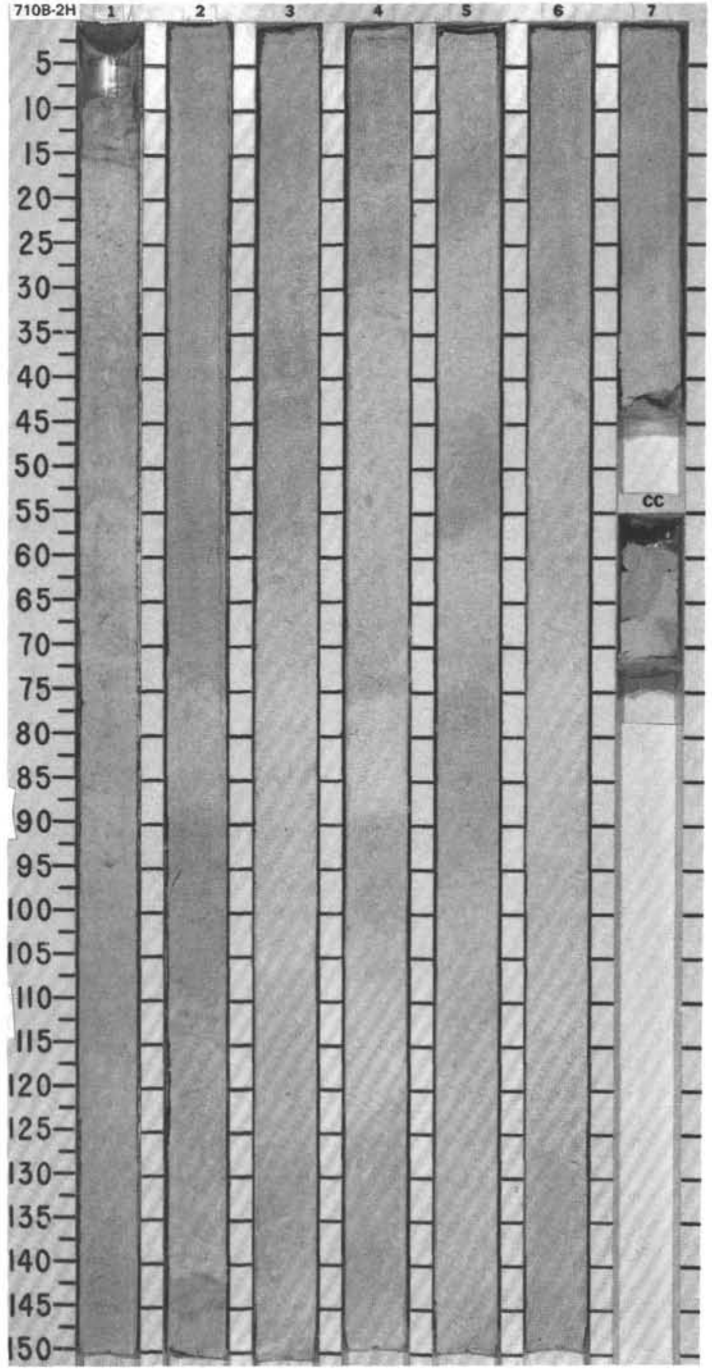

SITE 710 HOLE B CORE 3H CORED INTERVAL 3826.7-3836.3 mbsl; 16.2-25.8 mbsf

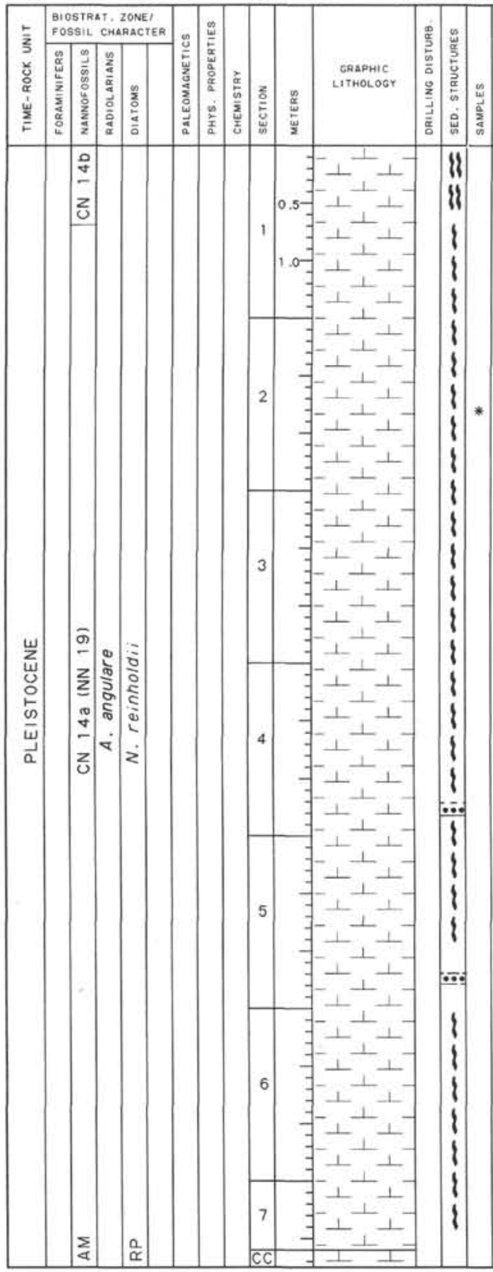

LITHOLOGIC DESCRIPTION

CLAY-BEARING, FORAMINIFER-BEARING NANNOFOSSIL OOZE

Major lithology: Clay-bearing, foraminifer-bearing nannofossil ooze, white (10YR 8/2), light gray (10YR 7/2), and very pale brown (10YR 8/3); numerous minor color changes. Bioturbated and mottled. Oxidized.

Minor lithology: Turbidites, foraminifer-nannofossil ooze, white (10YR 9/2). Sharp basal contacts, gradational upper contacts, normally graded. Section 4, 126-130 cm, and Section 5, 118-129 cm.

33 color changes and 2 turbidites.

SMEAR SLIDE SUMMARY (%):

	2, 80 D
TEXTURE:	
Sand	15
Silt	7
Clay	78
COMPOSITION:	
Quartz	Tr
Foraminifers	12
Nannofossils	78
Diatoms	3
Radiolarians	6
Sponge spicules	1
Silicoflagellates	Tr

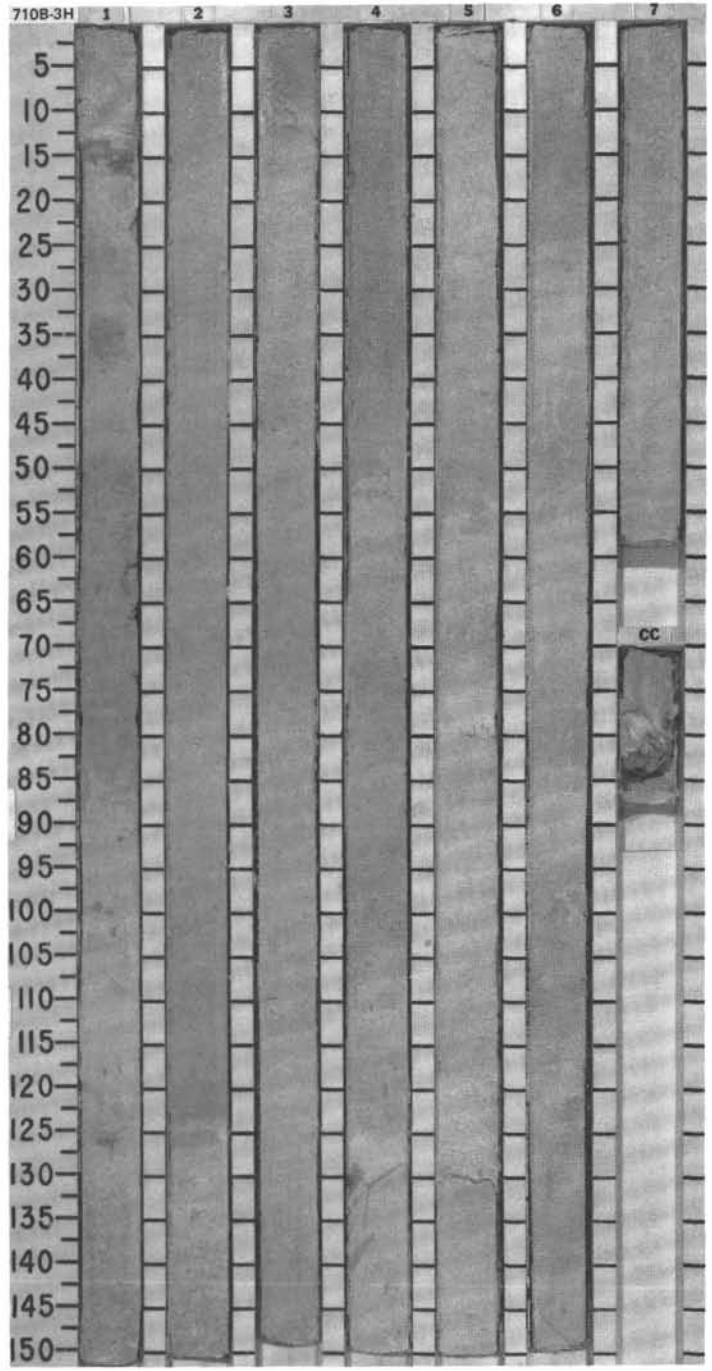

SITE 710 HOLE B CORE 4H CORED INTERVAL 3836.3-3845.8 mbsl; 25.8-35.3 mbsf

TIME-ROCK UNIT	BIOSTRAT. ZONE/FOSSIL CHARACTER: FORAMINIFERS	NANNOFOSSILS	RADIOLARIANS	DIATOMS	PALEOMAGNETICS	PHYS. PROPERTIES	CHEMISTRY	SECTION	METERS	GRAPHIC LITHOLOGY	DRILLING DISTURB.	SED. STRUCTURES	SAMPLES
UPPER PLIOCENE		CN 12d (NN 16)						1	0.5 / 1.0				*
								2					
								3					
LOWER PLIOCENE		CN 10c - CN 11 (NN 13 - NN 15)	*Spongaster pentas*	*N. jouseae*				4					
								5					
								6					
								7					
		AM	CG	FM				CC					

LITHOLOGIC DESCRIPTION

CLAY-BEARING NANNOFOSSIL OOZE

Major lithology: Clay-bearing nannofossil ooze, white (10YR 8/2) and very pale brown (10YR 7.5/2). Numerous very subtle color changes. Bioturbated throughout, oxidized.

Minor lithology: Turbidite, foraminifer-nannofossil ooze, white (10YR 8/2). Section 6, 63-67 cm.

23 color cycles and 1 turbidite.

Note: Drilling grease occurs inside core liner from Section 4 to the bottom of the core and in the next few cores.

SMEAR SLIDE SUMMARY (%):

	1, 80
	D
TEXTURE:	
Sand	5
Silt	10
Clay	85
COMPOSITION:	
Clay	Tr
Dolomite	Tr
Foraminifers	3
Nannofossils	86
Diatoms	3
Radiolarians	6
Sponge spicules	2
Silicoflagellates	Tr

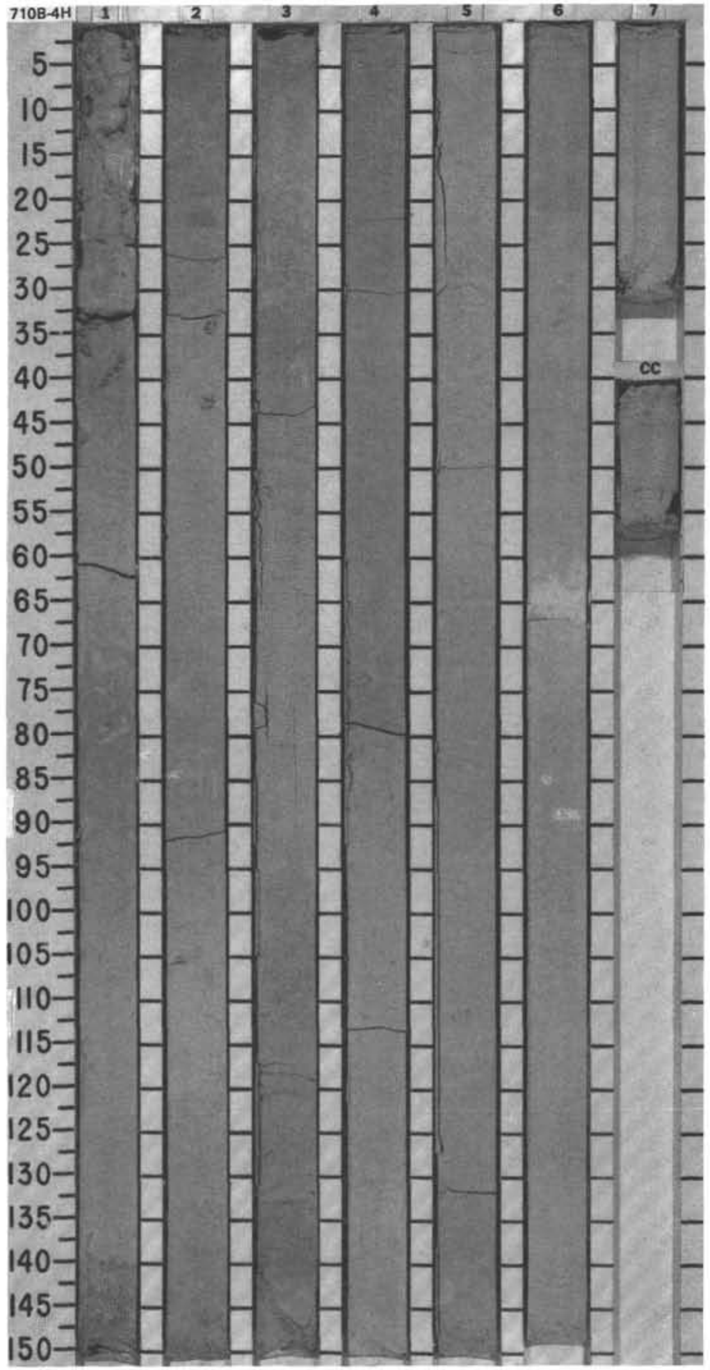

SITE 710 HOLE B CORE 5H CORED INTERVAL 3845.8-3855.4 mbsl; 35.3-44.9 mbsf

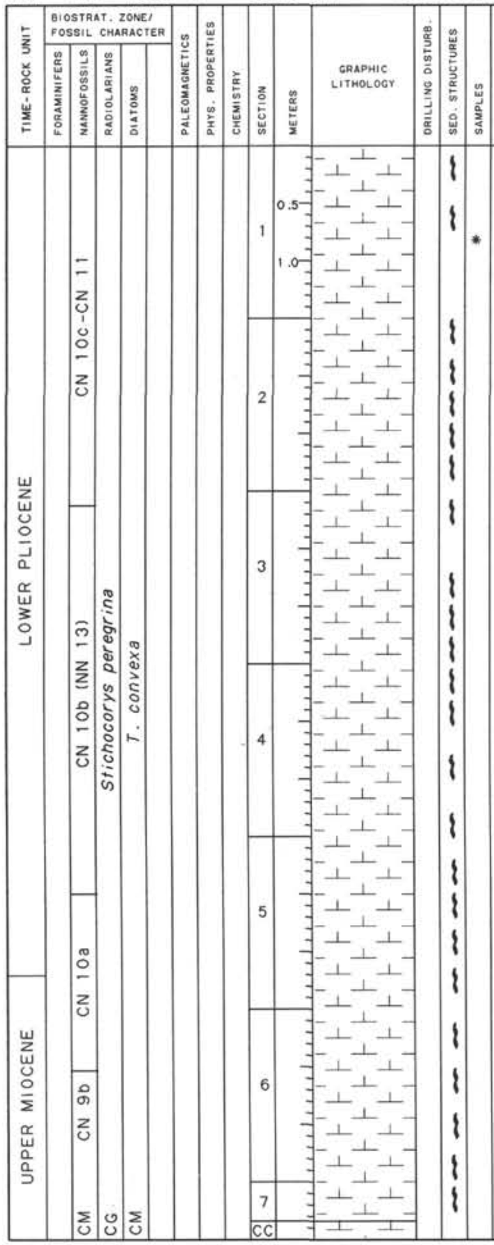

LITHOLOGIC DESCRIPTION

CLAY-BEARING NANNOFOSSIL OOZE

Major lithology: Clay-bearing nannofossil ooze, white (10YR 8/2) and light gray (10YR 7/2). Very subtle color changes. Some bioturbation, oxidized.

38 color changes and 0 turbidites.

Note: Drilling grease occurs inside core liner from all sections of this core.

SMEAR SLIDE SUMMARY (%):

	1, 80 D
TEXTURE:	
Sand	2
Silt	8
Clay	90
COMPOSITION:	
Feldspar	Tr
Volcanic glass	Tr
Foraminifers	1
Nannofossils	89
Diatoms	2
Radiolarians	4
Sponge spicules	4
Silicoflagellates	Tr

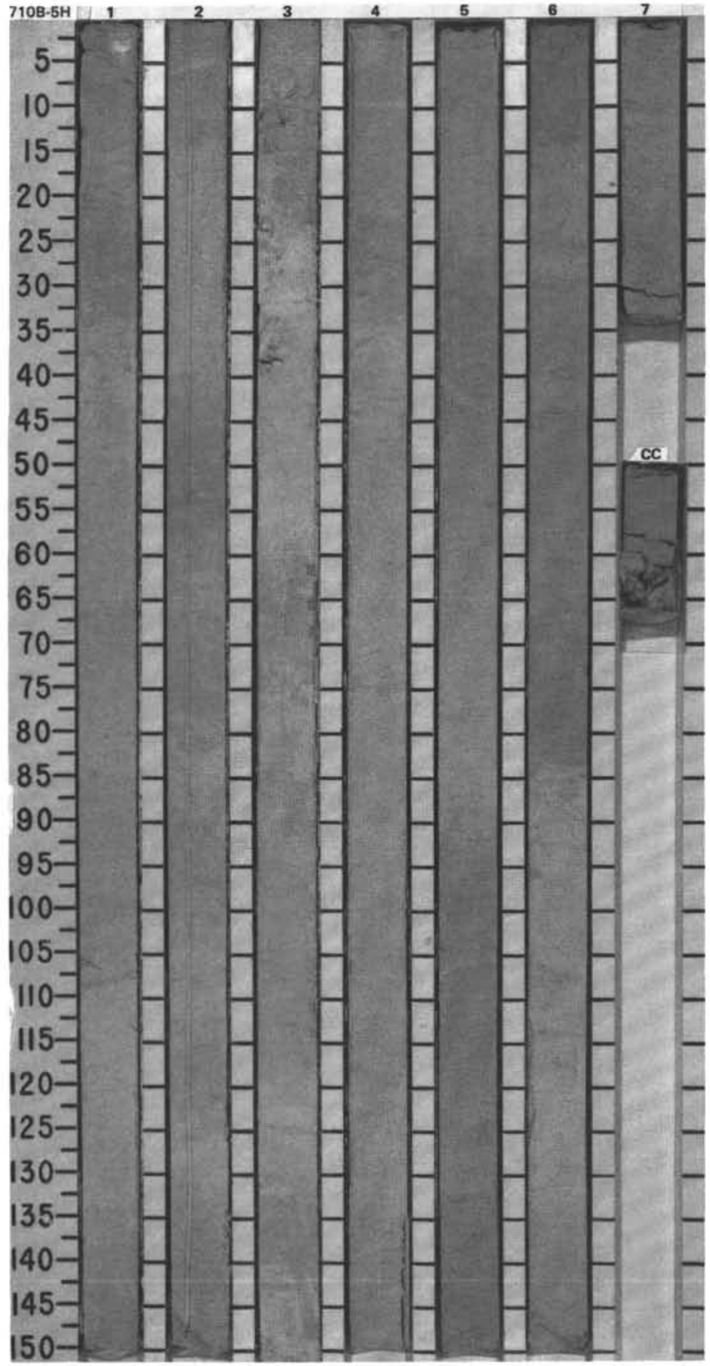

SITE 710 HOLE B CORE 6H CORED INTERVAL 3855.4-3865.0 mbsl; 44.9-54.5 mbsf

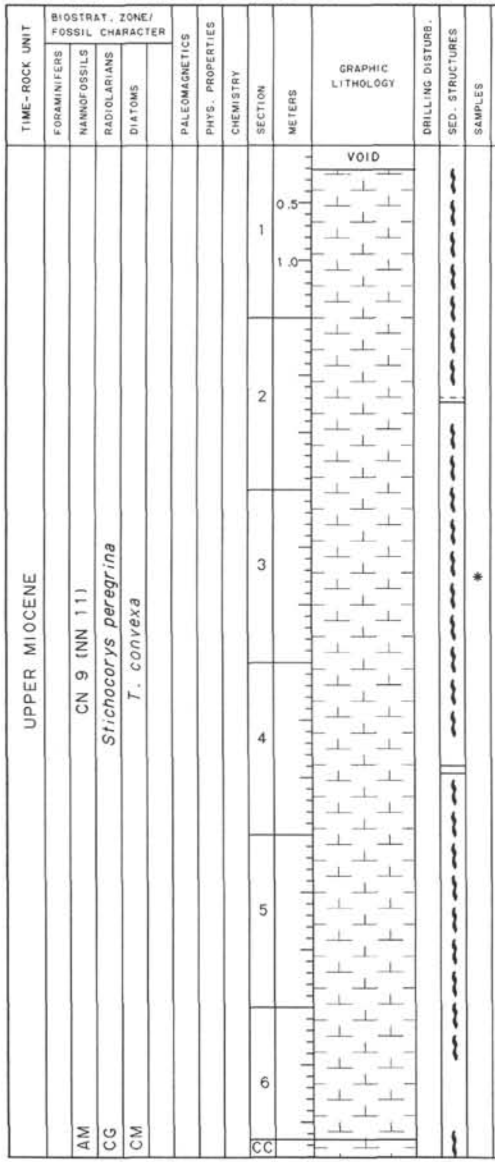

LITHOLOGIC DESCRIPTION

CLAY-BEARING NANNOFOSSIL OOZE

Major lithology: Clay-bearing nannofossil ooze, white (10YR 8/2, 5Y 8/1, 5G 8/1) and light gray (10YR 7/2, 5Y 7/1). Oxidized in Section 1, gradational in Section 2, and reduced in Section 3. Minor gray pyrite staining below Section 3.

Minor lithologies:
a. Turbidite, foraminifer-nannofossil ooze, white (N9). Section 2, 73–74 cm.
b. Clay-bearing nannofossil ooze, pale green (5GY 7/1) laminae, may be an altered ash. Section 4, 97 cm.

34 color changes and 1 turbidite.

SMEAR SLIDE SUMMARY (%):

	3, 80
	D
TEXTURE:	
Sand	5
Silt	10
Clay	85
COMPOSITION:	
Quartz	Tr
Foraminifers	Tr
Nannofossils	87
Diatoms	3
Radiolarians	8
Sponge spicules	2

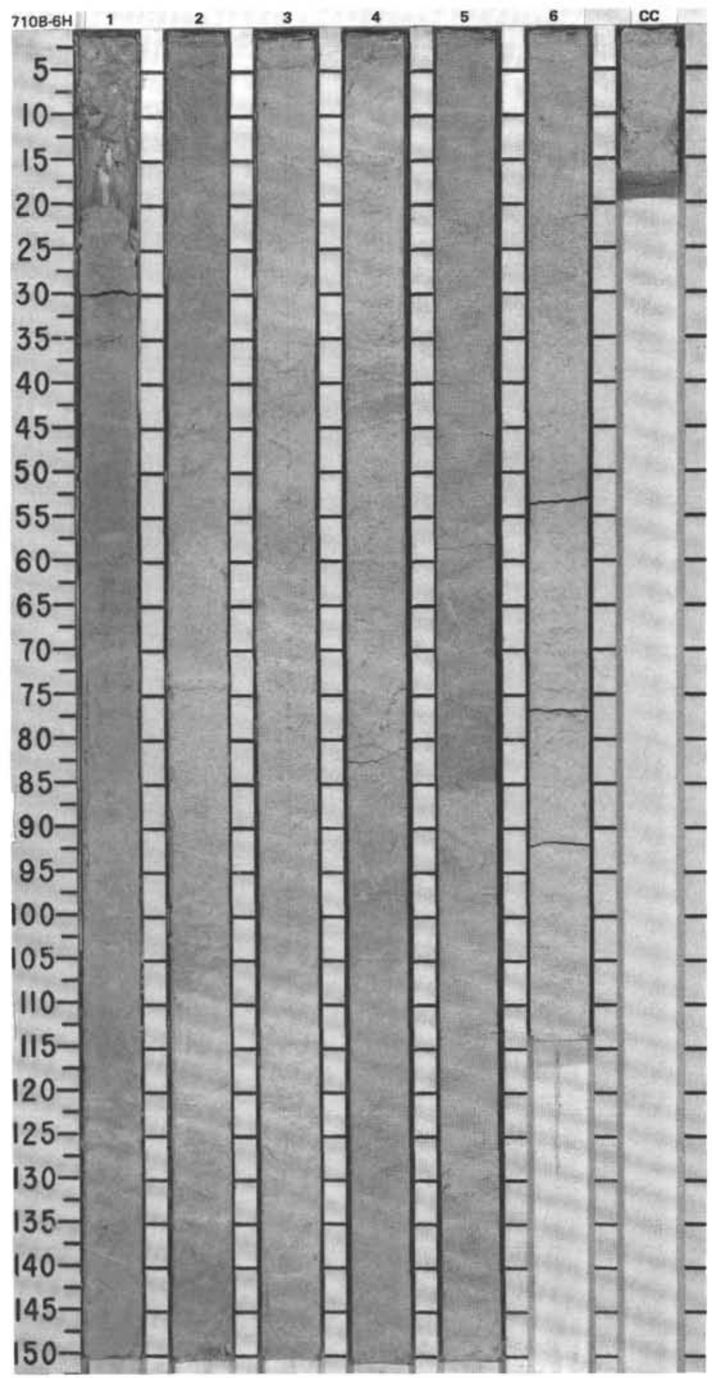

SITE 710 HOLE B CORE 7H CORED INTERVAL 3865.0-3874.7 mbsl; 54.5-64.2 mbsf

TIME-ROCK UNIT	BIOSTRAT. ZONE/FOSSIL CHARACTER: FORAMINIFERS	NANNOFOSSILS	RADIOLARIANS	DIATOMS	PALEOMAGNETICS	PHYS. PROPERTIES	CHEMISTRY	SECTION	METERS	GRAPHIC LITHOLOGY	DRILLING DISTURB.	SED. STRUCTURES	SAMPLES
UPPER MIOCENE		CN 9b (NN 11)	TRACE					1	0.5, 1.0				
								2					*
								3					
								4					
		CN 9a (NN 11)						5					
								6					
		AM						CC					

LITHOLOGIC DESCRIPTION

CLAY-BEARING NANNOFOSSIL OOZE

Major lithology: Clay-bearing nannofossil ooze, white (5G 8/1) and light gray (5Y 7/1, 5G 7.5/1). Very subtle color variations. Minor pyrite staining. Bioturbated throughout. Reduced.

Minor lithology: Turbidites, foraminifer-nannofossil ooze. Sharp basal contacts, gradational upper contacts. Gray (N4) pyrite-stained at the base. Section 4, 101-102 and 103-106 cm.

0 color changes in Section 6 and CC; 21 color changes in Sections 1-5; and 2 turbidites.

SMEAR SLIDE SUMMARY (%):

	2, 70 D
TEXTURE:	
Sand	5
Silt	5
Clay	90
COMPOSITION:	
Dolomite	Tr
Foraminifers	Tr
Nannofossils	90
Diatoms	3
Radiolarians	5
Sponge spicules	2
Silicoflagellates	Tr

710 B 8H NO RECOVERY

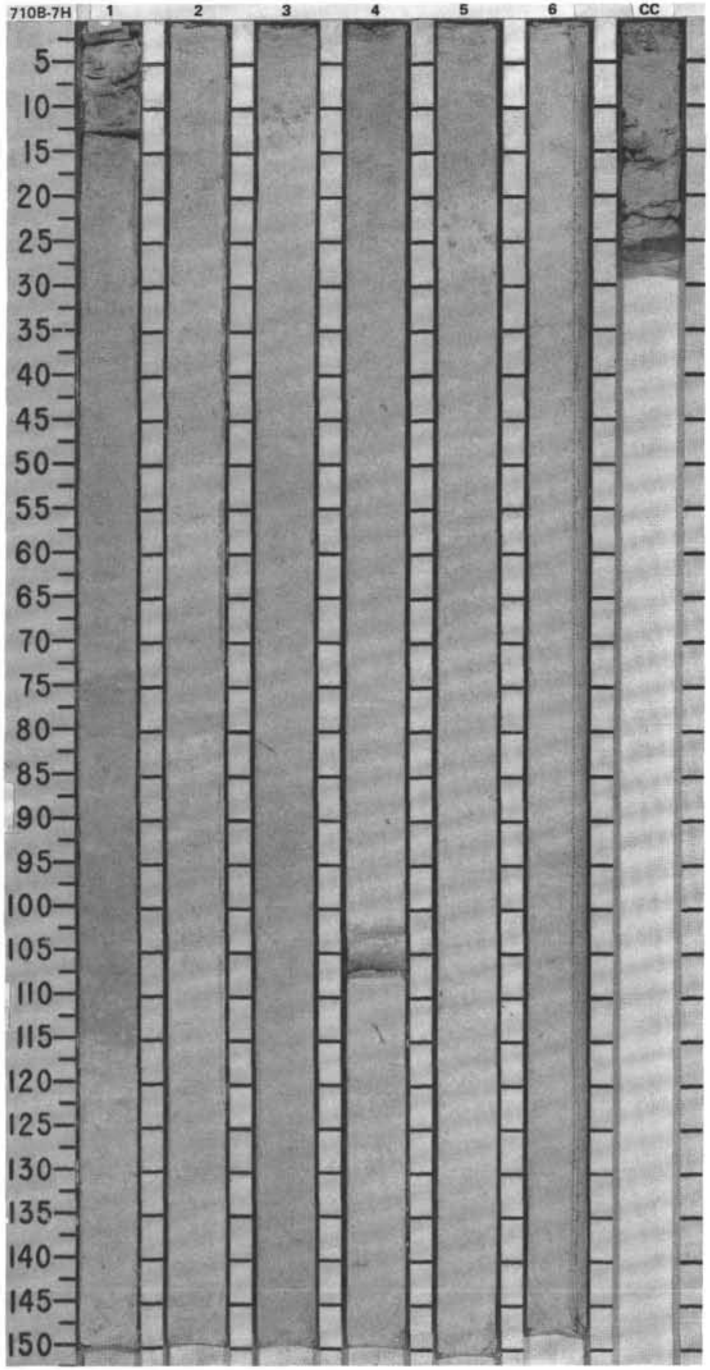

SITE 710 HOLE B CORE 9H CORED INTERVAL 3884.3-3893.9 mbsl; 73.8-83.4 mbsf

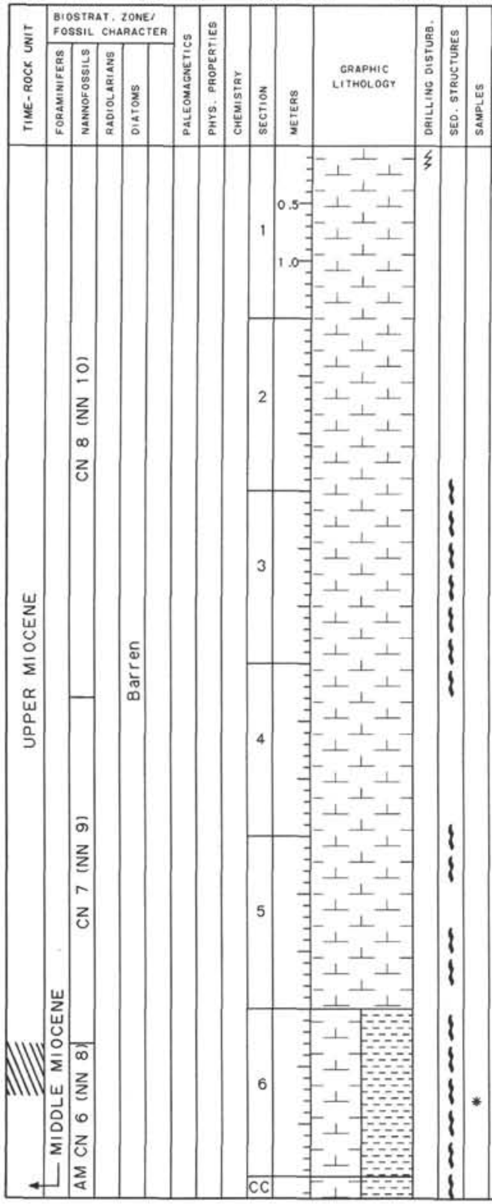

LITHOLOGIC DESCRIPTION

CLAY-BEARING NANNOFOSSIL OOZE and CLAY-NANNOFOSSIL OOZE

Major lithology: Clay-bearing nannofossil ooze in Sections 1-5 and clay-nannofossil ooze in Section 6 and CC. Light greenish gray (5GY 7/1) and light gray (5Y 7/1), reduced in Section 1. Grades to light gray (5Y 7/1) and pale yellowish gray (5Y 7/2) in Section 2, still reduced. Becomes oxidized gradually in Section 3 and below, where colors are white (10YR 8/2) and very pale brown (10YR 7.5/2). In Section 6 ooze becomes very pale brown (10YR 7/3, 7/4) and light yellowish brown (10YR 6/4).

0 color changes in Sections 1-3; 12 color changes in Sections 4, 5, 6, and CC.; and 0 turbidites.

SMEAR SLIDE SUMMARY (%):

	6, 80
	D
TEXTURE:	
Sand	3
Silt	5
Clay	92
COMPOSITION:	
Quartz	Tr
Mica	Tr
Clay	15
Foraminifers	Tr
Nannofossils	77
Diatoms	1
Radiolarians	5
Sponge spicules	2
Silicoflagellates	Tr